KOVINE ZLITINE TEHNOLOGIJE

METALS ALLOYS TECHNOLOGIES

LETO 28 št. 4 1994

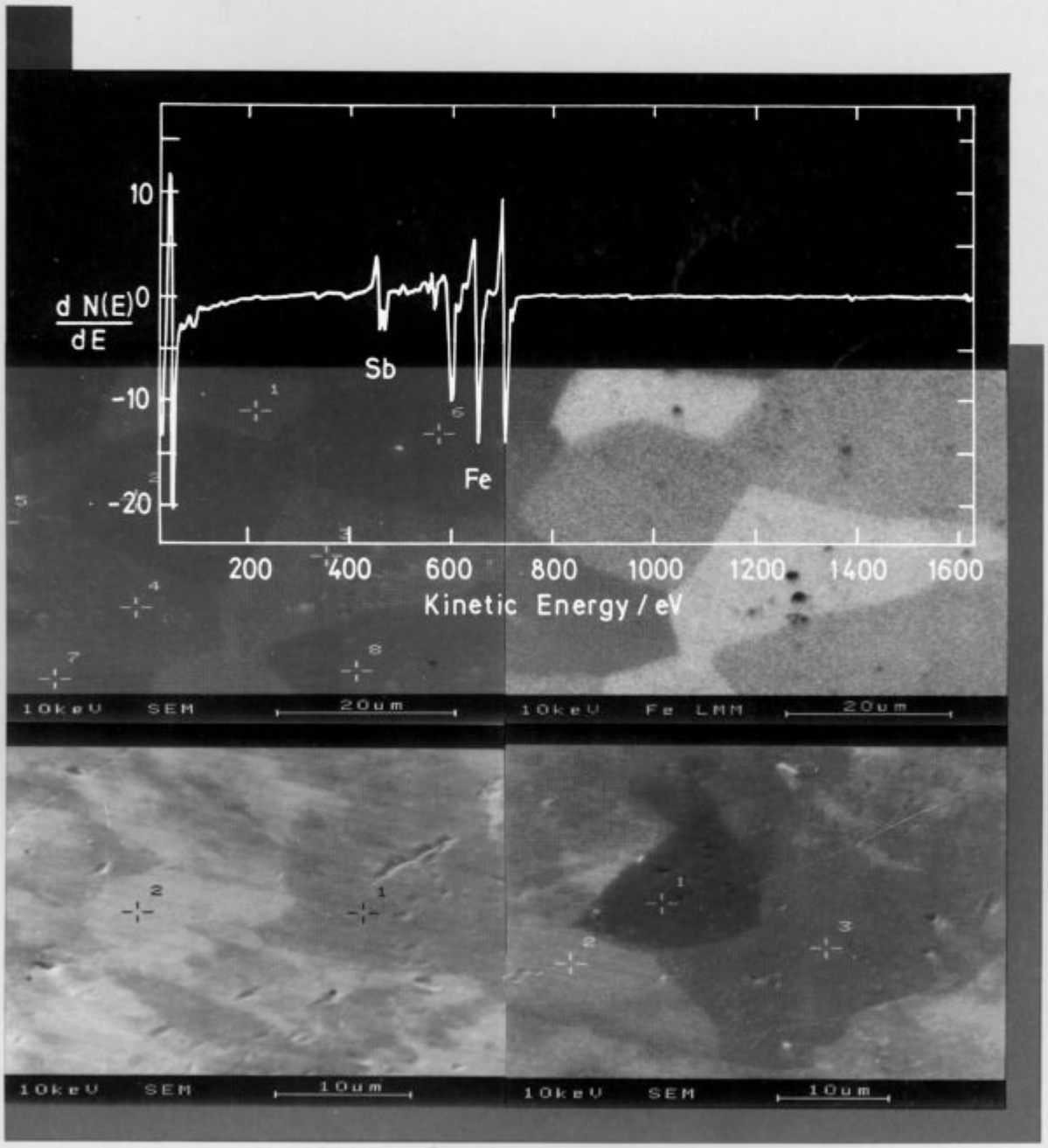

IZDAJAJO SŽ ACRONI JESENICE, METAL RAVNE, JEKLO ŠTORE IN INŠTITUT ZA KOVINSKE MATERIALE IN TEHNOLOGIJE LJUBLJANA

ISSN 1318-0010

Navodila avtorjem za pripravo člankov za objavo v reviji Kovine, zlitine, tehnologije

V letu 1992 uvajamo nov način tehničnega urejanja in priprave za tisk revije *Kovine, zlitine, tehnologije*. Da bi pocenili tiskarske stroške, skrajšali čas od prejema članka do njegove objave in prepustili avtorju končno odgovornost za morebitne neodkrite tipografske napake, smo se v uredništvu odločili, da izkoristimo možnosti, ki jih danes nudi namizno *založništvo*.

Avtor lahko pošlje članek napisan klasično – s pisalnim strojem. Zaželeno je, da avtor odda uredništvu članek oz. besedilo napisano na računalnik z urejevalniki besedil:

- WORDSTAR, verzija 4, 5, 6, 7 za DOS
- WORD za DOS ali WINDOWS
- WORDPERFECT.

Če je besedilo napisano z urejevalnikom besedil: CHI WRITER, naj ga avtor prekonvertira v WORDSTAR DOCUMENT.

Naprošamo avtorje, da pošljejo uredništvu disketo z oznako datoteke in računalniškim izpisom te datoteke na papirju.

Formule naj bodo v datoteki samo naznačene, na papirju pa ročno izpisane.

Vsebina članka

Kako naj članek izgleda vsebinsko, naj si avtorji ogledajo v starih izdajah Železarskega zbornika. Vsak članek pa mora vsebovati:

- slovenski in angleški naslovi članka,
- imena ter naslove avtorjev,
- povzetka v angleščini in slovenščini,
- reference, ki naj bodo v besedilu članka označene z zaporednimi številkami, primer[1–5]. Način citiranja članka: avtor, inicialkam naj sledi priimek, naslov članka, ime revije, letnik, strani, leto. Način citiranja knjige: avtor, naslov, založnik in kraj izdaje, leto, po potrebi poglavje ali strani.

Besedilo članka naj bo razdeljeno na razdelke (označene z zaporednimi številkami) in po potrebi še na podrazdelke (označene z decimalno številko, kjer celi del označuje razdelek.

Slike

Vse slike naj bodo na posebnih listih papirja, z jasno označeno številko slike. Slike naj bodo označene z zaporednimi številkami povsod v članku. Originali za vse vrste slik naj bodo ostri in brez šuma. *Risbe* naj bodo narisane s črnim na belem ozadju. Vse oznake in besedila na risbah naj bodo v istem jeziku kot besedilo članka in dovolj velike, da omogočajo pomanjšanje slike na 8 cm. Le izjemoma lahko slika sega čez obe koloni besedila (16,5 cm). *Fotografije* so lahko katerekoli običajne dimenzije, na svetlečem papirju in z dobrim kontrastom. Mikroskopska in makroskopska povečevanja označite v podpisu na sliki, še bolje pa z vrisanjem ustrezne skale na fotografiji.

Za vsako sliko naj avtor predvidi, kam naj se slika v besedilu članka uvrsti, kjer naj se nahaja ustrezen podnapis z zaporedno številko slike (na primer: "Slika 3 prikazuje...", nikakor pa ne: "Na spodnji sliki vidimo...").

Tabele

Avtor naj se izogiba zapletenih tabel z mnogo podatki, ki bralca ne zanimajo, posebej še, če so isti podatki tudi grafično ponazorjeni. Nad vsako tabelo naj se nahaja zaporedna številka tabele s pojasnilom. Tabele naj bodo povsod v članku označene z zaporednimi številkami.

Pisanje besedil na računalniku

Avtorje naprošamo, da pri pisanju besedil na računalniku upoštevajo naslednja navodila, saj le-ta precej olajšajo naše nadaljnje delo pri pripravi za tisk:

- ne puščajte praznega prostora pred ločili (pikami, vejicami, dvopičji) in za predklepaji oziroma pred zaklepaji,
- puščajte prazen prostor za vsemi ločili (pikami, vejicami, dvopičji) – razen decimalno piko,
- pišite vse naslove in besede z majhnimi črkami (razen velikih začetnic in kratic),
- besedilo naj ne vsebuje deljenih besed na koncu vrstice.

Če avtor pripravlja ilustracije na računalniku, ga naprošamo, da priloži datoteke s slikami na disketo z besedilom članka, s pojasnilom, s katerim programom so narejene.

Krtačni odtis

Krtačni odtis – končna podoba članka – bo poslan avtorju v končno revizijo. Avtorja naprošamo, da čim hitreje opravi korekture in ga pošlje nazaj na uredništvo. Hkrati naprošamo avtorje, da popravljajo samo napake, ki so nastale med stavljenjem članka. Če avtor popravljenega članka ne vrne pravočasno, bo objavljen nepopravljen, kar bo tudi označeno.

Uredništvo

KOVINE ZLITINE TEHNOLOGIJE

METALS ALLOYS TECHNOLOGIES

KOVINE ZLITINE TEHNOLOGIJE
Izdajajo (Published by): SŽ ACRONI Jesenice, METAL Ravne, JEKLO Štore in Inštitut za kovinske materiale in tehnologije Ljubljana

Izdajanje KOVINE ZLITINE TEHNOLOGIJE delno sofinancira:
Ministrstvo za znanost in tehnologijo

NASLOV UREDNIŠTVA (EDITORIAL ADRESS): KOVINE ZLITINE TEHNOLOGIJE,
ACRONI Jesenice d.o.o., 64270 Jesenice, Slovenija
Telefon: (064) 861-441
Telex: 37219
Telefax: (064) 861-412
Žiro račun: 51530-601-25734

Stavek: Majda Kuraš, **Tisk:** Gorenjski tisk, Kranj, **Oblikovanje ovitka:** Ignac Kofol,
Fotografija na naslovnici (opisi slik so v smeri urinega kazalca):
* SEM posnetek osmih zrn na površini neorientirane elektro pločevine legirane z 0.05% Sb. Površinska segregacija Sb je bila merjena z metodo AES na različno orientiranih zrnih.
* SAM posnetek Fe narejen na istem mestu
* SEM posnetek zrna z neanakomerno segregirano plastjo antimona
* SEM posntek segregirane plasti ogljika na zrnu 1.

Preko vseh posnetkov je prikazan AES spektre maksimalne ravnote-ne segregacije antimona dosežene pri 700°C za jeklo legirano z 0.05% Sb.
Vsi posnetki so bili narejeni z MICROLAG 310 D na Mx-Planck-Institut für Eisenforschug v Düsseldorfu, Nemčija.
Cover (captions in clock-wise):
* SEM image of eight grains on the surface of non oriented electrical steel sheet alloyed with 0.05% Sb. On the grains with different space orientation the antimony surface segregation was measured by AES;
* SAM image of Fe, measured on the same grains,
* SEM image of the grain with nonuniform antimony segregated layer and
* SEM image of carbon segregated layer on grain 1.

Across the images is AES spectra of maximum equilibrium atnimony segregation obtained after 15 minutes of annealing at 700°C.
All images were obtained with MICROLAB 310 D at Max-Planck-Institute für Eisenforschung in Düsseldorf, Germany.

Po mnenju Ministrstva za znanost in tehnologijo Republike Slovenije št. 23-335-92 z dne 09. 06. 1992 šteje KOVINE ZLITINE TEHNOLOGIJE med proizvode, za katere se plačuje 5-odstotni davek od prometa proizvodov.

Vsebina
Contents

Jenko Monika, F. Vodopivec, M. Godec, D. Steiner-Petrovič, H. Viefhaus, M. Lucas, M. Milun:
Surface Activated Recrystallization of Antimony Alloyed Non-Oriented Electrical Steel Sheet
Površinsko aktivirana rekristalizacija silicijevih elektro jekel, legiranih z antimonom ... 561–565

Kobe-Beseničar Spomenka, B. Saje, G. Dražič:
Use of the HDDR Process in Preparation of Zirconia Doped Nd-Dy-Fe-B High Coercivity Powder
HDDR postopek kot metoda za pripravo visoko koercitivnih Nd-Dy-Fe-B prahov 567–570

Vodopivec Franc, B. Ule, L. Vehovar, J. Žvokelj, V. Verbič:
Macro and Micromorphology of Service Cracking and Fracture of Turbine Blades
Makro in mikromorfologija razpok in zlomov nastalih med obratovanjem turbinskih lopatic 571–577

Schlomchack Georg Georgijevič, I. Mamuzič, F. Vodopivec:
The Role of Contact Friction and Rheology in the Deformation at Plastometric Tests of Rheologically Complex Materials
Vpliv kontaktnega trenja in reologije pri plastometričnih preizkusih reološko kompleksnih materialov 579–582

Schlomchack Georg Georgijevič, I. Mamuzič, F. Vodopivec:
Deformation Anomalies of Higher Order during the Plastic Extention of Rheologically Complex Materials
Deformacijske anomalije višje stopnje med plastičnim raztezanjem reološko kompleksnih materialov 583–587

Kejžar Rajko, L. Kosec:
Quality of Surfaced Running Wheels
Kvaliteta navarjenih tekalnih koles 589–593

Ule Boris, V. Leskovšek, B. Breskvar, K. Kuzman, D. Švetak, F. Kofol:
Cockroft - Latham Fracture Criterion and Bulk Formability of Copper Base Alloys
Cockroft Lathamov kriterij loma in masivna preoblikovalnost bakrovih zlitin 595–600

Šuštaršič Borivoj, B. Breskvar, V. Leskovšek, A. Rodič:
Properties of Cu-based Alloys - Powders for Brazing Prepared by Water Atomization
Lastnosti prahov-zlitin na osnovi bakra izdelanih z vodno atomizacijo 601–608

Koroušic Blaženko:
Use of a Mathematical Model GPRO to Describe Complex Gas - Metal Reactions
Uporaba matematičnega modela GPRO pri opisovanju kompleksnih reakcij med plinsko in kovinsko fazo 609–611

Borchardt Güntner, R. Turk, S. Javorič:
Protection of Carbon/Carbon Composites against Oxidation
Zaščita kompozitov tipa ogljik/ogljik pred oksidacijo 613–617

Kundak Mijo, J. Črnko:
Influence of the Scaling upon the Heating Process of Steel Slabs in a Pusher-type Furnace
Utjecaj ogorine na proces zagrijavanja čeličnih slabov u peči potisnog tipa 619–622

Index – Letno kazalo 623–628

Kovine, zlitine, tehnologije / letnik 28 / 1994 / številka 4 / strani 561 do 565

Surface Activated Recrystallization of Antimony Alloyed Non-Oriented Electrical Steel Sheet

Površinsko aktivirana rekristalizacija silicijevih elektro jekel, legiranih z antimonom

M. Jenko,* F. Vodopivec, M. Godec, D. Steiner-Petrovič, Inštitut za kovinske materiale in tehnologije, Ljubljana, Slovenia
H. Viefhaus, M. Lucas, Max-Planck-Institute für Eisenforschung, Düsseldorf, Germany
M. Milun,T. Valla, Institut za fiziku Sveučilišta u Zagrebu, Zagreb, Croatia

In the present paper the effect of antimony on recrystallization texture of non oriented steel sheets is discussed. The antimony surface and grain boundary segregation were investigated. Since the grain boundary segregation was negligible one can conclude that the texture formation results from orientation dependent effects of Sb on the surface energy and through them on grain boundaries.
Key words: non oriented steel sheet, recrystallization, grain growth, adsorption, surface and grain boundary segregation.

Raziskali smo vpliv antimona na teksturo rekristalizacije neorientirane elektro pločevine, kot tudi segregacijo antimona na površini in na mejah zrn. Segregacija antimona po mejah zrn preiskovanih jekel je zanemarljiva. Predpostavljamo, da se zaradi vpliva antimona na površini pločevine površinska energija zrn z orientacijo (100) zmanjša in vpliva na oblikovanje ugodne teksture.
Ključne besede: neorientirana elektro pločevina, rekristalizacija, rast zrn, adsorbcija, površinska segregacija, segregacija po mejah zrn.

1. Introduction

Low loss and high permeability non oriented silicon steels are needed for efficient electrical power generation and transformation, which is one of the conditions for energy conservation and environmental amelioration[1-5]. To attain the full potential of this highly developed material its recrystallization texture must be improved[10].

It has been found that small additions of certain elements (Sb,Sn,Se,Te) especially antimony, into the steel for non oriented electrical sheets, affect the recrystallization and lead to an increase of the number of ferrite grains with favorable orientation[6-9]. The effect on grain growth and orientation can be caused by surface and/or grain boundary segregation of Sb or else. The surface segregation, its kinetics and equilibrium were measured using Auger Electron Spectroscopy and Thermal Desorption Spectroscopy on and in steel doped with Sb.

2. Experimental

Experimental steels of the composition given in **Table 1**, were prepared in laboratory from the same base material. The specimens for the surface segregation studies, of dimensions 6 mm in diameter and thickness of 0.15 mm were mounted into the UHV system. The samples were heated up to 900°C for 10 minutes and then sputter clean, annealed in the temperature range from 450 to 950°C and investigated 'in situ' by AES. The antimony enrichment of the surface was determined by following the peak height ratio (PHR) of amplitudes between the dominant $Sb(M_5N_{4,5}N_{4,5})$ and $Fe(LM_{2,3}V)$. Auger transitions at kinetic energies of 454 and 650 eV, respectively[6,7,13-15].

Table 1: Chemical composition in mass contents in % of the experimental steels:

Steel	C	Mn	Si	S	Al	Sb
1	0.005	0.18	1.85	0.001	0.19	0.05
2	0.004	0.20	1.94	0.001	0.11	0.1
3	0.004	0.20	2.12	0.001	0.19	–

Cylindrical specimens for grain boundary segregation measurements were prepared from the ingots of the same base material, notched, encapsulated in quartz tubes evacuated to approximately 10^{-6} mbar, normalized for 24 hours at 1000°C, cooled and aged at 850, 700 and 550°C for different times, from 1 to 500 hours.

Also the grain boundary segregation was investigated by AES method. Cylindrical specimens were introduced into UHV system of AES spectrometer at basic vacuum $4x10^{-10}$ mbar and after cooling to approximately -120°C were impact fractured 'in situ'. The AES analysis were taken from as many intergranular fracture facets as possible[11,12,14-16].

The antimony desorption from the surface segregated layer was investigated by performing Thermal desorption

* doc. dr. Monika JENKO, dipl. inž.
IMT Ljubljana, Lepi pot 11, 61000 Ljubljana
e-mail: monika.jenko@guest.arnes.si

Spectrometry - TDS. The specimen was introduced in the UHV system of AES spectrometer additionally equipped with TDS and heated several times up to 950°C[18].

The grain orientation was determined by X-ray difractometry with Mo Kα radiation.

3. Results and discussion

The highest antimony surface segregation was established at 700°C until no further increase in Sb concentration could be observed and the sulfur concentration was acceptable low, **figure 1**.

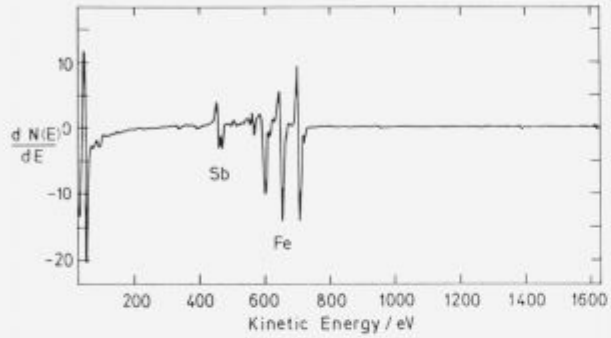

Figure 1: AES spectra of maximum equilibrium antimony segregation obtained at 700°C for steel with 0.05% Sb.

Slika 1: AES spekter maksimalne ravnotežne segregacije antimona dosežene pri 700°C za jeklo legirano z 0.05% Sb.

Table 2: Antimony to iron peak height ratios for all recordered AES spectra of Sb surface segregation measured on the different grains, shown in **figure 2**.

Grain	PHR (Sb/Fe650eV)
1	0.32
2	0.39
3	0.28
4	0.44
5	0.43
6	0.37
7	0.38
8	0.42

Table 2 shows antimony to iron peak height ratios for all recordered Auger spectra. The corresponding points on the different grains are noted on the SEM images, **figure 2**. The Sb/Fe650 eV peak height ratio varies between 0.28 and 0.44. There is not always a correlation of the peak height ratios and the intensity within the Sb SAM images and this may be due to a channeling effect of the primary electron beam. The intensity, especially of the iron Auger signal, depends on the angle of incidence for the primary electron beam with respect to the crystallographic orientation of the grains[11]. If we neglect this influence of possible channeling effects we can estimate the Sb surface concentration by comparison with the results on Sb surface segregation on single crystal surfaces of defined orientation. For the same primary energy of exciting electrons the following saturation peak height ratios were measured for single crystal surfaces of (100), (110) and (111) orientation:

Sb/Fe 650 eV = 0.42 for the (111) oriented surface
Sb/Fe 650 eV = 0.58 for the (110) oriented surface
Sb/Fe 650 eV = 0.40 for the (100) oriented surface

For the (100) oriented surface saturation coverage is half of a monolayer corresponding to a LEED c(2x2) overlayer pattern. For the other surface orientations no well defined ordered structure of surface coverage was observed[11]. But the peak height ratios are in the same order as for the polycristalline samples. The peak height ratio at saturation for the (100) surface was used as a calibration and the surface concentration for the polycrystalline samples at saturation were in the range of 0.2 to 0.6 of a monolayer.

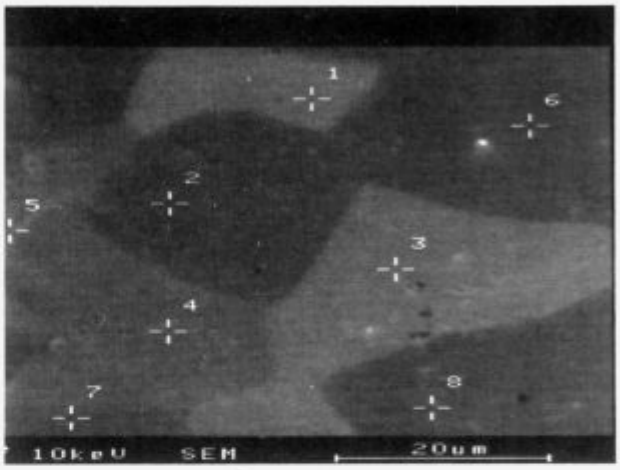

Figure 2: AES measurements of Sb surface segregation on the different grains. Antimony to iron peak height ratios for all recordered spectra are given in Table 2.

Slika 2: AES meritve površinske segregacije Sb na različnih zrnih. Razmerja vrhov antimona napram železu za posnete spektre so podana v tabeli 2.

It was found that even in one grain the antimony segregation layer is not uniform, close by grain boundary the segregated layer was thicker, **figure 3**.

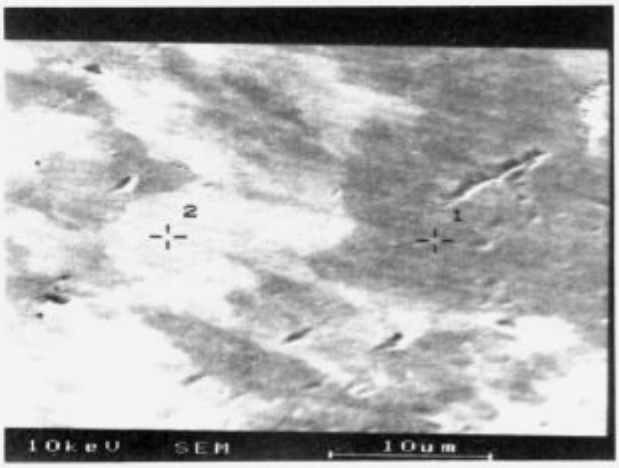

Figure 3: SEM image of the grain with segregated antimony layer. Close to grain boundary the segregated layer was found thicker.

Slika 3: SEM posnetek zrn s segregirano plastjo Sb. Ob meji zrna je bila segregirana plast Sb debelejša.

The kinetics of surface antimony segregation measured by AES at 700 and 800°C is shown in **figure 4**. It was found that at elevated temperatures T > 750°C, antimony surface segregation rate decreases. There are two possible explanation for this effect;

simultaneously antimony and sulfur segregation and/or Sb desorption from segregated layer.

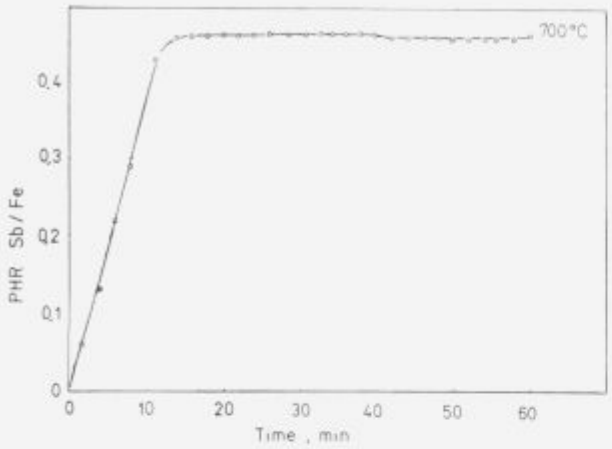

Figure 4: Kinetics of maximum equilibrium Sb surface segregation of steel alloyed with 0.05% Sb, obtained at 700°C.

Slika 4: Kinetika maksimalne ravnotežne površinske segregacije antimona za jeklo z 0.05% Sb, dobljena pri konstantnem žarjenju na temperaturi 700°C.

Sb desorption from the segregated layer was investigated by Thermal Desorption Spectrometry in temperature range from 20 to 950°C. In **figure 4** the results of TDS investigation are shown. Sb as well as S desorption from the segregated layer was established at T > 750°C.

Thus one can conclude that the effect of decrease of antimony segregation rate at elevated temperature T > 750°C is the result of both phenomena: antimony desorption and simultaneously segregation of Sb and S as we proposed in our earlier paper.[10]

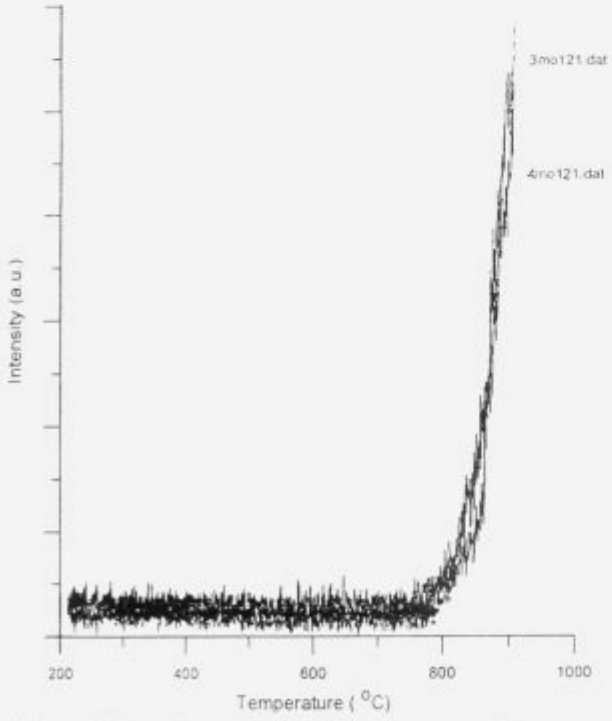

Figure 5: The antimony desorption from the segregated layer was established at T > 750°C, by Thermal Desorption Spectrometry.

Slika 5: Odparevanje antimona iz segregirane plasti smo izmerili z metodo TDS pri temperaturah T > 750°C.

Also grain boundaries of the material were analyzed by AES after annealing at 850, 700, 600 and 550°C for 1 to 500 hours. We found that the grain boundary segregation of antimony and also of other solute elements was negligible[8] which is not in agreement with our earlier findings[5]. However the Sb grain boundary segregation was established in a crack open to the surface of cylindrical specimen. It is therefore possible that in the earlier work the surface antimony segregation and not grain boundary segregation was measured. Strong interaction and cosegregation of Ni and Sb was observed at the grain boundaries[14-17] but in our investigation it is not to be expected because of very low Ni content. Bryant[16] and Gas[17] reported that they found grain boundary segregation of antimony in pure Fe-Sb alloy after 200 and 500 hours of annealing in vacuum at 550°C. After the same thermal treatment of the investigated steels, the present investigation revealed that grain boundary segregation of antimony and also of other solute elements was negligible.

The influence of antimony on recrystallization and grain growth was studied on steel alloyed with 0.05% Sb and on comparative steel. The kinetics of grain growth and the final grain size was determined in the temperature range from 700 to 800°C, there was no clear effect of Sb on the rate of the grain growth, while the recrystallization was slow in the antimony alloyed steel, **figure 5**.

The grain orientation for both steel alloyed with Sb and comparative steel was determined with X-ray difractometry,

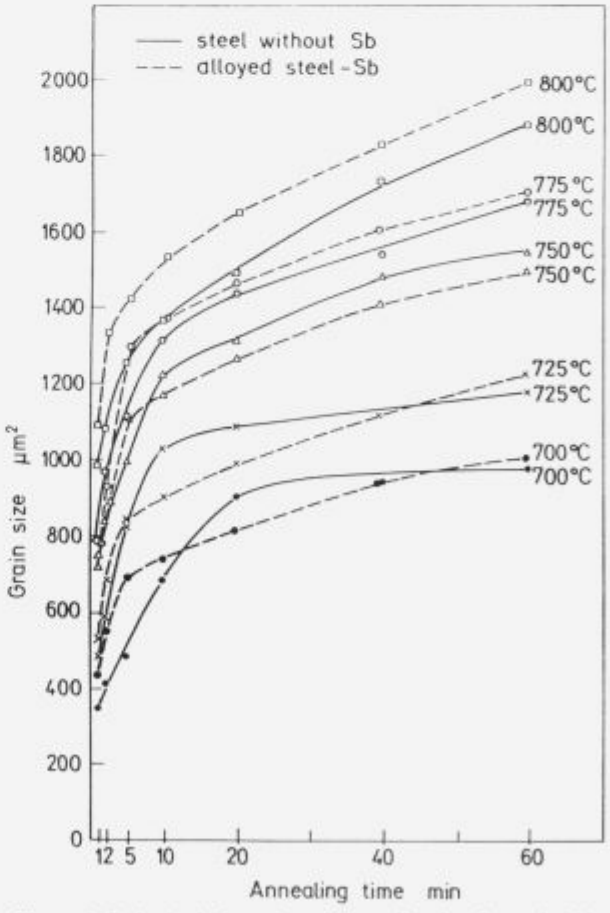

Figure 6: Grain size in dependence of annealing time for steels with 0.05% Sb and without Sb10.

Slika 6: Velikost zrn v odvisnosti od časa žarjenja za jeklo z 0.05% Sb in primerjalno jeklo brez Sb10.

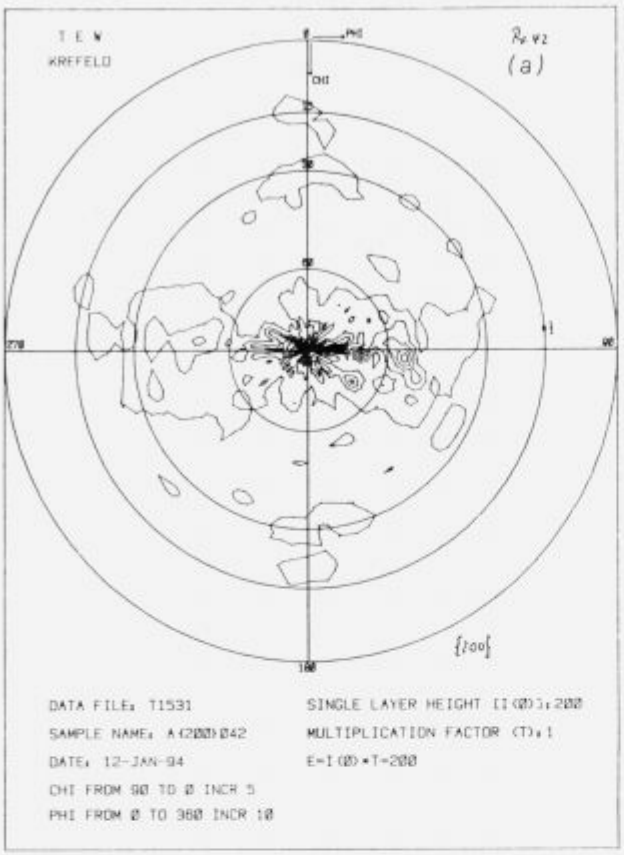

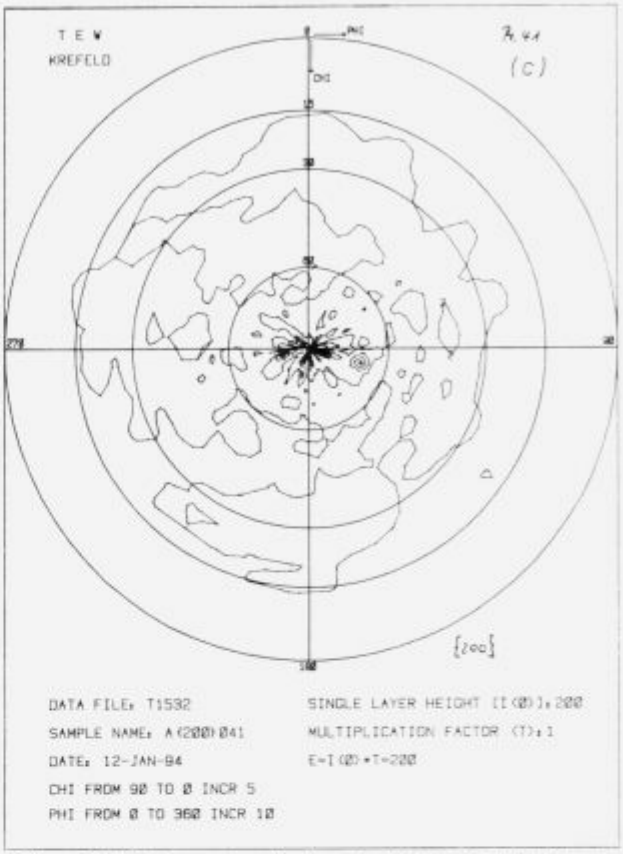

Figure 7: Pole figures of steels alloyed with 0.05% Sb, 0.1% Sb and comparative steel established by X-ray difractometry, using Mo-Kα radiation. Small share of grains with the texture (100)(001) was obtained in 0.05% Sb steel(a), for 0.1% Sb steel a weak texture with (111)(001) orientation was established.

Slika 7: Polove figure jekel legiranih z 0.05% Sb, 0.1% Sb in za primerjalno jeklo brez Sb smo določili z metodo rentgenskega uklona z uporabo Mo Kα sevanja. V jeklu z 0.05% Sb je bil ugotovljen manjši delež zrn z orientacijo (100)(001) (a); za jeklo z 0.1% Sb pa je bila določena šibka tekstura (111)(110), (b).

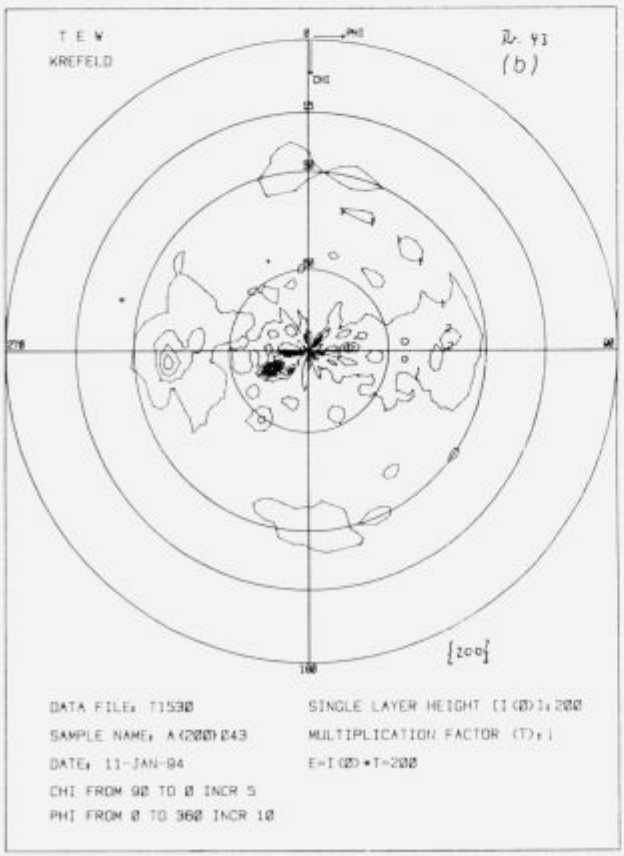

using Mo Kα radiation. Ordered pole figures are shown in **figure 6**, for comparative steel. For both steels alloyed with antimony a week orientation is estimated. Small share of grains with the texture (100) (001) was obtained in steel with 0.05% Sb, while for the steel alloyed with 0,1% Sb a weak texture of (111) (110) orientation was established. Similar results of grain orientation were obtained by performing an etch pits method, as reported already[8].

The results of this investigation, support the hypothesis that the texture formation results from orientation dependent effects of Sb on the surface energy, but not from effects on the grain boundary stability and mobility.

4. Conclusions

The antimony surface segregation depends on grain orientation. The maximum antimony surface segregation coverage at saturation was found at 700°C by AES.

The Sb surface segregation depends on grain orientation. The peak height ratio at saturation for the (100) single crystal surface was used as a calibration and the maximal surface concentration for the polycrystalline samples at saturation was 0.6 of a monolayer.

Grain boundary segregation of antimony and of other solute elements e.g., S, C, P, Si, Al, in the experimental steels were negligible.

The desorption of antimony and sulfur was established at T > 750°C, by TDS method. Thus one can conclude that the decrease in antimony segregation rate at elevated temperature is the result of simultaneously segregation of antimony and sulfur as well as of antimony and sulfur desorption.

5. References

[1] G. Lyudkovski, P. K. Rastogi, M. Bala, *Journal of Metals*, 1 (1986) 18

[2] G. Lyudkovski, P. K. Rastogi, *Metall. Trans. A.*, 15A (1984) 257

[3] H. Shimanaka, T. Irie, K. Matsumura, K. Nakamura, *J. Magn. Magn. Mat.* 19 (1980) 63

[4] P. Marko, A. Šolyom, V. Frič, *J. Magn. Magn. Mat.* 41 (1984)

[5] F. Vodopivec, F. Marinšek, D. Gnidovec, B. Praček, M. Jenko, J. *Magn. Magn. Mat.* 97, (1991) 281

[6] M. Jenko, F. Vodopivec, B. Praček, *App. Surf. Sci.* 70/71 (1993) 118

[7] M. Jenko, F. Vodopivec, B. Praček, M. Godec, D. Steiner, *J. Mag. Mag. Mat.* 133 (1994) 229

[8] G. Lyudkovski, *IEEE Trans. Magnetics mag.* 22 (1986)5, 508

[9] G. Lyudkovski, A. G. Preban, J. M. Shapiro, *J. Appl. Phys.* 5 (1982) 3, 2419

[10] M. Jenko, F. Vodopivec, H. J. Grabke, H. Viefhaus, B. Praček, M. Lucas, M. Godec, *Steel research*, 65 11, (1994) 500,

[11] V. Rusenberg, H. Viefhaus, *Surf. Sci.* 172 (1986) 615

[12] H. J. Grabke, *Iron and Steels, ISIJ int.* 29 (1989) 529

[13] H. J. Grabke, *Kovine zlitine tehnologije* 27 (1993) 1-2 9

[14] C. Lea, M. P. Seah, *Phil. Mag.* 35, 1 (1977) 213

[15] E. D. Hondros, M. P. Seah, *Metal Trans.* 8A (1977) 1363

[16] C. L. Briant, M. Ritter, *Acta metall.* 32 (1984) 2031

[17] P. Gas, M. Guttman, J. Bernardini, *Acta metall.* 30 (1982) 1309

[18] D. P. Woodruff, T. A. Delchar, *Modern Techniques of Surface Science*, Cambridge University Press, 1994

slovenske železarne

ACRONI

SŽ ACRONI d.o.o. Cesta železarjev 8, 64270 Jesenice
tel. centrala: +386 64 861-441
tel. direktor: +386 64 861-443
tel. komerciala: +386 64 861-474
Fax: +386 64 861-379
Telex: 37219 ZELJSN SI Slovenija

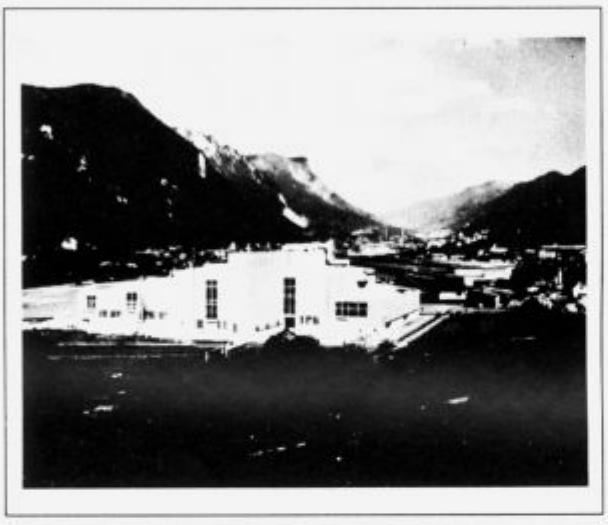

OUR PRODUCTION PROGRAM INCLUDES:

* general structural steels
* finegrained and HSLA structural steels
* carbon and alloyed steels
  - for quenchig and tempering
  - case herdening
* silicon steels for electrical sheets
* stainless steels

* hot rolled plates, wide and slit strips and bars
* cold rolled sheets, wide and slit strips
* cold rolled sections
* metal door posts
* blanks

WE ALSO OFFER:

* hot and cold rolling
* blankig
* torch cutting by drawing
* straightening
* heat treating of plates, strips and sheets

ELECTRICAL SHEETS AND STRIPS

STAINLESS STEELS

MICROALLOYED STEELS

HIGH CARBON STEELS for herdening and tempering

Kovine, zlitine, tehnologije / letnik 28 / 1994 / številka 4 / strani 567 do 570

Use of the HDDR Process in Preparation of Zirconia Doped Nd-Dy-Fe-B High Coercivity Powder

HDDR postopek kot metoda za pripravo visoko koercitivnih Nd-Dy-Fe-B prahov

S. Kobe Beseničar,* B. Saje, G. Dražič, Jožef Stefan Institute, Ljubljana, Slovenia

The present paper deals with the use of the HDDR process as the preparative method for obtaining zirconia doped high coercive Nd-Dy-Fe-B powders. The influence of the dopant and of the processing parameters on the HDDR mechanism and the magnetic properties of the powders obtained, was studied. The material was characterized by magnetisation measurements at various stages of the HDDR process. Electron microscope studies on the Nd-Dy-Fe-B powders were performed to observe the influence of zirconia addition on the crystallisation during the recombination process.
Key words: Nd-Fe-B magnets, coercivity, processing.

HDDR postopek (Hidrogenacija Disproporcionacija Desorpcija Rekombinacija) smo uporabili kot metodo za pripravo finih visoko koercitivnih Nd-Dy-Fe-B prahov dopiranih s cirkon oksidom. Študirali smo vpliv dopanta in procesnih parametrov na mehanizem poteka HDDR postopka in na končne morfološke in magnetne lastnosti tako dobljenih prahov. Vzorce smo karakterizirali na različnih stopnjah HDDR postopka z magnetnimi meritvami. Prahove smo opazovali z elektronskim mikroskopom in študirali vpliv cirkonovega oksida na potek kristalizacije med postopkom rekombinacije.
Ključne besede: Nd-Fe-B magneti, koercitivnost, procesiranje.

Introduction

One of the well known methods for preparation of isotropic Nd-Fe-B coercive powders is the HDDR process, as reported in several papers[1-4]. It was also established previously that an anisotropic powder can be produced by the addition of small amounts of Zr to the initial composition. The intrinsic coercivities of powders prepared by this method are reported to be up to 1100 kA/m (13.8 kOe)[5,6].

In our previous work the beneficial influence of zirconia on the microstructure and consequently on the magnetic properties and corrosion resistance of sintered Nd-Dy-Fe-B magnets was reported[7,8].

The purpose of the present work was to prepare high coercive Nd-Dy-Fe-B powders by the HDDR processing route, using the same composition of the basic alloy, together with the addition of 1 wt.% of ZrO_2, as previously employed[8]. High coercivity powders were intended for use as the basic material for the preparation of resin bonded magnets. This paper only deals with the powder processing and its characterization.

Experimental

The basic alloys for the HDDR process were prepared by arc melting the alloys NdFe, DyFe, FeB and Fe powder in a pure Ar atmosphere. The alloy composition was $Nd_{15-x}Dy_xFe_{76}B_8$ ($0<x<3$). In order to prevent oxidation, a Ti sponge was used as a getter for oxygen. 1 wt.% of zirconia was added before arc melting. The melted buttons were then subjected to HDDR processing. They were treated in hydrogen at room temperature (20kPa) first and then heated to different temperatures between 750°C and 850°C and exposed to further hydrogenation for two hours. A thermopiezic (TPA) analysis and DTA analyses were performed to follow the absorption process. The procedure was followed by evacuating the system and after exposing the samples to maximum temperature and high vacuum (10^{-3} Pa) for one hour they were furnace cooled[6].

Samples were lightly crushed and the powders obtained were characterized by magnetic measurements. For the mass magnetization measurements a DSM8 magnetometer - susceptometer was used; the intrinsic coercivity measurements were performed using a permeameter. Comparability of the measurements was attained by using always the same quantity of examined powder and binding material (epoxy) (wt.% 85/15). Samples were pulsed in a field of 4000 kA/m and demagnetized with a field of cca 2000 kA/m. Powders were observed by means of a SEM/EPMA (JEOL JXA 840 A). Phase analyses were performed using a TEM (JEOL 2000 FX).

Results and discussion

Figure 1 shows the demagnetizing curves of powders obtained by the HDDR process at different temperatures. Samples with and without zirconia addition are compared. The basic composition of those samples is $Nd_{15}Dy_1Fe_{76}B_8$. Z0 samples are without zirconia addition and Z1 with 1 wt%

* dr. Spomenka KOBE BESENIČAR,
Inštitut Jožef Stefan, Jamova 39, 61000 Lj.,

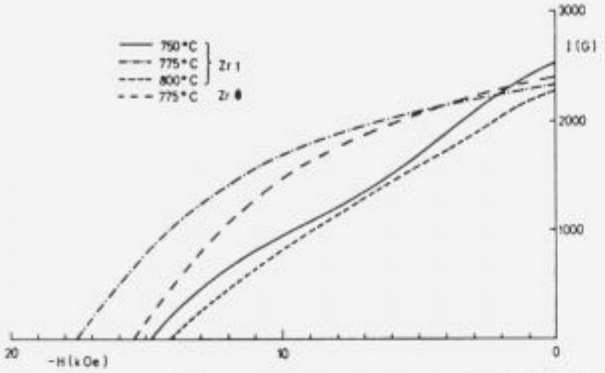

Figure 1: Demagnetizing curves of powders obtained by the HDDR process at different temperatures. Samples with and without zirconia are compared.

Slika 1: Demagnetizacijske krivulje prahov, dobljenih po HDDR postopku pri različnih temperaturah. Primerjava vzorcev z in brez dodatka cirkon oksida.

of zirconia additive. A maximum value of the intrinsic coercivity of 1400 kA/m (17.5 kOe) was attained when samples with the addition of zirconia were processed at 775°C. This value exceeds the coercivity of samples without zirconia and processed under the same conditions for about 13 % of the value obtained with samples without additive. At 750°C the poorer magnetic properties obtained were attributed to the presence of free iron. Grain growth at 800°C causes a decrease in coercivity.

Figure 2 shows the difference in the mass magnetization between samples with and without ZrO_2 addition processed at different temperatures. Several experiments in two different laboratories showed reproducible results. Samples with zirconia addition revealed a higher magnetization at lower temperature (750°C) than samples free of this additive. In **Figure 3** the SEM micrographs of the samples without addition of zirconia (A) and with zirconia addition (B) are shown. Both samples were processed under the same conditions. They were treated at 750°C. There is obvious difference in the grain size, which is around 0.3 μm in the samples without ZrO_2 addition and in the range between 0.3 μm and 1 μm in the samples with the additive. The most probable reason for the recombination process starting at lower temperatures and consequently the higher magnetization of doped samples, lies in the different reaction kinetics of zirconia doped samples. At temperatures of the recombination

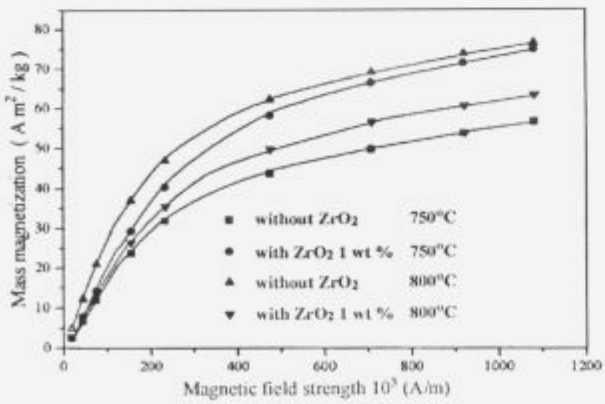

Figure 2: Mass magnetization measurements of samples with and without ZrO_2 addition, processed at different temperatures.

Slika 2: Magnetizacija vzorcev z in brez dodatka cirkon oksida, pripravljenih pri različnih temperaturah, kot funkcija jakosti magnetnega polja.

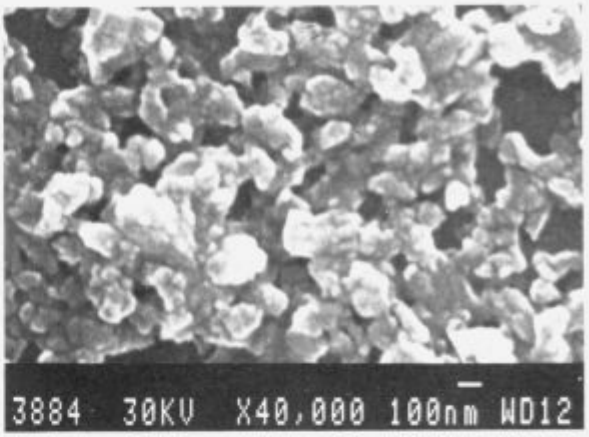

A

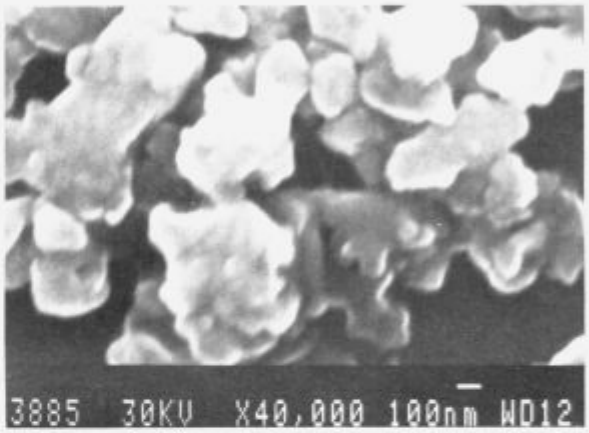

B

Figure 3: SEM micrographs of the samples processed under the same conditions (750°C): A - without zirconia, B - with zirconia addition.

Slika 3: SEM posnetki vzorcev pripravljenih pri enakih pogojih (750°C): A - brez cirkon oksida, B - s cirkon oksidom.

process higher than 750°C the mass magnetization is normally always higher in samples free of additive.

Our TEM observations confirmed the presumption about different reaction kinetics of zirconia doped samples. When the samples are exposed to the recombination process at 750°C, nano crystals of Nd rich phase which occurs within the origin grains are at least an order of magnitude smaller in the case of zirconia free samples (2 nm) (**Fig. 4A**) than in the case of samples with zirconia addition (up to 20 nm) (**Fig. 4B**).

In addition the crystallites of hard magnetic phase within the origin grains are at least an order of magnitude bigger in zirconia doped samples (**Fig. 5B**) comparing to the zirconia free sample (**Fig. 5A**), where nano crystals do not exceed 10-20 nm.

In **Figure 6** EDX spectra of 2-14-1 phase in samples without (A) and with zirconia (B) addition are shown. The $Fe_{K_\alpha}/Nd_{L_\alpha}$ peak-height ratio is lower in the case of sample (A) (cf. **Fig. 5**) indicating that several small Nd-rich particles were also present in the analysed volume. In the case of sample B, the particle size of Fe-rich phase is large enough to obtain just the spectrum of this phase without the interference from Nd-rich phase.

TPA analysis of the absorption process showed the disproportionation starting at higher temperature and proceeding slower in zirconia doped samples (**Fig. 7**). These results were confirmed also with a DTA analysis (**Fig. 8**). It is obvious that disproportionation of the samples without zirconia addition starts at lower temperature.

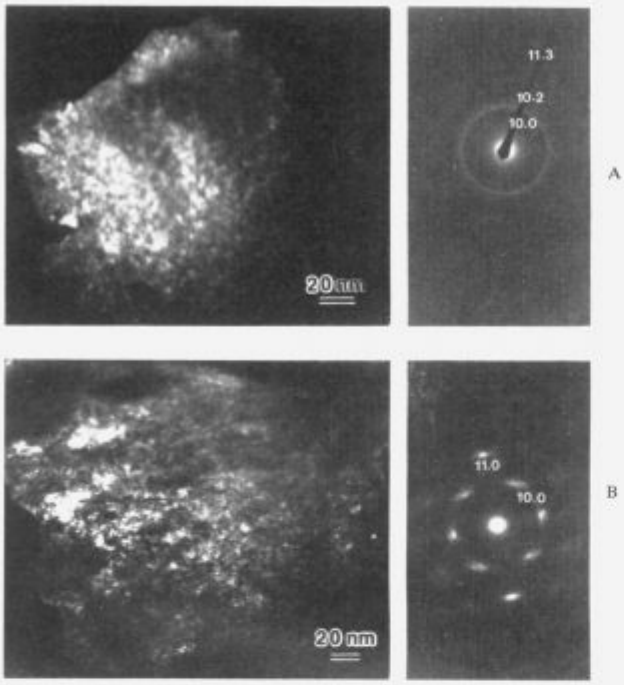

Figure 4: TEM micrographs (dark field) and corresponding diffraction patterns of NdDyFeB samples - Nd rich phase: A - zirconia free, B - zirconia added.

Slika 4: TEM posnetki (temno polje) in odgovarjajoči difraktogrami vzorcev NdDyFeB - faza bogata z Nd: A - brez cirkon oksida, B - z dodatkom cirkon oksida.

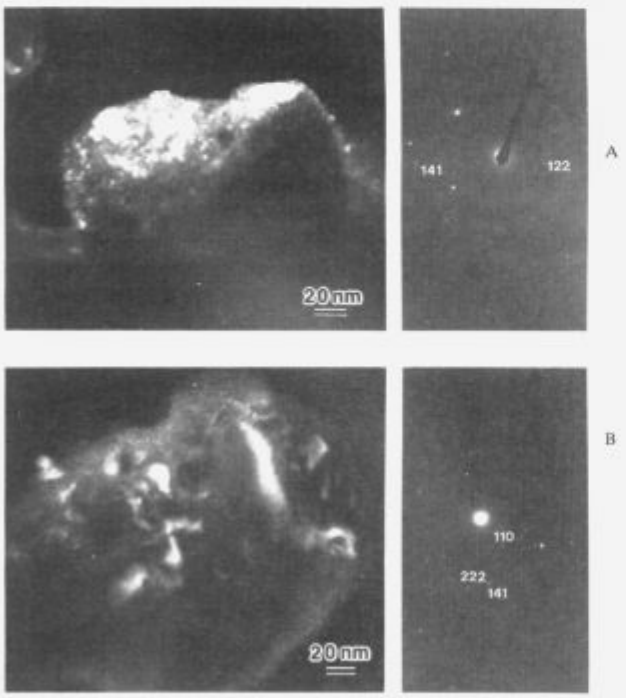

Figure 5: TEM micrographs (dark field) and corresponding diffraction patterns of NdDyFeB samples - $Nd_2Fe_{14}B$ phase: A - zirconia free, B - zirconia added.

Slika 5: TEM posnetki (temno polje) in odgovarjajoči difraktogrami vzorcev NdDyFeB: faza - $Nd_2Fe_{14}B$ A - brez cirkon oksida, B - z dodatkom cirkon oksida.

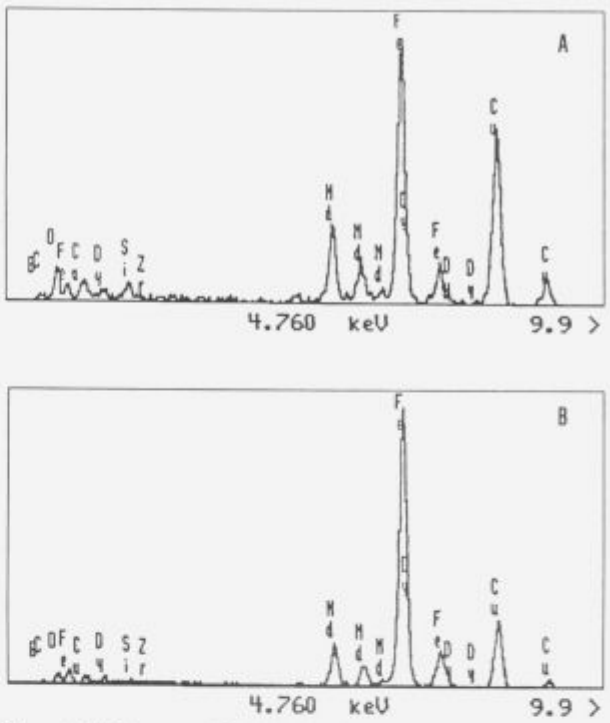

Figure 6: EDX spectra of 2-14-1 phase in samples without A and with B zirconia addition.

Slika 6: EDX spektri 2-14-1 faze v vzorcih brez A in z dodatkom cirkon oksida B.

A tentative explanation is that the statement about the local stabilization of 2-14-1 phase with respect to disproportionation, when elements such as Zr are added to the basic alloy[9] could be also transmitted in the case of zirconia addition. With the addition of zirconia the so called cells remain unaffected by the disproportionation and they act as nucleation centres in the recombination process. This model which explains anisotropy of such powders can tentatively also explain our TEM observations. A certain texture structure of the Nd-rich crystals formed during the recombination process in zirconia doped samples was detected (**Fig. 4B**, diffraction pattern). In the samples without ZrO2 addition the structure consists of randomly oriented nano crystallites (**Fig. 4A**). A detailed analysis with TEM on solid samples will give us more information about phase composition. There are

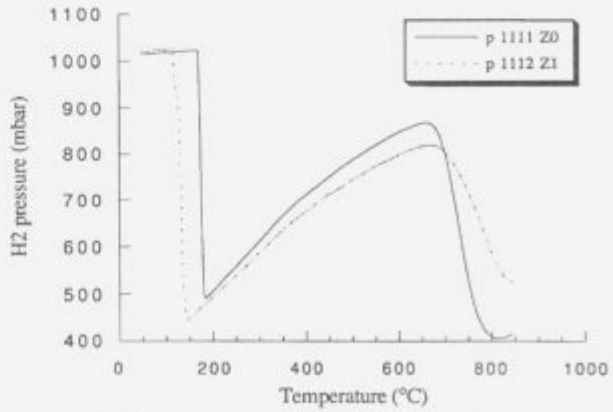

Figure 7: TPA traces for zirconia free (Z0) in zirconia added (Z1) $Nd_{11}Dy_1Fe_{82}B_6$ samples.

Slika 7: TPA analiza vzorcev $Nd_{11}Dy_1Fe_{82}B_6$: Z0 - brez cirkon oksida, Z1 - z dodatkom cirkon oksida.

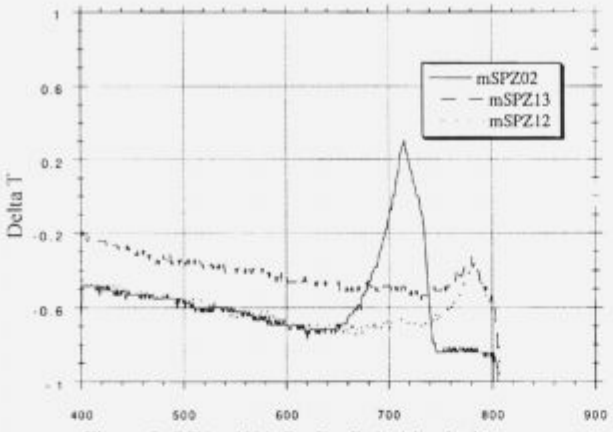

Figure 8: DTA of $Nd_{15}Dy_1Fe_{76}B_8$ in 1 bar hydrogen (note: graphs are not calibrated to the mass)

Slika 8: DTA analiza vzorca $Nd_{15}Dy_1Fe_{76}B_8$ pri 1 bar vodika (grafi niso kalibrirani na maso).

some indications about the presence of a phase based on Fe and Zr and this will also help us to explain the results of our first TEM analyses.

On the basis of these results, one can conclude that the HDDR processing route for the preparation of high coercive zirconia doped Nd-Dy-Fe-B powders reaches its optimum at 775°C for the present processing conditions (temperatures tested were: 750°C, 775°C, 800°C, 850°C). Further work will study the preparation of anisotropic magnets by different established techniques.

Acknowledgment

The financial assistance of the Ministry of Science and Technology and the British Council, UK are gratefully acknowledged. Part of the work was performed at the University of Birmingham, School of Metallurgy and Materials. Authors (S. Kobe Beseničar and B. Saje) would like to thank Prof. I. Rex Harris for his guidance and fruitful discussions. Prof. I. Rex Harris is also gratefully acknowledged for his critical review of the manuscript. The assistance of Mr. F. Dimc for the magnetic measurements and Mr. Z. Samardžija for SEM observations are gratefully acknowledged.

References

[1] T. Takeshita, R. Nakayama, *Proceedings of the 10. International Workshop on Rare Earth Magnets and their Applications*, Kyoto, (1989) 551

[2] P. J. McGuiness, X. J. Zhang, X.J. Yin, I.R. Harris, *J. Less Common Metals*, 158 (1990) 359

[3] I. R. Harris, P. J. McGuiness, *J. Less Common Metals*, 172 (1991) 1273

[4] X. J. Zhang, P. J. McGuiness, I. R. Harris, *J. Appl. Physics*, 68(8) (1991) 5838

[5] T. Takeshita, R. Nakayama, *Proceedings of the 11. International Workshop on Rare Earth Magnets and their Applications*, Pittsburgh, PA, (1990) 7

[6] P. J. McGuiness, C. L. Short, I. R. Harris, *IEEE Trans. on Magn.*, 28, (1992) 5, 2160-2162

[7] S. Beseničar, B. Saje, G. Dražič, J. Holc, *JMMM* 104-107, (1992) 1175

[8] S. Kobe Beseničar, J. Holc, G. Dražič, B. Saje, *IEEE Trans. on Magn.*, 30, 2, (1994) 693-696

[9] I. R. Harris, *Proceedings of the 12. International workshop on rare-earth magnets and their applications*, Canberra (1992) 347

Kovine, zlitine, tehnologije / letnik 28 / 1994 / številka 4 / strani 571 do 577

Macro and Micromorphology of in Service Cracking and Fracture of Turbine Blades

Makro in mikromorfologija razpok in zlomov nastalih med obratovanjem turbinskih lopatic

F. Vodopivec*, B. Ule, L. Vehovar, J. Žvokelj, Institute of Metals and technologies, Ljubljana, Slovenia
V. Verbič, TNT, Obrenovac, Serbia

After the break down cracked and fractured blades were extracted from the turbine and the macro and micromorphology of cracks and fractures surface were investigated. Three modes of propagation were identified: stable propagation by HISC, stable propagation by HISC and fatigue and instable brittle and ductile propagation. The micromorphological characteristics of the different modes of propagation are explained.
Key words: Turbine blades, steel, cracking, fracture, corrosion, fatigue, microstructure.

Po zlomu so bile počene in zlomljene lopatice vzete iz turbine in bila je raziskana makro in mikromorfologija razpok in zlomov. Identificirani so trije mehanizmi širjenja: stabilno širjenje zaradi HISC, stabilno širjenje zaradi HISC in utrujenosti ter nestabilno krhko in duktilno širjenje. Opisane so mikromorfološke značilnosti posameznih načinov širjenja.
Ključne besede: Jeklo, turbinske lopatice, razpokanje, zlom, korozija, utrujenost, mikrostruktura.

1. Experimental work

The experimental work consisted of:
- examination of microstructure;
- analysis of impurities on cracks surfaces, and
- macro and micro examination on the cracks and fractures surface.

The data on the composition of the steels and mechanical properties will be reported later and will be considered in this paper only when necessary to explain better the findings relative to the microstructure and the aspect of the cracks and fractures surface.

The composition of all examined blades corresponded to that required for the martensitic stainless steel X21CrMoV 121 and also the mechanical properties sufficed the requirement of the buyer of the turbine. It should be noted that a very low notch toughness of 15 J was required. Four different cases of cracking and fracturing of the blades were identified on the basis of visual examination:- one case of cracking on the rounded trailing edge in the passage between the root and the blade:
- some cases of cracking in the first root grove mostly at a distance up to 50 mm from this edge **(fig. 1, 2 and 3)**, and
- fracture of precracked blade in the turbine in the first root grove with an initial crack **(fig. 4)** or without such crack **(fig. 5)**.

On some in service cracked blades the crack surface was opened for examination by bending in laboratory, generally after cooling in liquid nitrogen.

On the base of the macromorphology of the crack surface three types of in service crack propagation were identified:
- surface showing near the initial point no fatigue striations but with such striations on the remaining area of the crack **(fig. 2 and 6)**,
- surface of cracks without fatigue striations **(fig. 3)**, and
- surface with fatigue striations from the starting point of cracks propagation.

Figure 1: Crack on the trailing edge in the first root grove of blade 436.
Slika 1: Razpoka na izhodnem robu v prvem korenskem žlebu lopatice 436.

2. Micromorphology of cracks and fractures

Several form of propagation were observed on specimens cut from different parts of the fracture of blades and on laboratory

* Prof. dr. Franc VODOPIVEC,
IMT Ljubljana, Lepi pot 11, 61000 Lj.

Figure 2: Surface of a crack with areas with and without fatigue striations.

Slika 2: Površina razpoke z deli z in brez utrujenostnih brazd.

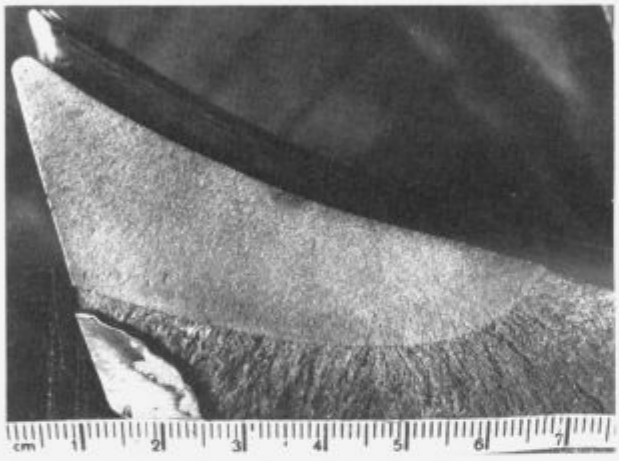

Figure 3: Surface of a crack without fatigue striations.

Slika 3: Površina razpoke brez utrujenostnih brazd.

Figure 4: Fracture of the blade 447 extracted from the disc after the break down. The initial crack is on the left side.

Slika 4: Prelom lopatice 447, ki je bila iz turbine vzeta po havariji. Začetna razpoka je na levi strani.

Figure 5: Fracture of the blade 379 extracted from the disc after the break down.

Slika 5: Prelom lopatice 379, ki je bila vzeta iz turbine po havariji.

Figure 6: Surface of the crack on the blade on fig. 4.

Slika 6: Površina razpoke na lopatici na sl. 4.

specimens. In order to make the matter easier to follow the fracture micromorphology is described separately for different areas: initial point, stable propagation and brutal (instant) rupture on laboratory specimens and in the turbine.

2.1. Initial point of cracking and stable propagation

Generally, the surface of cracks near the initial point was covered with corrosion products and also after a very careful cleaning it was rarely possible to find at SEM observation reliable details, which would characterize the mechanism of initiation. An exception was the specimen in **fig. 7**, where several crack initials with a perfectly clean surface were found. Near the tip of the pitting with a size of appr. 0,25 mm the fracture surface is brittle trans and intergranular **(fig. 8)** without fatigue striations. The micromorphology of the transgranular surface is featherlike and similar to that reported frequently for high strength steels with a martensitic microstructure and with an increased content of hydrogen. This suggests that in presence of the pitting the nucleation of the crack was induced by the overcharging of the steel with hydrogen produced by the corrosion process at the tip of the pitting. A similar detail of micromorphology of fracture surface near the nucleation point was observed also on the blade 436 **(fig. 9)**. It shows mixed propagation and small contamination with corrosion products, visible more clearly on the intergranular surface. On the clean part of cracks surface without striations near the border of the brutal fracture the micromorphology was similar as in **fig. 8** and **9** and it showed mixed trans and intergranular propagation with the featherlike surface of transgranular cleavage **(fig. 10)**.

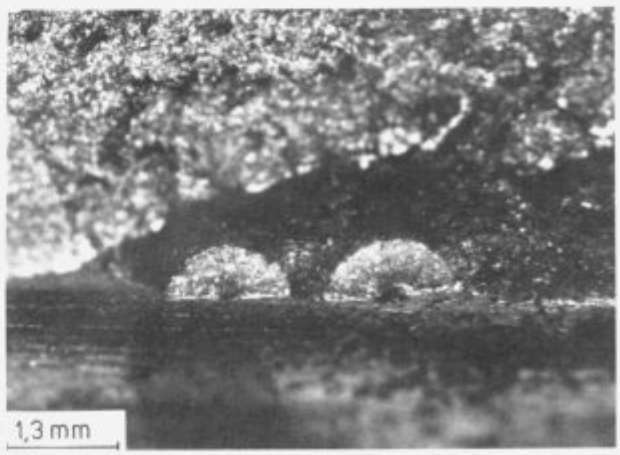

Figure 7: Fracture initials on blade 450.

Slika 7: Začetki preloma na lopatici 450.

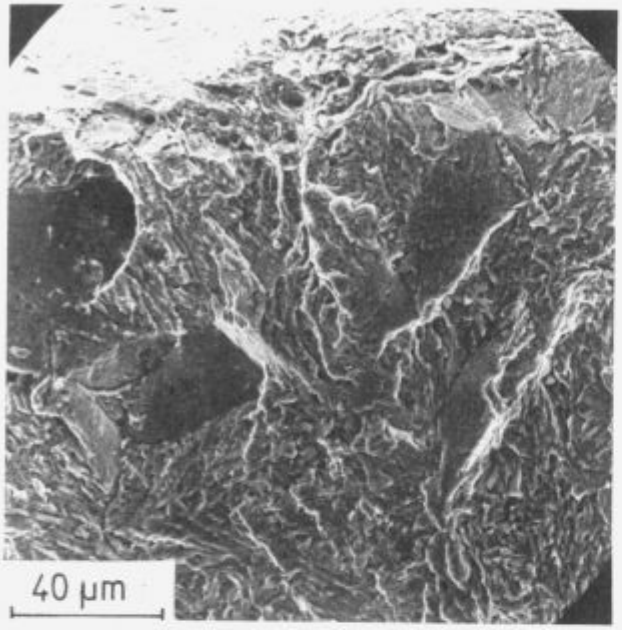

Figure 8: Surface of one of the cracks in fig. 13 near the bottom of the pitting.

Slika 8: Površina ene od razpok na sl. 13 ob dnu zajede.

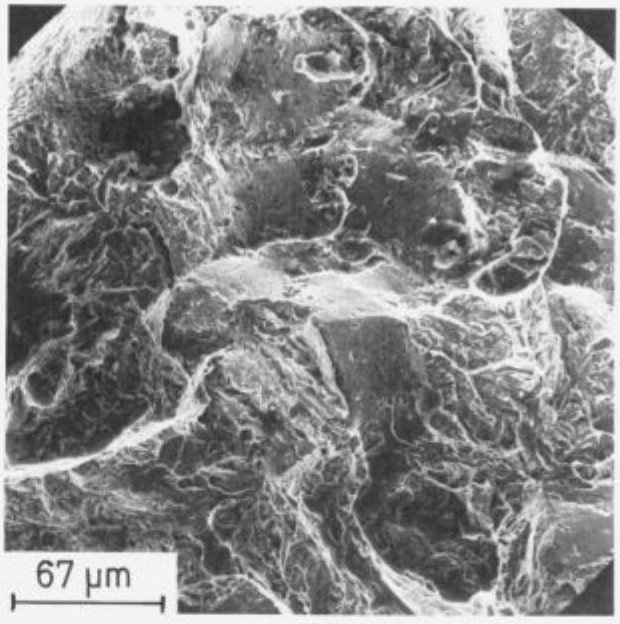

Figure 10: Surface of the crack in fig. 3 near the border line of the brutal rupture of the blade.

Slika 10: Površina razpoke na sl. 3 ob meji z nasilnim zlomom.

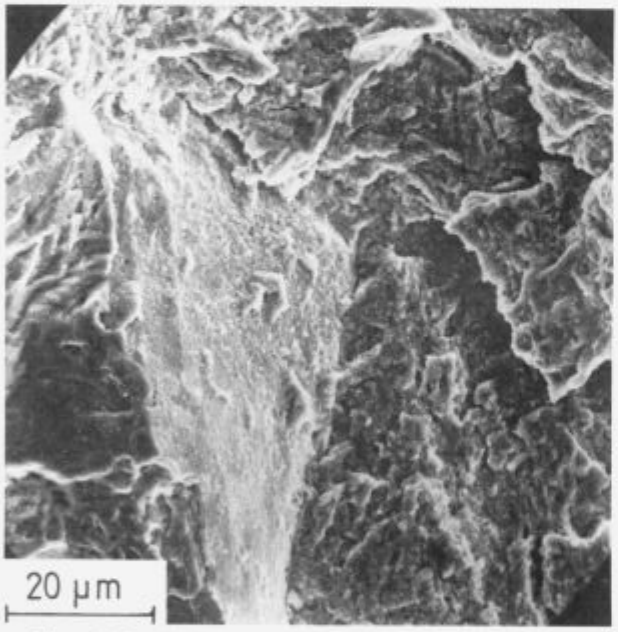

Figure 9: Detail of the crack surface without fatigue striations.

Slika 9: Detajl površine razpoke brez utrujenostnih brazd.

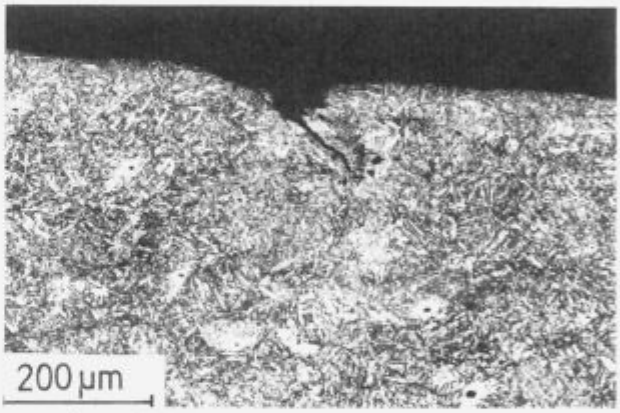

Figure 11: Pitting and microcrack in the first root grove.

Slika 11: Zajeda in mikrorazpoka v prvem žlebu korena.

Corrosion pits were the initials of all the cracks in the first grove of the root, also pitting as small as 0,05 mm **(fig. 11)**.

In all cases when the cleaning was sufficient to reveal details the surface of cracks without fatigue striations showed a micromorphology similar to that in **fig. 10**, thus brittle trans and intergranular propagation.

Fatigue striations were found on crack surface of several blades at various distance from the starting point on the surface. That shows that two mechanisms of stable propagation were active in the growth of cracks. Consequently, on cracks surface two different micromorphologies of propagation were found. Pure fatigue with striations of different width **(fig. 12)** was found only in the crack situated in the rounded passage between the root and the leaf of the blade. The propagation is transgranular and the micromorphology is independent upon the width of the striation. The main feature are striations and small edges oriented in the direction of crack propagation. It seems safe to conclude that the cause for propagation was the amplitude of fatigue stress and that large striations represent the operation of the turbine in range of critical number of revolutions. Also the width of the narrowest striation is considerable (0,01 mm) and indicates to a relatively high amplitude of dynamic stress. In the second case the crack surface showed by macroscopic observation an apparent pure fatigue propagation. By appropriate magnification is SEM a mixed micromorphology was observed **(fig. 13)**. It consisted of groups of steps and microcracks orthogonal to the direction of propagation alternated with wider bands where the surface indicates a specific mechanism of transgranular propagation. Microridges parallel to the direction of the propagation of cracks trespassed sheafs of steps and microcracks orthogonal to the

direction of propagation. The conclusion is that the crack propagated in conditions when corrosion and fatigue prevailed alternatively, thus a propagation by fatigue corrosion.

As already shown, all the findings indicate that the initials of cracking in the first grove of the root were corrosion pits, also pits as small as 0,05 mm (**fig. 11**). The steel at the top of the pits was charged with hydrogen, that decreased it fracture toughness and cracks with mixed trans and intergranular propagation were

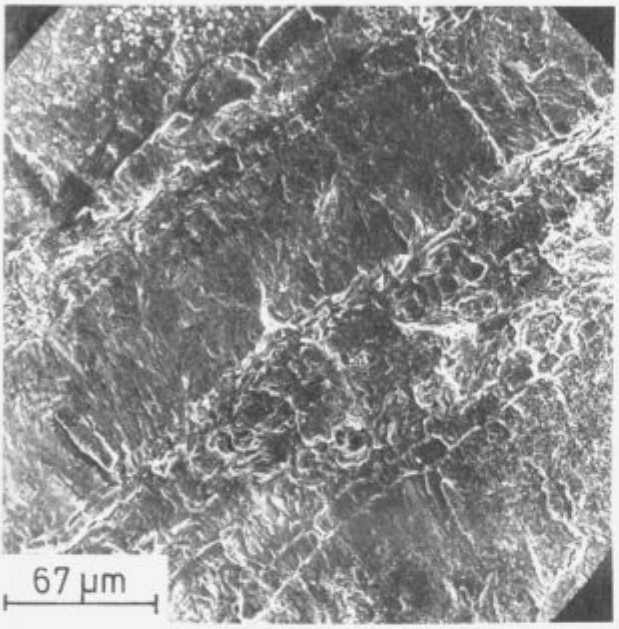

Figure 12: Surface of the fatigue crack in the rounded area of the transition from the root to leaf of the blade.

Slika 12: Površina utrujenostne razpoke na zaobljenem prehodu iz korena v list lopatice.

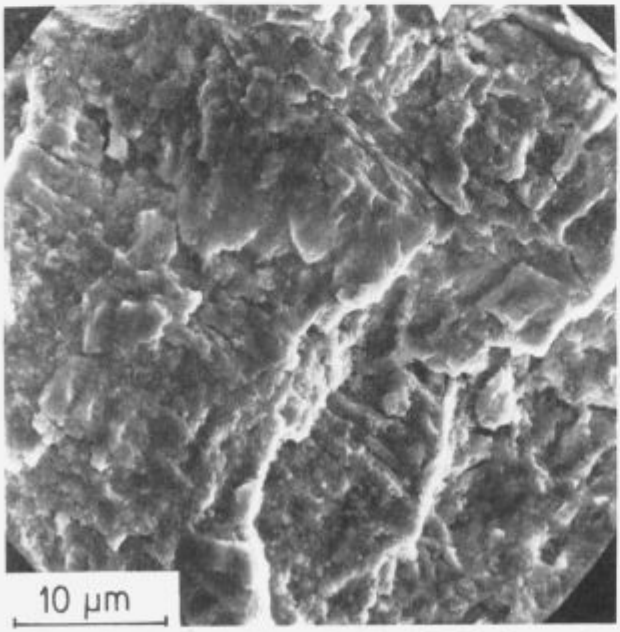

Figure 13: Microdetail of the crack surface in fig. 2 in the area of fatigue striations.

Slika 13: Mikrodetajl površine razpoke na sliki 2 na področju utrujenostnih brazd.

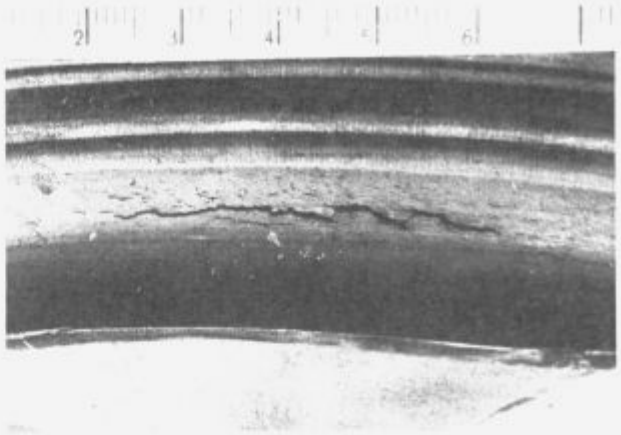

Figure 14: Step like crack on the working side in the first root grove. Blade 435.

Slika 14: Stopničasta razpoka na delovni površini v prvem korenskem žlebu. Lopatica 435.

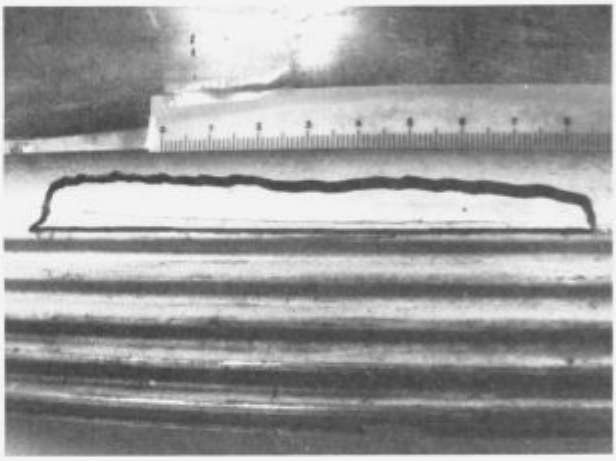

Figure 15: Straight crack on the working side in the first root grove of blade 411.

Slika 15: Ravna razpoka na delovni strani v prvem korenskem žlebu lopatice 411.

initiated because of static or dynamic stresses. The initiation took place either on several points and single microcracks coalesced in a steplike macrocrack (**fig. 14**) or in one point and the microcrack did grow in a harline slightly curved macrocrack (**fig. 15**). If the corrosion process was continued, the crack continued to propagate by the same mechanism and a crack surface without striations was obtained. If the intensity of corrosion was diminished or the corrosion was stopped, the propagation continued by sufficient stress amplitude in conditions of pure fatigue.

In **ref. 1** it is reported that the enrichment of impurities in the first drops of condensate could reach several orders of magnitude. The presence of pittings in the first grove of the root shows that the first drops of contaminated condensate appeared in this area of the blade, where the static and dynamic stress made them particularly harmful. The presence of pittings demonstrates naturally also a poor quality of boiler water, at least in some periods of the work of the power station.

2.2. Brutal fracture

This type of fracture was obtained in three different ways:
– in service,

– on laboratory specimens and
– by bending of cracked blades in laboratory.

Brutal in service fracture was observed on blades 379, 434, 442 and 447. **Fig. 16** shows the micromorphology of the fracture in area I on blade 379 fractured without precrack and shown in **fig. 5**. The micromorphology shows a quasi ductile propagation under shearing stress with very rare intercrystalline details. In area II of the same blade the micromorphology is identical. In area III, where the propagation occurred in conditions of plane strain (1), the micromorphology is brittle, mixed trans and intergranular **(fig. 17)**. Virtually identical was the micromorphology of the fracture of blade 434, which failed in service probably at the same time and in similar stress conditions. Also the micromorphology of the brutal fracture of blades 442 **(fig. 4)** and 447, two blades broken in service or during the break down and precracked in the first grove of the root is similar as that in area III of blade 379.

On notch toughness specimens the more intercrystalline brittle propagation was found the lower was the value of notch toughness. By a level of 70 J and more the propagation was ductile **(fig. 18)** with mostly small dimples, which indicate that only a thin layer of metal both sides of the crack lips was deformed

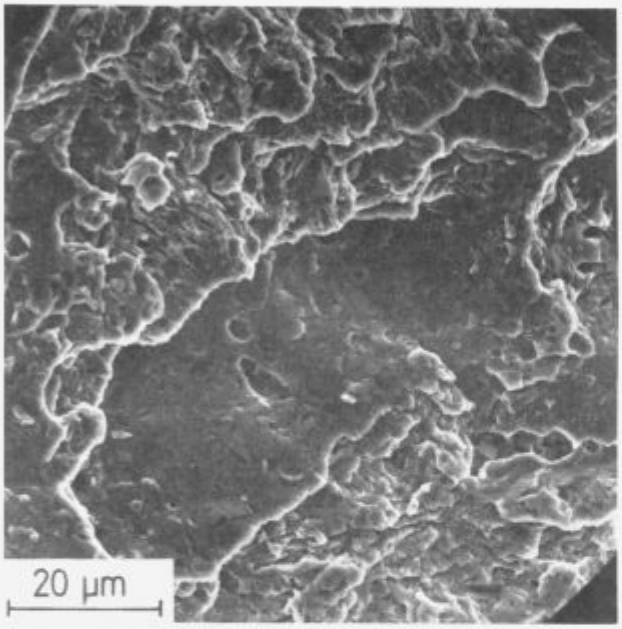

Figure 16: Microdetail of the rupture surface of the blade on fig. 5 in area I.

Slika 16: Mikrodetajl površine preloma lopatice na sl. 5 v področju I.

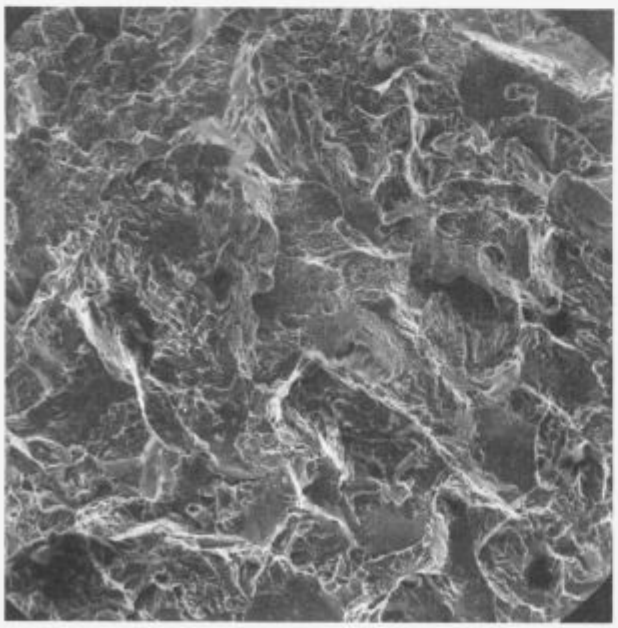

Figure 17: Microdetail of the rupture surface of the blade on fig. 5 in area III.

Slika 17: Mikrodetajl površine preloma lopatice na sl. 5 v področju III.

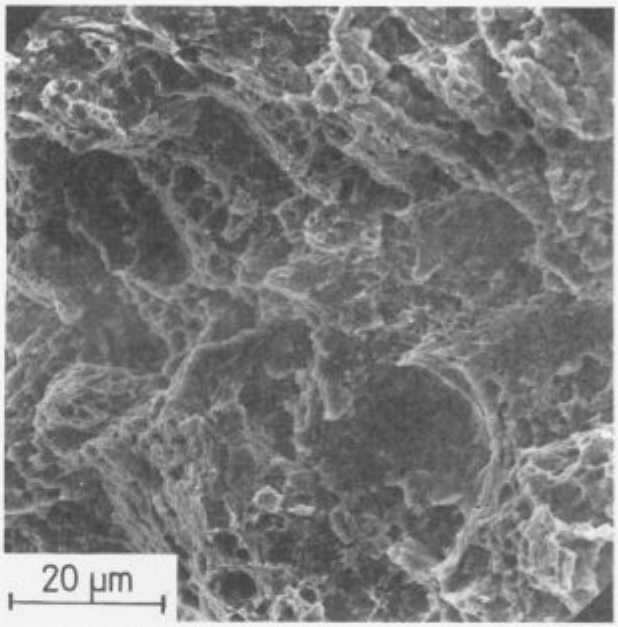

Figure 18: Fracture surface by a notch toughness of 110 J.

Slika 18: Prelomna površina pri zarezni žilavosti 110 J.

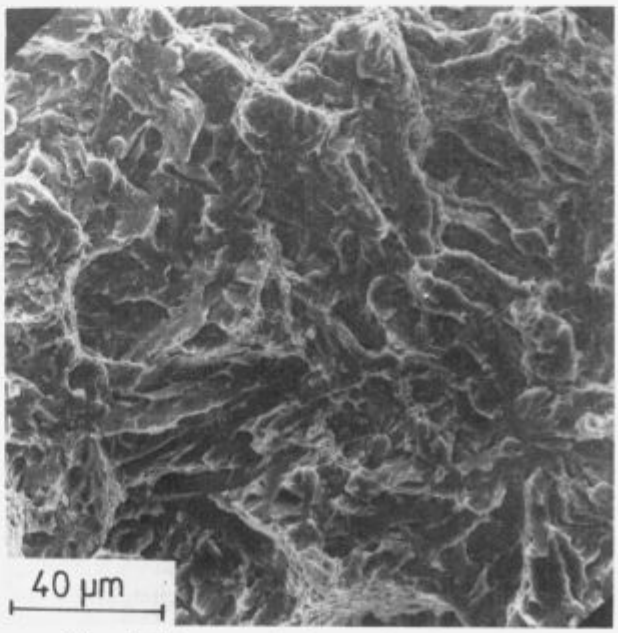

Figure 19: Fracture surface by a notch toughness of 52 J.

Slika 19: Prelomna površina pri zarezni žilavosti 52 J.

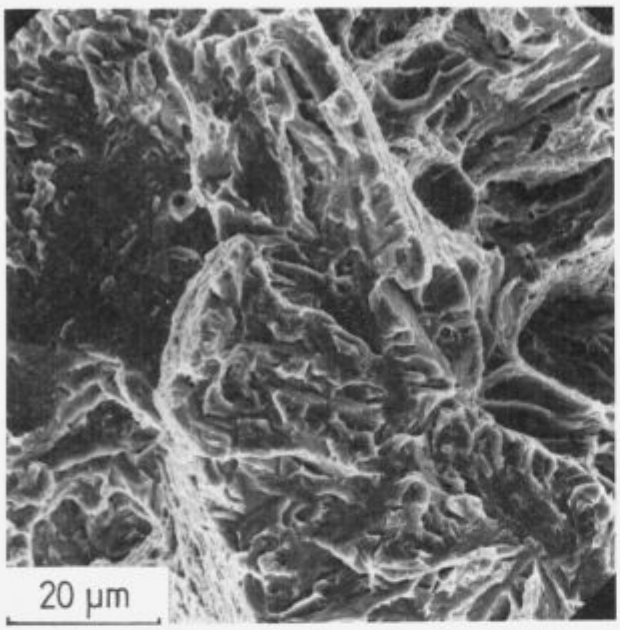

Figure 20: Fracture surface by a notch toughness of 35 J.
Slika 20: Prelomna površina pri zarezni žilavosti 35 J.

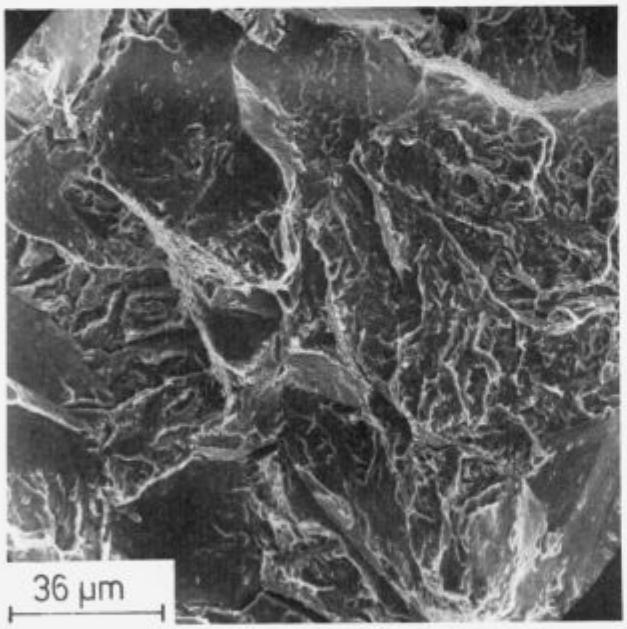

Figure 21: Fracture surface by a notch toughness of 22 J.
Slika 21: Prelomna površina pri zarezni žilavosti 22 J.

during the formation of the voids. Below a toughness of 60 J the surface shows a quasi brittle propagation with frequent areas of propagation through martensite platelets lying in the plane of the fracture and rare ductile details **(fig. 19)**. By a notch toughness of 34 J in a similar transcrystalline matrix intergranular facets are found **(fig. 20)** and by a notch toughness of 24 J the intergranular brittle propagation predominated **(fig. 21)**. It seems thus that the diminution of toughness below a level of appr. 35 J is connected to an increasing part of intergranular brittle crack propagation. The micromorphology of fracture toughness and of notch toughness specimens of the same steel was virtually identical.

3. Contamination of crack surface and mechanism of stable crack propagation

On some of the cracked blades broken by bending in laboratory small relatively clean areas of crack surface were obtained. On two such surfaces, one with and the second without fatigue striations the presence of some elements was determined with surface scanning in a SEM equipped with two wavelength dispersive spectrometers. Because of the uneven surface no quantitative analysis was possible, therefore the results given in **table 1** have only a comparative value. It seems logical to conclude that all the analysed elements were present on the crack surface as compounds, since all of them could not reach the crack surface as pure elements. It is assumed also, considering the traces of corrosion on the surface of the blades, that sulphur and chlorine are present in form of sulphate rsp. chloride which in water solution strongly increase the corrosivity of the droplets in the first area of steam condensation (2, 3, 4). The very great difference in the level of contamination offers a logical support for the following explanation of the difference in the process of stable crack propagation and the resulting difference in the morphology of the surface of cracks.

Table 1: Results of the analysis of crack surfaces.
Tabela 1: Rezultati analize površine prelomov.

Blade No.	Mode of crack propagation	Element, mg/cm²					
		Cl	Na	Ca	Si	S	Cl+S
435	without fat. str.	47.7	48.4	55.6	112	50.2	97.9
436	with fat. str.	1.6	0.17	5.2	12.4	0.19	1.79

Chloride ions break the passive layer on the surface on the blade, cause a rapid local process of corrosion and pittings are formed because the cathodic area is much greater than the anodic area. On the bottom of the pittings the condition for the initiation of cracks are present: an aggressive solution, small active tip, great passive lateral surface as well as brittle steel charged in hydrogen produced at the tip by the corrosion process through the following electrochemical reactions: $M \rightarrow M^{+} = e$, and

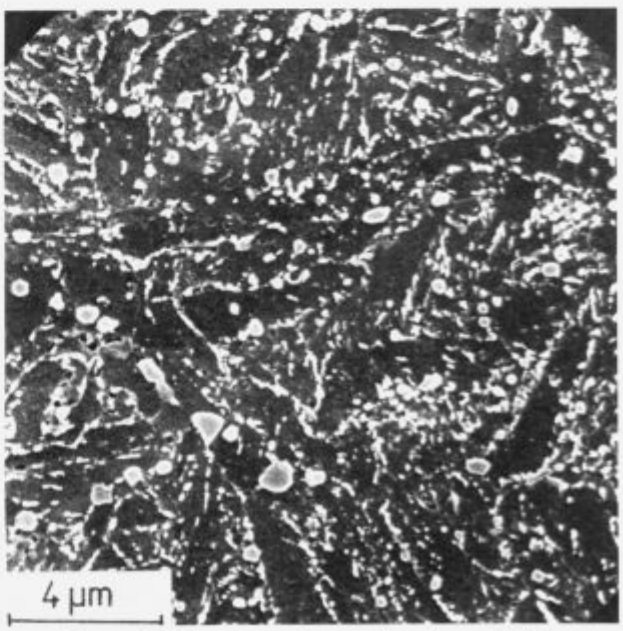

Figure 22: Microstructure by a notch toughness of 110 J.
Slika 22: Mikrostruktura pri zarezni žilavosti 110 J.

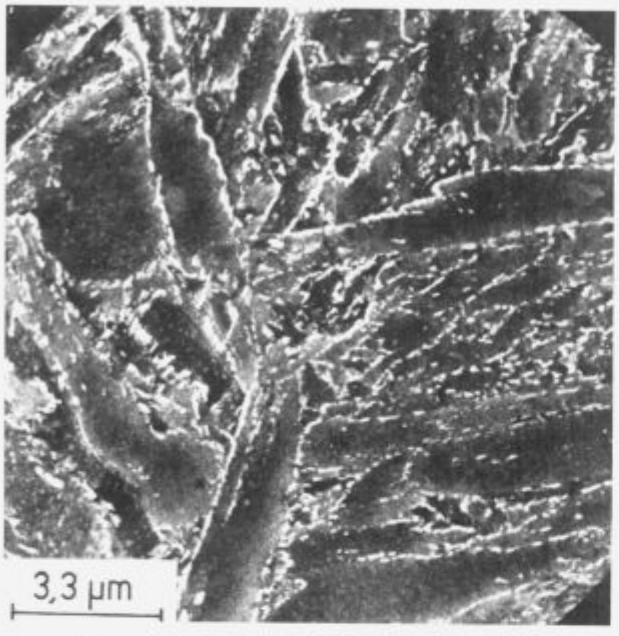

Figure 23: Microstructure by a notch toughness of 35 J.
Slika 23: Mikrostruktura pri zarezni žilavosti 35 J.

$M^+Cl^- + H_2O = MOH + Cl^- + H^+$. Metal chloride produces through hydrolysis metal hydroxide as deposit on the crack surface and ions of hydrogen and chloride. The formation of acid in the pitts lowers the pH value, produces hydrogen ions which promote the hydrogen induced stress cracking (HISC). In references 2, 3 and 4 the brittle cracking of martensitic stainless steel in the presence of a corrosion process which generates hydrogen ions in cathodic areas is confirmed. Typical features of this type of cracking are non branched cracks, which were found in all the blades cracked in the first grove of the root, while in case of stress corrosion cracking the cracks are branched. Hydrogen in interstitial solution segregates to areas of tensile stress concentration, lowers the ductility and the fracture toughness of the steel and causes a mixed trans and intergranular brittle fracture.

4. Microstructure and notch toughness

The examination in optical microscope did not show significant differences in microstructure of the steel, while the observation in SEM was more instructive. In all cases the microstructure consisted of tempered mostly acicular martensite. By observation in SEM it was possibly to connect partly the microstructure, especially the size and distribution of tempered carbide particles, to the notch toughness. By high notch toughness the carbide particles are coarse and the habitus of martensite poorly marked **(fig. 22)**. By intermediate toughness level the particles of carbide are smaller, frequently aligned along grain boundaries and along martensite platetels, and the habitus of martensite is well marked **(fig. 23)**. By a very low notch toughness of 20 J the microstructure is similar. A careful evaluation indicates that the difference in notch toughness and the increasing part of intergranular fracture can not be explained only in terms of microstructure. The tempering temperature required for a high limit of elasticity for this type of steel is in the range of reversible intergranular segregation of some elements, especially phosphorus (5). It seems thus that the intergranular fracture by low toughness is partly due also to the brittleness produced by intergranular segregation. This conclusion is confirmed by the fact that frequently intergranular facets are perfectly smooth **(fig. 21)**, thus typical for intergranular brittleness produced by reversible intergranular segregation (5).

Conclusions

In the paper the results of the investigation of the cracks and fractures surface of turbine blades are presented.

On the base of the cracks macro and micromorphology three mechanisms of stable crack propagation were established:
– mixed inter and transgranular propagation by HISC and
– transgranular propagation by corrosion fatigue, and
– transgranular propagation by fatigue.

In the first two cases cracks started on corrosion pits as small as 0,05 mm. Brutal fracture in turbine and in laboratory occurred by mixed brittle trans and intergranular propagation. On the initial part of the in turbine rupture of the blades without crack the fracture was ductile, in the second area the propagation was brittle trans- and intergranular while the fracture of precracked blades was completely brittle. The lowering of the notch toughness of the steel below appr. 35 J is characterised by an increasing part of intergranular fracture with a smooth surface suggesting that the steel brittleness was connected to the microstructure as well as to an intergranular segregation of phosphorus.

References

[1] M. Bodmer: *Brown-Boveri Mitt.* 6, 1977, 343-351.

[2] J. Bohnstedt, P. H. Effertz, P. Forchammer, L. Hagn: *Der Maschinenschaden* 51, 1987, 73-79.

[3] F. Gelhaus: "SCC in Steam Turbine Materials" in *Metals Handbook*, Volume 13, Corrosion, p. 952-959.

[4] O. Jonas: Corrosion of Steam Turbines in *Metals Handbook*, Volume 13, Corrosion, p. 993-1001.

[5] H. Erhart, H. J. Grabke: *Železarski zbornik* 15, 1981, 149.

INŠTITUT ZA KOVINSKE MATERIALE IN TEHNOLOGIJE, LJUBLJANA
KEMIJSKI INŠTITUT, LJUBLJANA
INŠTITUT JOŽEF STEFAN, LJUBLJANA
SLOVENSKO DRUŠTVO ZA MATERIALE
SLOVENSKO KEMIJSKO DRUŠTVO – SEKCIJA ZA POLIMERE IN KERAMIKO
DRUŠTVO ZA VAKUUMSKO TEHNIKO SLOVENIJE

organizirajo

3. SLOVENSKO KONFERENCO O MATERIALIH IN TEHNOLOGIJAH

4.–6. oktober 1995, Portorož

in vabijo

strokovnjake iz industrije, inštitutov in univerz, ki delajo na teh področjih k aktivnemu sodelovanju. Konferenca je namenjena predstavitvi temeljnih in aplikativnih raziskovalnih ter razvojnih dosežkov s področja tehnologije in uporabe materialov.

Obravnavana bodo naslednja področja:

– sinteza sodobnih kovinskih, polimernih, keramičnih in kompozitnih materialov
– razvoj modernih tehnologij proizvodnje materialov
– matematično modeliranje in računalniška simulacija procesov in tehnologij
– degradacija gradiv
– sodobne termične obdelave
– karakterizacija materialov
– vakuumska tehnika in tehnologije
– tanke plasti in površine
– tribologija
– varstvo okolja

V tehnični sekciji bodo lahko razstavljalci predstavili najnovejše proizvode in opremo.

V okviru konference bomo organizirali razstavo, na kateri se bodo predstavila slovenska in tuja podjetja, proizvajalci in uporabniki materialov, gradiv in opreme.

Delovna jezika konference sta slovenski in angleški jezik.

Vabimo vas k aktivnemu sodelovanju na področjih znanstvenega programa konference.
Program bo obsegal vabljena predavanja, govorne prispevke mladih raziskovalcev in postrske prispevke.

Zadnji rok za oddajo abstraktov je 15. maj 1995.

Dela, uvrščena v program konference, bodo natisnjena v prvi številki znanstvene revije Kovine, zlitine, tehnologije v letu 1996.

Dodatne informacije: tajništvo IMT Ljubljana, telefon: (061) 125 11 61, fax: (061) 21 37 80

Kovine, zlitine, tehnologije / letnik 28 / 1994 / številka 4 / strani 579 do 582

The Role of Contact Friction and Rheology in the Deformation at Plastometric Tests of Rheologically Complex Materials

Vpliv kontaktnega trenja in reologije pri plastometričnih preizkusih reološko kompleksnih materialov

G. G. Shlomchack*, Dnepropetrovsk Metallurgical Institute, Ukraine
I. Mamužič, Metalurški fakultet, Sisak, Croatia
F. Vodopivec, Institute of metals and technologies, Ljubljana, Slovenia

The deformation anomalies of higher orders at plastometric test are studied on easily deformable lead alloys-models of different rheological complexity by original testing methods. It is ascertained that the development of deformation anomalies depends upon the degree of rheological complexity of the material. Simple strain anomalies are due to the inadequate conditions of contact friction, while those of the higher orders results mainly from microrelief of the sample butts. Recommendations for the obtention of homogeneity of deformation at plastometric tests are given. The tests show that the deformation of rheologically complex metals develops according to laws basically different of the contemporary notions of the mechanics of plastic deformation.
Key words: plastic deformation, rheology, deformation anomalies, contact friction, homogeneous deformation

Opredeljene so deformacijske anomalije višjega reda pri plastometričnih preizkusih svinčevih spojin z različno reološko kompleksnostjo. Razvoj anomalij je odvisen od reologije materiala. Enostavne anomalije so posledica neustreznega stičnega trenja, anomalije višjega reda pa so predvsem odvisne od mikroreliefa stične površine. Priporočeni so ukrepi za doseganje homogene deformacije pri plastometričnih preizkusih. Ti kažejo, da deformacija reološko kompleksnih materialov poteka po zakonih, ki se razlikujejo od sodobnega razumevanja mehanizma plastične deformacije.
Ključne besede: plastična deformacija, reologija, deformacijske anomalije, kontaktno trenje, homogena deformacija.

1. Introduction

The development of new technologies of pressure shaping depends on the knowledge of rheological properties of the plastically deformed material. The dependence between the resistance to deformation σ and the deformation rate ϵ at different strain rates σ and temperatures T is a family of curves σ-ϵ, it is specific for each steel and alloy and it is a rheological passport of the material. The most reliable are rheological curves obtained by compression tests on cam plastometer **(fig. 1)** at constant strain rates (1). The condition σ = const is ensured by the cam profile which is given by the logarithmic law

$$\frac{h_0}{h_0 - \Delta h} = \exp\left(\frac{\varepsilon}{v} \cdot x\right),$$

with h_0 – initial height of the cylindrical specimen 4;
Δh – absolute cogging of the specimen all over its height;
v – circumferential speed of the drum 1;
x – length of the cam profiled part 2.

The ensurance of the specimen deformation homogeneity (2), thus the elimination of barrel formation, twisting, shift, bending and other deformation anomalies is the basic requirement in plastometric tests.

It is generally accepted that contact friction forces only influence the deformation of the specimen during its plastic compression. The present investigations refute this point of view and show experimentally that the development of deformation anomalies depends to a great extent upon the rheological complexity of the deformed metal.

2. Rheology of the investigated material

Non-strengthenable materials of the first rheological class and monotonously strengthenable materials of the second rheological class are regarded as rheological simple (3). Rheological complex materials differ from them by presence of extrema on the σ-ϵ curves.

In this work steels and alloys with one maximum on σ-ϵ curves are examined which belong to the most widespead third rheological class (4) of metallic materials with the characteris-

* Dr. sc. Georg GEORGIJEVIČ SHLOMCHACK, Dnepropetrovsk Metallurgical Institute, Ukraine

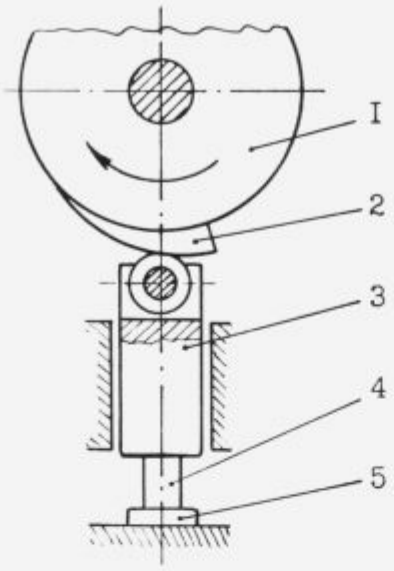

Figure 1: Scheme of cam plastometer: 1 - drum; 2 - profiled cam; 3 - plunger; 4 - specimen; 5 - force-measuring element.

Slika 1: Shema tlačnega (cam) plastometra: 1 - valj, 2 - profiliran nastavek, 3 - bat, 4 - preizkušanec, 5 - merilnik sile.

tic deformation σ_s at the maximum of resistance to deformation σ_{max} (5). The smaller is the value σ_s within the limits of the rheological class, the higher is the degree of the material rheological complexity. In **fig. 2** rheological curves of carbon steel (a) with a characteristic degree of deformation σ_s = 0.4...0.6 (6), high-speed alloy steel (B) with σ_s = 0.3...0.4 (7), and as unique for it degree of rheological complexity (C) a zirconium alloy (8) are shown. The characteristic degree of deformation of the cirkonium 2.5% Nb alloy is only σ_s = 0.03...0.05 and its rheological curves could be better qualified as "curves of unstrengthening" than as "curves of strengthening". The deformation of such materials occurs according to laws which are different in principle of the modern conception of the mechanics of material plastic deformation. The close study of the development of deformation anomalies of higher order (4) of rheologically complex materials would probably promote the development of the theory and technology of metal pressure shaping.

Easily deformed lead alloys-models of different rheological complexity were developed for the modelling new processes of metal pressure shaping at the Ukrainian Metallurgical Academy. **Fig. 3** shows some σ-ϵ curves for a technically pure lead (99.98% Pb, curve A) and alloys with 99.9% Pb (curve B), 99.4% Pb (curve C) and 99.0% Pb (curve D) obtained by cam plastometric tests in compression at the temperature of 15°C and strain rate σ=0.3 s^{-1}. If pure lead is qualified as a second order rheological monotonously strengthenable material ("A") then, depending on the content of additions, the alloys have a maximum on curves σ-ϵ, which shifts to a smaller deformation degree, from σ_{sb} = 0.63 to σ_{sd} = 0.23, which complicates their rheology.

It should be noted that earlier the rheological (but not deformational) complexity of lead was observed either at high temperatures (9) or by static loading (10) what made it unsuitable for the use in physical quantitative modelling of the pressure shaping processes based on the similarity theory.

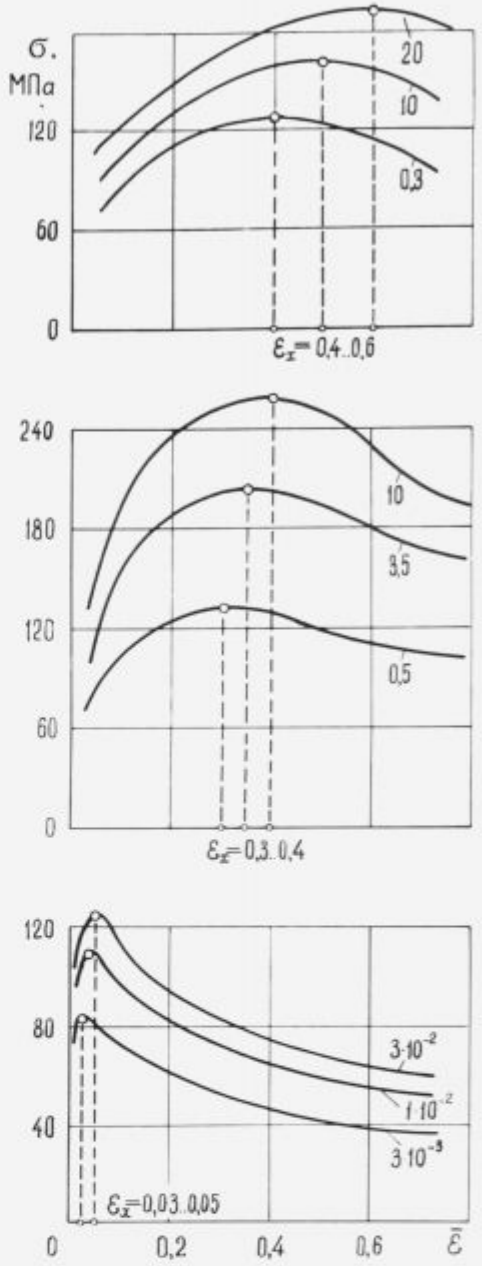

Figure 2: s-s curves of different rheological complexity: a - steel with 0.19% C; 0.04% Si; 0.86% Mn; 0.022% P; 0.029% S at 900°C (6); b - high speed steel with 0.88% C; 0.39% Si; 0.23% Mn; 0.03% P; 0.011% S; 3.3% Cr; 6.39% W; 4.72% Mo; 2.23% V at 1100°C (7); c - zirconium alloy with 2.5% niobium at 775°C. (8) all at the indicated values of strain rate in s-1.

Slika 2: s-s krivulje z različno stopnjo reološke kompleksnosti: a - jeklo z 0,19% C; 0,04% Si; 0,86% Mn; 0,022% P in 0,029% S pri 900°C (6); b - hitrorezno jeklo z 0,88% C; 0,39% Si; 0,23% Mn; 0,03% P; 0,011% S; 3,3% Cr; 6,39% W; 4,72% Mo in 2,23% V pri 1100°C (7); c - cirkonijeva zlitina z 2,5% Nb pri 775°C. (8) vse pri označeni deformacijski hitrosti v s-1.

3. Specimens and methods of testing

After vacuum melting and chemical checking the ingots of lead alloys of 50 mm diameter and 10 mm high were pressed into rods of diameter of 5.9 mm and cut into initial blanks of 11.5...11.8 mm of lentgh. In **fig. 4** press mould details used for the calibration of specimens and the simultaneous indentation of a regular microrelief on their butts in form of concentrical trian-

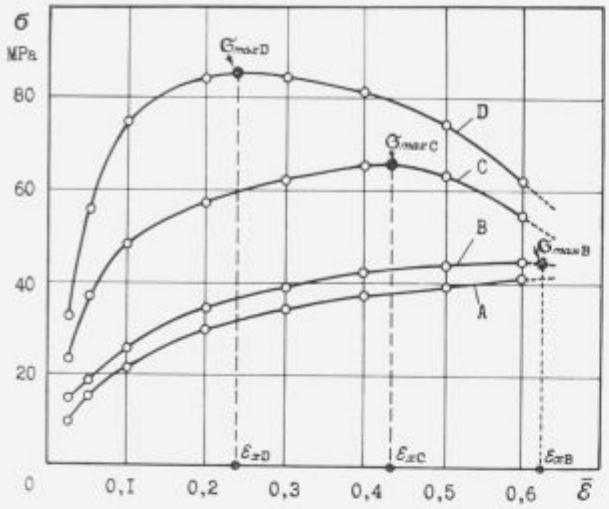

Figure 3: Rheological curves of technically pure lead S1 (99.98% Pb, "A" curve) and alloys of 99.9% ("B" curve), 99.4% ("C" curve) and 99.0% lead ("D" curve).

Slika 3: Reološka krivulja za tehnično čisti svinec S1 (99.98% krivulja A) in zlitine z 99.9% (krivulja B), 99.4% (krivulja C) in 99.0% svinca (krivulja D).

gular juts 0.3 mm high by the plungers 2 and 4 are shown. The final dimensions of the specimen were: diameter - 6.0 mm and height - 11.0 mm. Before the plastometric tests the specimens were annealed at 100°C during an hour and then aged during thirty days at room temperature.

Fig. 5 shows the container for the compression tests of cylindrical specimens. The initial adjustment of the specimen 3 and the plungers 1 and 4 in the container 2 is obtained by means of a simple centring device. Polished working surfaces of plungers and profiled butts of the specimens are covered with layers of viscous lubricant Litol 42 and separated by thin rubber, polyethylene or polyurethane foils. The number of layers of lubricant ensuring the homogeneity of deformation was determined experimentally. If in the process of compression the specimen becomes

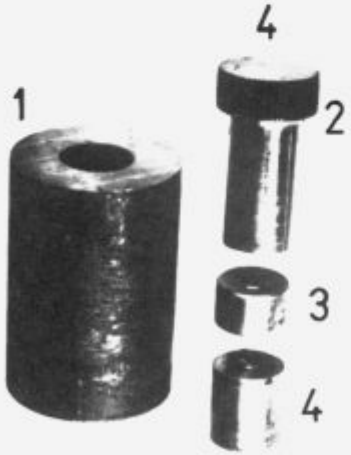

Figure 4: Press mould for pressing and calibration of specimens for plastometric tests: 1 - body; 2 - upper die; 3 - calibrating matrix; 4 - lower die.

Slika 4: Orodje za stiskanje in kalibriranje preizkušancev za plastometrične preizkuse: 1 - ohišje, 2 - zgornja matrica, 3 - kalibracijska matrica, 4 - spodnja matrica.

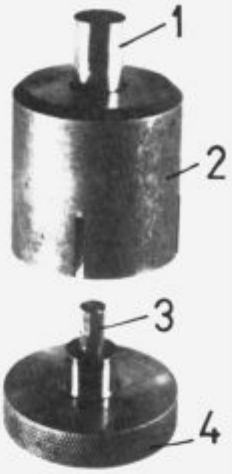

Figure 5: Container for plastometric tests by compression: 1 - upper die; 2 - body; 3 - specimen; 4 - lower die.

Slika 5: Container za plastometrične tlačne preizkuse: 1 - zgornja matrica, 2 - ohišje, 3 - preizkušanec, 4 - spodnja matrica.

barrel-shaped, the number of layers is increased, if it becomes concave then their number is diminished.

4. The influence of contact friction on the growth of deformation

In case when the radial displacement of metal on the working surface of the plungers is hampered, the butts of the specimens are formed with the contact of it lateral surface and the plunger. **Fig. 6b** shows a pressed pure lead specimen covered with chalk on the initial contact area. The light circle on the butt is the unstrained initial surface, dark circle is a part of the contact area lifted from the lateral surface of the specimen. Also the initial form and the shape after a true homogeneous deformation of the specimen during plastometric tests as a result of the proper lubrication of the contact area are shown in **fig. 6**.

In **fig. 7** specimens of pure lead after sagging at plastometer with strain rate $\sigma = 0.3\ s^{-1}$ by identical parameters, but different conditions of friction on the contact are shown.The specimen 2 was pressed with dry contact surfaces, and a barrel shape was obtained. The specimen 3 was deformed homogeneously as a result of the optimal selection of the lubricant. The concave shape of the specimen 4 which was obtained by increasing the number of layers of lubricant to three with two intermediate rubber separators. In this case the friction force vector changed to the opposite sign and the friction became active in promoting the strong radial displacement of metal adjacent to the contact and the concave lateral surface of the specimen was obtained.

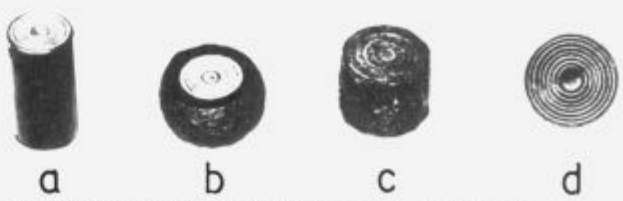

Figure 6: Heterogeneous (b) and homogeneous (c) deformation of pure lead samples S1 (a - initial form of the sample, d - butt relief of the sample).

Slika 6: Heterogena (b) in homogena (c) deformacija preizkušancev iz čistega svinca S1 (a - začetna oblika preizkušanca, d - relief na osnovni ploskvi valjastega preizkušanca).

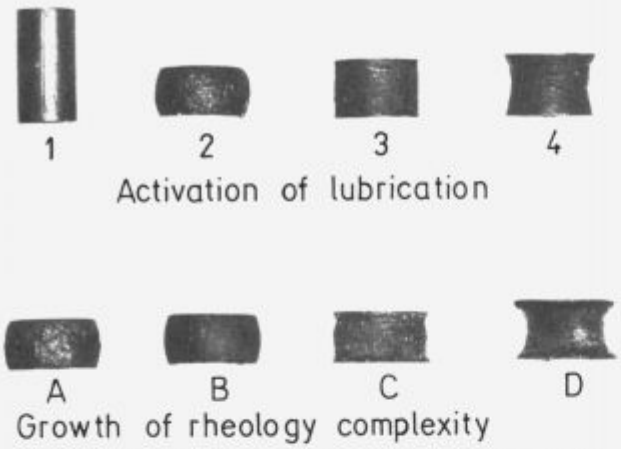

Figure 7: Strain development in pure lead samples by increase of lubrication of butts (2-4) and lead alloys specimens from fig. 3 by different degree of rheological complexity (A-D).

Slika 7: Razvoj deformacije v preizkušancih iz čistega svinca pri povečanem % mazanju stičnih ploskev (2-4) in preizkušancev iz svinčevih zlitin s slike 3 pri različnih stopnjah reološke kompleksnosti (A-D).

Evidently, by plastometric tests of rheologically simple materials the significance of lubricant is very substantial. With modification of the conditions of friction on the contact surfaces it is possible to regulate the development of deformation and achieve its homogeneity.

5. The role of metal rheological complexity in development of deformation

Let us now present some results of plastometric tests of rheologically complex alloys at the same conditions (ϵ=0.6; σ=0.3 s^{-1}) without lubrication.

Fig. 7 (A-D) shows samples of the tested alloys by order of rheological complexity: A - pure lead, B - "B" alloy, C - "C" alloy, D - "D" alloy. As in the previous series of tests the specimen of pure lead (A) is barrel-shaped. The shape of the specimen of alloy "B" with a maximum (σ_{max}) on the rheological curve at σ_s = 0.63 (see **fig. 3**) is also barrel shaped. Since only a deformation below σ = 0.63 was achieved the rheological complexity of the alloy did not come to evidence and the specimen was deformed according to the simple strengthenable material of the second class. The specimen of "D" alloy inspite of the sagging without lubrication assumed a quite different shape, a strongly marked concavity of the lateral surface. The rheological curve of the alloy "D" (third rheological class in **fig. 3**) shows that if the deformation is increased above the characteristic value, the resistance to deformation is decreased sharply from σ_{max} = 95 MPa at σ_s=0.23 to 60 MPa at ϵ = 0.6. Simple calculations show that before the deformation has embraced all the specimen volume the triangular juts of it butts did deform to the extent of ϵ = 0.4...0.6. This started a deformation with strengthening of the metal in the bulk volume of specimen and unstrengthening of metal in layers adjacent to the contact. The resistance to deformation of these layers in the very initial stage is smaller and they flow in radial direction with higher speed than the inner layers forming the specimen with concave lateral surface. It should be noted, that in spite of the small depth of the butt relief (0.3 mm) the volume of this unstrengthenable metal is sufficient to initiate the deformation of metal more distant from the contact.

The deformation anomalies in the process of sagging of the alloy "C" (**fig. 7C**) is of special interest. The characteristic degree of deformation of the alloy "C" is achieved by σ_s = 0.43. Up to this moment the adjacent to contact volumes of metal, on account of the greater deformation of the butt microrelief, are strengthened more intensively than those in the depth and the sample becomes barrel-shaped. By further sagging the deformation of metal layers adjacent to the contact above σ_s start to unstrengthen and in the last stage rush intensively in radial direction outstripping the layers in the depth. The specimen acquires a specific shape: concavity near the contact with the tool and barrel-shaping during the final stage of the process. It is concluded, therefore, that the deformation homogeneity must be achieved during all the test.

It is possible to eliminate deformation anomalies of higher orders at plastometric tests of rheological complex alloys by means of greater friction on the contact specimen-tool with the deposition of chalk. Also it can be achieved by selecting the proper specimen butts asperity.

Conclusions

1. The development of deformation anomalies at plastometric tests depends substantially on the degree of metal rheological complexity. Deformation anomalies are caused by inadequate conditions of contact friction while deformation anomalies of higher orders result from the primary deformation of specimen microrelief on the contact with the tool.
2. The homogeneity of deformation at plastometric tests of rheologically complex metals can be achieved by the proper roughness of the specimen surfaces in contact with the tool. Friction at this place either prevents or promotes the radial displacement of the deformed metal.
3. By plastometric tests of metals and alloys it is necessary to control the deformation of the specimen during the whole process in order to reveal and eliminate intermediate deformation anomalies.

References

[1] Poluhin P. I., Gun G. Ya, Galkin A. M., Resistance to plastic deformation of metals and alloys, *M. Metallurgia*, 1983, 352.

[2] Trefilov V. Y., Moiseyev V. F., Pechkovsky E. P., Gornaya M. D., Vasiliev A. D., Strain hardening and failure of polycrystalline metals, *Naukova dumka*, Kiev, 1989, 256.

[3] Shlomchack G. G., *Deformation features of rheologically complex metals*, Deposited in UkrNIINTI 13.08.91, N 1167.-Uk91, Kiev, 11.

[4] Shlomchack G. G., Reological classes of materials. *International conference:* "Materials for Building" Works. Dnepropetrovsk, 1993, 69-70.

[5] Shwartsbart Y. S., Resistance to deformation of steels and alloys at continuous hot rolling, *Izvestia AS USSR, "Metals"*, 1980, 1, 87-91.

[6] Suzuki H., *Report of Unst. of Industrial Science the University of Tokyo*, 18, 1968, 3, 139-240.

[7] Lehmann G., Tiets A., *Neue Hutte*, 24, 1979, 9, 325-327.

[8] *The Hot Deformation of Austenite* (edited by J. B. Ballance) AIME New-York: 1977, 631.

[9] Bailey I., Singer A., *J. of Inst. of metals*, 92, 1963-64, 5, 288-289; 12, 404-408.

[10] Thomson E., Young C., Koboyashy, *Sc. Mechanics of plastic deformation at metal working*, Transl. from English, M., Mashinostroenie, 1969, 504.

Kovine, zlitine, tehnologije / letnik 28 / 1994 / številka 4 / strani 583 do 587

Deformation Anomalies of Higher Order during the Plastic Extention of Rheologically Complex Materials

Deformacijske anomalije višje stopnje med plastičnim raztezanjem reološko kompleksnih materialov

G. G. Shlomchack*, Dnepropetrovsk Metallurgical Institute, Ukraine
I. Mamuzić, Metalurški fakultet, Sisak, Croatia
F. Vodopivec, Institute of metals and technologies, Ljubljana, Slovenia

New deformation anomalies of rheologically complex materials were discovered and demonstrated. It was found out that in the process of axial extention during the decrease of resistance to deformation secondary deformation heterogeneities take place alternated with deformation homogeneities due to changes in resistance to deformation.
Key words: rheology, tensile test, deformation, heterogeneities

Odkrite so bile nove deformacijske anomalije reološko kompleksnih materialov in dokazane z raztržnimi preizkusi primernih kovin. Ugotovljeno je, da pri aksialnem raztezanju med zmanjševanjem odpora proti deformaciji prihaja do sekundarnih deformacijskih heterogenosti in homogenosti zaradi sprememb v odpornosti materiala proti deformaciji.
Ključne besede: reologija, raztržni preizkus, deformacija, heterogenosti

1. Introduction

The plasticity is essential for the irreversible change of form of materials and the obtention of a finished product. The measure of plasticity is the extent of deformation energy accumulated in the material up to the failure[1] and it is generally established by testing in conditions of stress-strained state identity. The simplest of such tests is the linear tension or compression of the specimens when the concepts of deformability and plasticity are identic.

Kaibishev defines good plasticity as "high stability" against formation of the neck "at uniaxial extention of the specimen" and explains the possibility of using veritable stress-strain diagrams ∂-ϵ for the estimation of the plasticity[2]. Beside of the uniform elongation and necking the test shows some parameters of the sensitivity of the material to the strengthening rate as well as quantitative data on the plasticity. However the question remains of how to obtain better informations on the materials deformability by means of real stress-strain curves.

Modern metallophysics investigates the separate and combined influence of many factors on plasticity of metals and alloys. For example, on the basis of the analysis of extensive experimental data M. Y. Dzugutov tried to explain why the plasticity of high-alloyed steel decreases and worked out a classification of this multiform phenomenon[3].

However, the complex interrelation between various factors and their influence upon the deformation processes makes the problem of the prediction of the deformability unsolvable without special appropriate experiments. In **ref. 3** the importance of plastometric tests is pointed out, but no suggestion is proposed how to use their results for deformability forecasts.

In literature extensive informations on rheological ∂-ϵ curves obtained by plastometric tests of various metals and alloys are found[4,5]. Their analysis shows that plastically deformed materials can be devided into rheological simple with invariable or strictly increasing function ∂-ϵ and rheologically complex with extreme on ∂-ϵ curves.

Rheological anomalies are well-known and explained. Initial strain anomalies observed as necking of specimens at tensile strain are known too, but the regularities of their development are not fully explored. The influence of test rate and temperature[6], as well as that of the material structure[7] were investigated, however no attempts to study the dependence between the regularities of strain and rheological anomalies were published so far.

This problem was solved by the experimentally discovered and theoretically explained phenomenon of highest order strain anomalies during the tests of rheologically complex materials by plastic stretching.

2. Theoretical analysis

In the phenomenological analysis it is necessary to keep in mind the condition of identity of rheological curves ∂-ϵ obtained by stretching and by compression and the fact that in the integral aspect these curves hold all the information on the changes in the material during the plastic deformation.

* Dr. sc. Georg GEORGIJEVIČ SHLOMCHACK,
Dnepropetrovsk Metallurgical Institute, Ukraine

During the tensile tests of unstrengthenable material any casual reduction of specimen cross-section leads to rupture, if it is not compensated by strain hardening and the deformation in form of the necking preceding the rupture. Let's call this well known simple strain heterogeneity "simple strain anomaly".

During tensile tests of strengthenable material the deformation with decreasing cross-section is localised in one section earlier than in others which strengthen because of liquations, favourable orientation of crystallite, etc. and ceases to deform, while other sections of the specimen less strengthened are involved in the flow.

Consequently in the beginning the deformation spreads within the whole volume of the material - we observe the well-known quasi-homogeneous strain of the specimen. According to phenomenological concepts it will be called "homogeneous strain of the first order". The following formation of the neck on the specimen will be called "heterogeneous strain of the first order" or "strain anomaly of the first order".

On the base of the analysis of true ∂-ϵ diagrams and their explanation all materials are classified by the degree of their rheological complexity **(Fig. 1)**.

The first rheological class are simple unstrengthenable materials. By stretching the specimens are deformed according to simple heterogeneous strain with formation of the neck and rupture **(Fig. 1,I)**.

In the second rheological order one finds simple strengthenable materials with a strictly increasing ∂-ϵ function **(Fig. 1,II)**. A typical feature of such materials is the homogeneous strain of the first order, the formation of the neck - strain anomaly of the first order and rupture of the specimen.

The third to fifth classes are rheological complex materials. The third rheological class is charasterized by a maximum on ∂-ϵ curves. The material **(Fig. 1,III)** of this type is stretched through the stage of the first order homogeneous strain, then the neck is formed. The reason is not a lack of plasticity as in second rheological class, but the influence of other mechanisms. The diminution of the resistance to deformation is reached after a limited uniform elongation of the specimen. The process is followed by a considerable decrease of the relative elongation due to the accelerated formation of the neck, however, the value of relative necking is not decreased at the same moment. This anomaly was called "heterogeneous strain anomaly of the second order"[8].

For the fourth rheological class of materials two extreme on ∂-ϵ curve and an subsequent increase of resistance to deformation after the first one **(Fig. 1,IV)** are typical. As in the case of materials of the second class, the extention of the specimen begins with a homogeneous strain of the first order and then, in the materials of the third class, a heterogeneous strain of the second order is observed: the neck starts to form before the elongation ϵ_t is attained. Here the material reveals its remarkable property: the specimen does not fracture, but it is stretched homogeneously in the region of the already formed neck[9]. The explanation is the secondary increase of the material resistance to deformation in the neck before ϵ_t **(Fig. 1,IV)**. Outside the process is similar to the homogeneous strain of the first order, embracing only the neck region or, to be more exact, the transition zone from the neck to the main volume of the specimen. This strain anomaly is called according to the proposed terminology as "homogeneous strain of the second order". Many metals (copper, aluminium, lead, etc.) have the remarkable property to restore the plasticity in this way. The further extension of the specimen brings the formation of a localised neck on the earlier elongated neck and causes "a heterogeneous strain anomaly of the third order".

The fifth rheological class of materials is characterized by relations ∂-ϵ with three or more extrema **(Fig. 1,V)**. During the extension the specimen passes through stages of strain typical for the IV rheological class, however without rupture in the localised necks but with further strengthening and uniform elongation due to the homogeneous strain. This anomaly, is called "homogeneous strain of the third order". The following stage is the formation of a new localized neck on the elongated neck of "heterogeneous strain anomaly of the fourth order", and so on.

Multistage strain anomalies of the highest orders on materials of the fifth rheological class are not evident as it is shown schematically in **Fig. 1,V**. The reason are anomaly smooth changes between the different stages and thus the changes are found only by very careful observation.

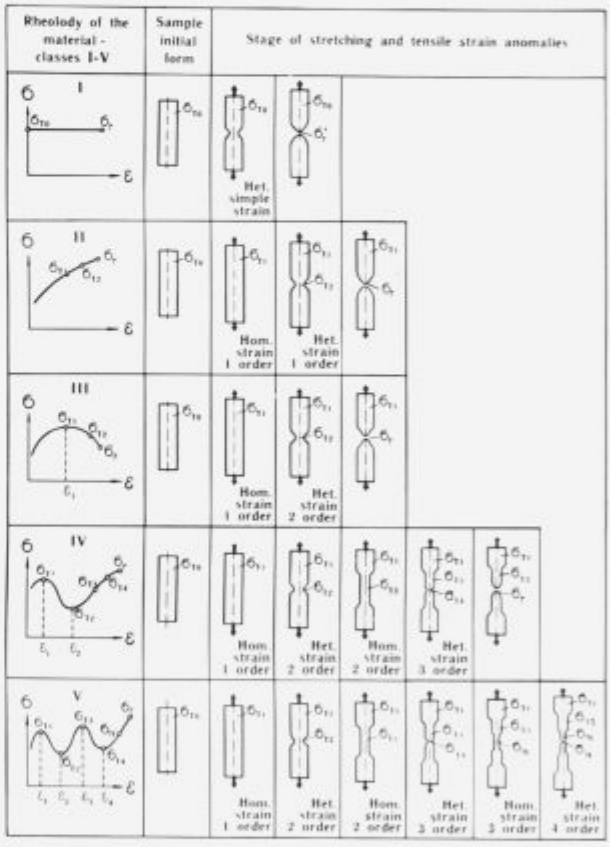

Figure 1: Tensile strain anomalies of materials with different rheology.
Slika 1: Anomalije pri natezni deformaciji materiala

Fig. 2 shows a family of rheological curves for hot-rolled annealed pure titanium (99.9%)[5] which is at 900°C typical representative of an unstrengthenable material of the first rheological class, deformable according to the simple strain heterogeneity type, while at 700°C it is a typical representant of the second rheological class. **Fig. 3a** shows rheological curves for a carbon steel (0.43% C, 0.26% Si, 0.74% Mn, 0.022% P, 0.016% S) representing a very numerous third class of rheologically complex materials. **Fig. 3c** shows ∂-ϵ curves

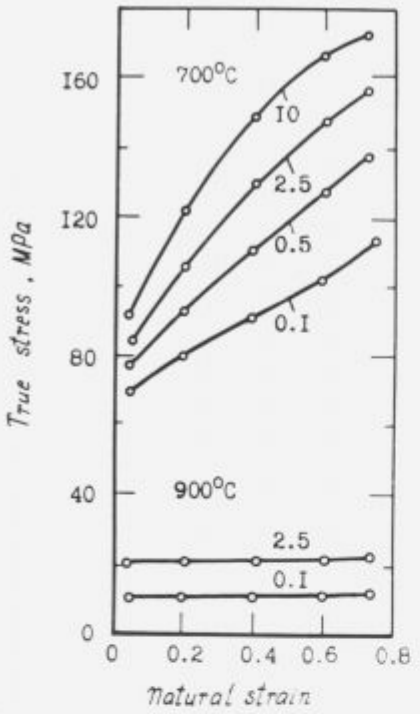

Figure 2: Rheological curves of hot-rolled and annealed Ti (99.9%).
Slika 2: Reološke krivulje toplo valjanega in žarjenega Ti (99.9%).

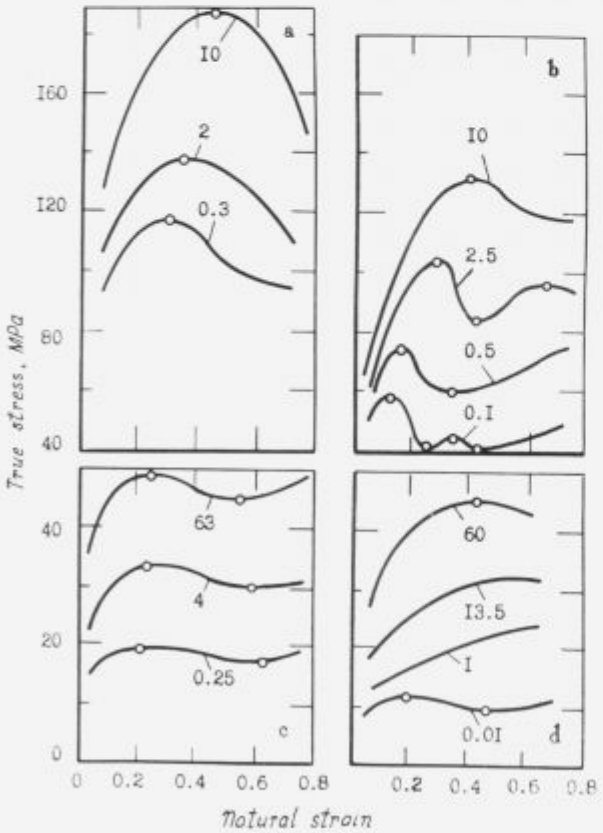

Figure 3: Rheological curves:
a - steel C 45 at 900°C;b - copper (99.99%) at 600°C;
c - aluminium (99.5%) at 480°C6; d - lead C1 (99.98%) at 20°C.
Slika 3: Reološke krivulje:
a - jeklo C 45 pri 900°C; b - baker (99.99%) pri 600°C;
c - aluminij (99.5%) pri 480°C6; d - svinec C1 (99.98%) pri 20°C.

for a technically pure aluminium (99.5%)[7] which is a rheologically complex material of the fourth class with two extrema on the ∂-ϵ curves. Copper (99.99%) is at 600°C[8] a rheologically complex materials of the fifth class with three of more extrema on ∂-ϵ curves **(Fig. 3b)**.

3. Experimental investigations

The experimental investigations of strain anomalies were performed on lead, which has the remarkable property to recrystallize at room temperature **(Fig. 4)**. Processes of its plastic deformation are similar to those during the hot deformation of steels and alloys. It is therefore exceptionally convenient for the modelling[11,12]. The rheological properties of lead are unique. **Fig. 3d** shows rheological curves of lead (99.98%) obtained on a cam plastometer at 18-20°C[13]. At strain rate $\epsilon = 0.005\ s^{-1}$ lead softens completely by recrystallization and it can be thus regarded as a rheologically simple unstrengthenable material of the first class. At the speed of $\epsilon = 0.01$ to $0.1\ s^{-1}$ it has complex relation ∂-ϵ with two extrema inherent to rheologically complex materials of the fourth class. By moderate strain rates (ϵ = 0.1 to 0.5 s^{-1}) lead is a rheologically simple strengthenable material of the second class, while at higher rates it is a rheologically complex material of the third class.

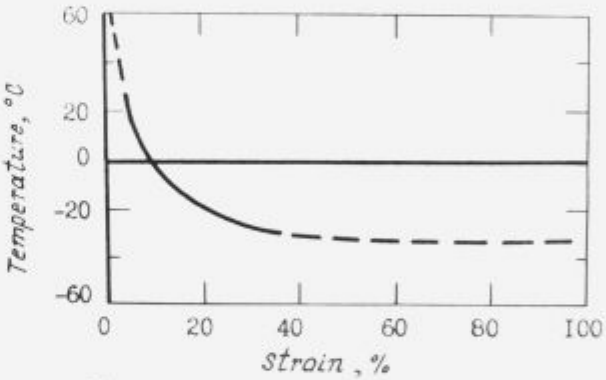

Figure 4: Recrystallization temperature of lead.
Slika 4: Temperatura rekristalizacije svinca.

The diversity of rheological properties of lead makes it suitable for the study of materials deformability with various rheology at stable conditions and room temperature. Specimens 10 x 20 mm cross-section were extruded with a deformation ratio of 18:1. After thickening of the ends by forging the specimens were annealed an hour at 100°C. The properties were then stabilized by aging at 30°C for 60 days and the microstructure was controlled. **Fig. 5** shows the microstructure after annealing and ageing. No grain growth was observed during the thermal treatment. Even slight impurities can change significantly the lead rheology quantitatively as well as qualitatively[13]. In order to have a constant chemical composition the specimens were made of the same melt.

In the analysis of the rheological properties of different metals it was ascertained that at a temperature slightly above the recrystallization temperature the complexity of rheology is revealed more evidently at low strain rates. For this reason the experiments were performed at a temperature of 33-34°C, thus different from the temperature by which the rheological curves

Figure 5: Microstructure of lead.
Slika 5: Mikrostruktura svinca.

∂-ϵ in Fig. 3d were obtained. Investigations were performed on "Fritz Hekkert" FP-10 and FP 100/1 machines at a stretching rates of 0.5; 1; 200 and 1500 mmpm.

It was ascertained that the character of specimen deformation depends at a given rate on the specific rheological relation given by the ∂-ϵ curve from the family of rheological curves in **Fig. 6**.

To ensure an average strain rate of $\epsilon = 0.004\ s^{-1}$ longer specimens were used **(Fig. 6, specimen No 1)**. At this rate lead deformed as materials of the first rheological class with a distinct formation of the neck, thus with a simple strain anomaly. Specimens No 1, No 2 and No 3 were stretched with the same pre-set relative elongation $\epsilon = 40\%$.

The average strain rate of specimen No 2 was $0.02\ s^{-1}$ **(Fig. 1, IV)** and a curve of the fourth rheological class was obtained. After a short deformation in the stage of strain homogeneity of the first order the deformation continued by strain heterogeneity of the second order and a local neck was formed. As the extension went on, deformation proceeded according to the secondary homogeneity type. The neck elongated on account of near-by metal volumes and the specimen acquired the shape given in **Fig. 6**, No 2. Though quantitatively rheological anomalies (ϵmax and ϵmin deviations) of lead at this speed are only marked, strain anomalies and differences between them are observed quite distinctly.

Specimen No 3 (200 mmpm) deformed as rheologically simple strengthenable material of the second class in conditions of homogeneous strain.

Specimen No 4 (1500 mmpm) passed a short stage of homogeneous deformation according to heterogeneous strain type and fractured attaining scarcely an elongation of $\epsilon = 38\%$ while retaining the value of .. = 100% waist. The fall of plasticity is due in this case to the strain anomaly of the second order. At this strain rate rheological curve of lead shows one maximum, which is a characteristic for materials of the third rheological class.

The repetition of experiments confirmed the reliability of the findings. The investigation of strain anomalies of higher orders and the regularity of their occurrence suggest a solution of some interesting problems and reveal the nature of the formation of the strain nidus during the rolling of rheologically complex steels[14].

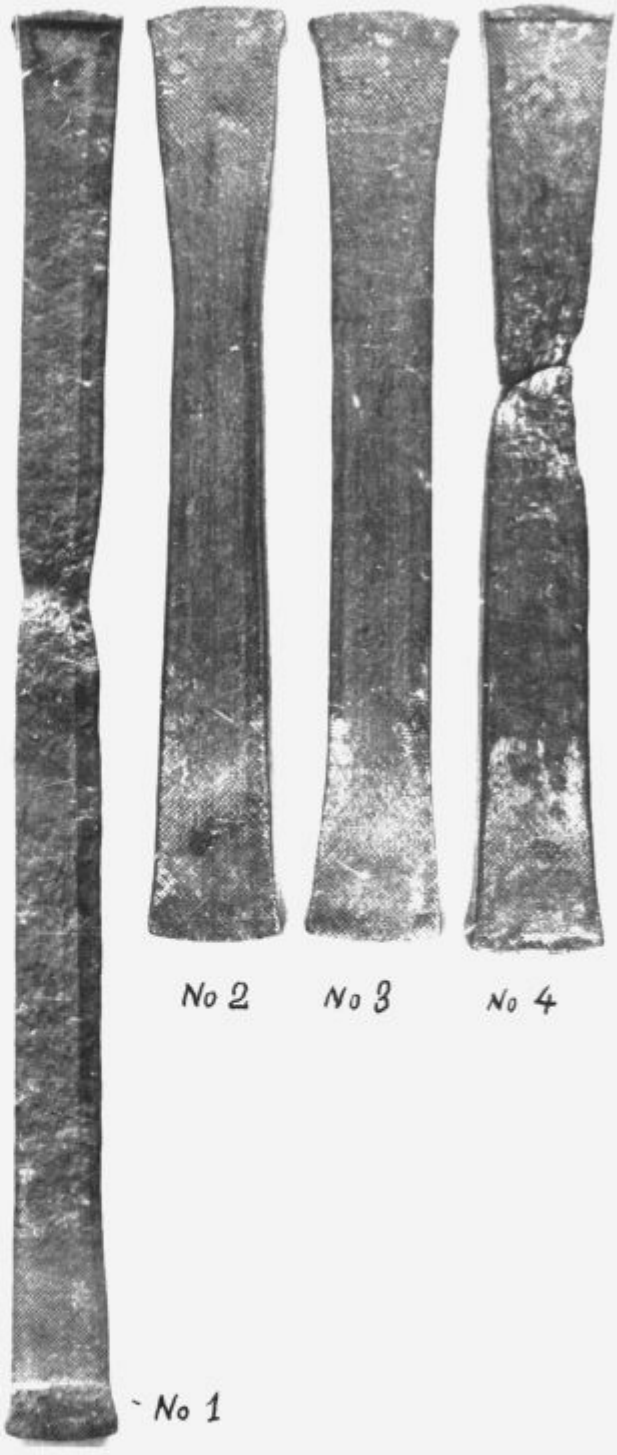

Figure 6: Form of lead specimens stretched at strain rate of mmpm: No 1 - 0.5; No 2 - 1.0; No 3 - 200; No 4 - 1500.
Slika 6: Oblika svinčenih preizkušancev, deformiranih s hitrostjo deformacije: št.1 - 0.5; št.2 - 1.0; št.3 - 200; št.4 - 1500.

4. Conclusion

A phenomenon of strain anomalies of higher orders of rheologically complex materials was determined experimentally and explained. It reveals itself in the process of plastic uniaxial extension, according to the rheological curve ∂-ϵ. Secondary and further strain heterogeneities appear

alternated with secondary and following homogeneities which increase the resistance to deformation.

Considering the proposed rheological classification of materials the understanding of regularities of strain anomalies can be used for the solution of theoretical and technological problems connected with the prediction of the development of plastic deformations and of the rupture of rheologically complex materials.

References

[1] U. L. Colmogorov, A. A. Bogotov, B. A. Migachov, E. G. Zudov, M. E. Freidzon: *Metalurgia*, 1977, 336.

[2] O. A. Caybishev: *M. Metallurgia*, 1975, 280.

[3] M. Y. Dzugutov: *M. Metallurgia*, 1977, 480.

[4] P. I. Poluhin, G. Y. Gun, A. I. Galkin: *Metallurgia*, 1983, 352.

[5] H. Suzuki: *Report of Inst. of Industrial Science*, University of Tokyo, 18, 1968, 3, 139-240.

[6] A. V. Bobiliov: Mechanical and technological properties of metals Manual; *Metallurgia*, 1980, 290.

[7] D. Rittel, R. Aharonov, G. Feigin, I. Roman: *Acta Metallurgica et Materialia*, 39, 1991, 4, 719-724.

[8] G. G. Shlomchack: *Strain Features of rheologically complex metals*; Kiev, 1991, Dep. in UkrNIINTI 18.8.91, No 1167-Uk 91.

[9] G. G. Shlomchack: *Regularity of strain heterogeneity and plasticity anomalies of rheologically complex and extra - complex materials*; Kiev, 1991, Dep. in UkrNIINTI 12.1.291, No 1589-Uk 91.

[10] A. Burkhard: Mechanical and technological properties of pure metals; *M. Metallurgizdat*, 1941, 443.

[11] G. G. Schlomchack, G. A. Fen, V. G. Kutsay: *Izvestia vuzov. Chernaya metallurgia*, 1980, 3, 61-65.

[12] G. G. Shlomchack: *Izvestia AN USSR*, Metals, 1976, 6.

[13] G. G. Shlomchack, V. G. Vrublevsky, R. N. Filchakov: *The change of rheological properties of lead by modification*; Kiev, Dep. in UkrNIINTI, 16.0589, No 1267 - Uk 89.

[14] G. G. Shlomchack: *The modelling of the rolling process*; Coloured film, 35 mm., parts 1 and 2. Produced by laboratory of technical education of the Ministry of ferrous metallurgy, USSR, Dnepropetrovsk, 1991.

3rd SLOVENIAN CONFERENCE ON MATERIALS AND TECHNOLOGY

October 4–6, 1995, Portorož, Slovenia

organizired by

INSTITUTE OF METALS AND TECHNOLOGY, LJUBLJANA
NATIONAL INSTITUTE OF CHEMISTRY, LJUBLJANA
INSTITUTE JOŽEF STEFAN, LJUBLJANA

Materials scientists from Industry, Universities and Institutes are cordially invited to attend the Slovenian Conference on Materials and Technology and to contribute to its scientific programme.

The Scientific programme covers:

- Synthesis of advanced metallic, polymer, ceramic and composite materials
- Development of advanced manufacturing technology
- Mathematical modeling and computer simulation of processes and technology
- Degradation of materials
- Advanced thermal treatment
- Characterization of materials
- Vacuum technique and technology
- Thin films and surfaces
- Tribology
- Environmental protection

Exhibitors will be able to present their latest products and equipment in a Technical session.

During the Conference a technical exhibition of materials, equipment and scientific literature will be held.

Conference languages are Slovene and English.

You are invited to sumbit contributed papers in the fields of scientific programme of the Conference. There will be plenary session of invited lecturers, oral session for young scientists and poster sessions.

Deadline for abstract submission is May 15, 1995.

The Conference Proceeding will be published as a special issue of Slovenian scientific journal Metals, Alloys, Technologies in January 1996.

Information: Institute of Metals and Technology, 61001 Ljubljana, Slovenia, Lepi pot 11, PO Box 431, Telephone: 386 61 125 11 61, Fax: 386 61 21 37 80.

Kovine, zlitine, tehnologije / letnik 28 / 1994 / številka 4 / strani 589 do 593

Quality of Surfaced Running Wheels
Kvaliteta navarjenih tekalnih koles

R. Kejžar*, ZRMK Ljubljana, Slovenia
L. Kosec, FNT - Montanistika (Metalurgija), Ljubljana, Slovenia

Results of tribologic testing of samples of running crane wheels as well as of crane rails show that wear resistance of running wheels can be considerably improved by surfacing. The wear of the wheels coated with higher-alloyed claddings is insignificant. It is only the wear of crane rails which becomes significant, and which increases with the increase of hardness of the running wheel surface (it depends only on alloying of the surfaced cladding). Hard running wheel surfaces are interesting mostly in the case of greater stresses because they permit operation with lower friction moment, and consequently lower heating of contact surfaces in sliding as well as in rolling friction.
Key words: wear of running crane wheels, submerged-arc surfacing, alloyed agglomerated fluxes, tribologic testing of wear resistance of surfacings.

Rezultati tribološkega testiranja vzorcev tekalnih koles žerjavov in tirnice so pokazali, da lahko z navarjanjem znatno izboljšamo obrabno ostojnost tekalnih koles. Obraba koles, ki jih platiramo z močneje legiranimi prevlekami, je neznatna. Pomembna postane samo obraba tirnice, ki pa se s trdoto tekalne površine kolesa (odvisna je od legiranja navarjene prevleke) povečuje. Trde tekalne površine koles so zanimive predvsem pri večjih obremenitvah, ker zagotavljajo obratovanje z nižjim momentom trenja in s tem manjše segrevanje stičnih površin tako pri drsnem kot tudi kotalnem trenju.
Ključne besede: Obraba tekalnih koles žerjavov, navarjanje pod praškom, legirani aglomerirani praški, tribološke preiskave obrabne odpornosti navarov.

1. Introduction

Wear mechanisms are simulated by tribologic testing. The state of stress of a material depends on the load applied, number of revolutions, and slip. Stresses generated in a material due to the operation of a machine element exert a decisive influence on its applicability[1-6].

Quality of the surfaces subject to wear is of extreme importance. Life of the machine element depends on the steel or alloy applied. Its making of high-alloy steels or special alloys, which would result in its high wear resistance, however, would be very expensive. It is surfacing processes which make it possible that solely the surfaces and edges subject to wear during operation need to be made of special wear-resistant steels or alloys[7-9]. The very submerged-arc surfacing of wheels with alloyed wire "EPP Cr 6" and with fused flux somewhat improves their wear resistance with regard to that of unsurfaced wheels. An even more distinct improvement of wear resistance of the wheels can be achieved if running wheel surfaces are submerged-arc surfaced with alloyed agglomerated fluxes or high-efficiency alloyed thick-coated electrodes to obtain higher-alloyed and harder claddings. These filler materials permit us to surface structural unalloyed steels in one layer with high-alloyed claddings[10-12].

2. Quality of samples for tribologic testing

Multi-layer submerged-arc surfacing of worn-out running wheels with wire "EPP Cr 6" and fused flux provides quite an acceptable quality of the repaired running wheels. The running wheels repaired in this way are even a little more wear-resistant than the unsurfaced ones. This was proved also by tribologic testing[13,14].

Surfacing of the worn-out running wheels with alloyed wire "EPP Cr 6" can be replaced by submerged-arc surfacing with unalloyed wire "EPP 2" and alloyed agglomerated flux. The surfacing is alloyed with chromium and other selected elements coming from the alloyed agglomerated flux. The compositions of one-layer and multi-layer surfacings, i.e. deposited metals, obtained in submerged-arc surfacing with unalloyed wire "EPP 2" and with the new alloyed agglomerated flux "0–7 SM" correspond very well to those of the surfacings obtained in submerged-arc surfacing with wire "EPP Cr 6" and fused flux (see **Table 1**).

Testing of wear resistance of the surfacings has shown that the alloyed agglomerated welding flux "0–7 SM" in combination with the unalloyed wire "EPP 2" is quite a suitable substitute to be applied for submerged-arc surfacing of the running wheels with alloyed wire "EPP Cr 6" and fused flux.

For surfacing of higher-alloyed wear-resistant claddings, high-alloyed agglomerated welding fluxes "U-Mo 1" and "BM-2" have been developed in addition to the alloyed agglomerated welding flux "0–7 SM".

Samples for tribologic testing **(Fig.1)** have been made of steel Č.4732. They have been automatically submerged-arc sur-

* Dr. Rajko KEJŽAR, dipl. inž.,
ZRMK Ljubljana, Dimičeva 12, 61000 Ljubljana

Table 1: Chemical analyses of one-layer and multi-layer submerged-arc surfacings (deposited metals) made with wires
– EPP Cr 6 and fused flux and
– EPP 2 and alloyed agglomerated flux "0-7 SM" respectively.

Tabela 1: Kemične analize enoslojnega in večslojnega navara (čistega vara) z žico
– EPP Cr 6 pod taljenim praškom in
– EPP 2 pod legiranim aglomeriranim praškom "0-7 SM"

Surfacing	C (%)	Si (%)	Mn (%)	Cr (%)	Mo (%)
EPP Cr 6/fused flux					
– one-layer	0,20	0,24	0,65	4,53	–
– multi-layer	0,10	0,25	0,70	7,00	–
EPP 2/alloyed flux "0–7 SM"					
– one-layer	0,32	0,35	0,87	3,56	0,31
– multi-layer	0,11	0,55	1,21	9,12	0,48

faced with wire "VAC 60" ∅1.2 mm (I = 140 A, U = 21 V, and $v_{weld.}$ = 30cm/min; q = 5 KJ/cm) and alloyed agglomerated fluxes "0-7 SM", "U-Mo 1", and "BM-2" which, during surfacing, heated up to the temperature of 350°C. Cooling rates of the surfacing and of the heataffected zone correspond to those in surfacing of preheated running wheels carried out in practice[13,14].

Chemical compositions and hardness values for the surfacings and the heat-affected zones are given in **Table 2**.

Table 2: Chemical compositions and hardness values of the samples surfaced for tribologic testing (50 % overlapping of runs)

Tabela 2: Kemične sestave in trdote navarjenih vzorcev za tribološke preiskave (50%-no prekrivanje varkov)

Surfacing	C (%)	Cr (%)	Mo (%)	W (%)	V (%)	Hardness in HV: Final layer	Weld centre	HAZ
VAC 60/0-7SM	0,31	5,3	0,3	–	–	410	366	183
VAC 60/U-Mo 1	0,55	9,8	2,3	–	0,9	687	556	172
VAC 60/BM-2	0,85	5,1	4,2	5,0	1,9	707	586	163

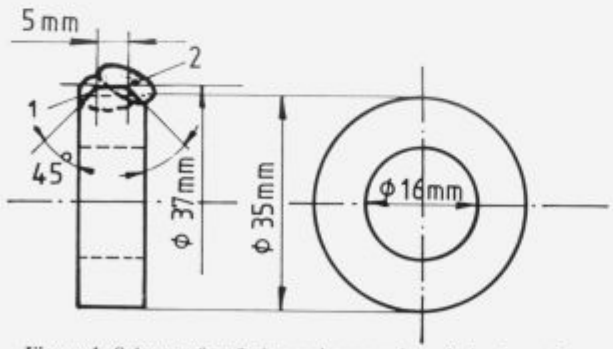

Figure 1: Scheme of surfacing and preparation of a hard running surface by specimens for tribologic testing (1 - first surfacing, 2 - second surfacing).

Slika 1: Skica navarjanja in priprave trde tekalne površine pri vzorcih za tribološke preiskave (1 - prvi navar, 2 - drugi navar)

Quality running surfaces of the surfaced rollers are obtained if the surfacings are broached at an angle of 45 (**Fig. 1**). The samples of the rail not being broached, it is the surfaced samples which determine the gap width in tribologic testing (5 mm). The running contact surfaces of the rollers surfaced and of the rail samples have been ground and polished to Ra = about 0.3 mm before being tested on a tribometer "Amsler".

3. Results of tribologic testing of the surfacings and of the rail

Parameters for tribologic testing of the running crane wheels and of the rail have been chosen in such a manner that Hertz's pressure in the case of our test carried out between two rollers (Amsler) is the same as that in actual condition existing the running wheel and the crane rail[13].

Testing conditions in rolling friction are as follows:
P = 600 N/cm, 1200 N/cm, and 2000 N/cm
v = 200 r.p.m. (0.42 m/s), and 400 r.p.m. (0.84 m/s)
t = 24 min

Diagrams of friction moment are given in **Fig. 2**.

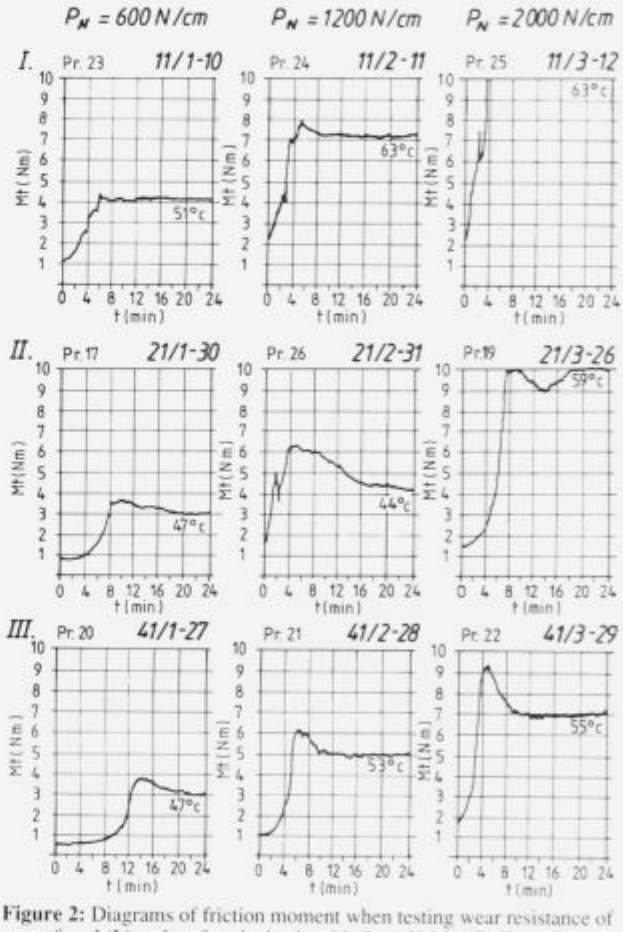

Figure 2: Diagrams of friction moment when testing wear resistance of unsurfaced (I.) and surfaced wheels with flux "U-Mo 1" (II.) and "BM 2" (III.); v = 400 r.p.m. or 0.84 m/s.

Slika 2: Diagrami momenta trenja pri testiranju obrabne obstojnosti nenavarjenih (I.) ter navarjenih koles pod praškom "U-Mo 1" (II.) in "BM 2" (III.); v = 400 obr./min. oz. 0.84 m/s

Wear of the wheels surfaced with higher-alloyed claddings is insignificant. It is only wear of the rail which becomes important and which increases with the increased hardness of the running wheel surface (which itself depends on alloying of the cladding surfaced). Hard running wheel surfaces are of interest most of all with higher stresses because they make possible op-

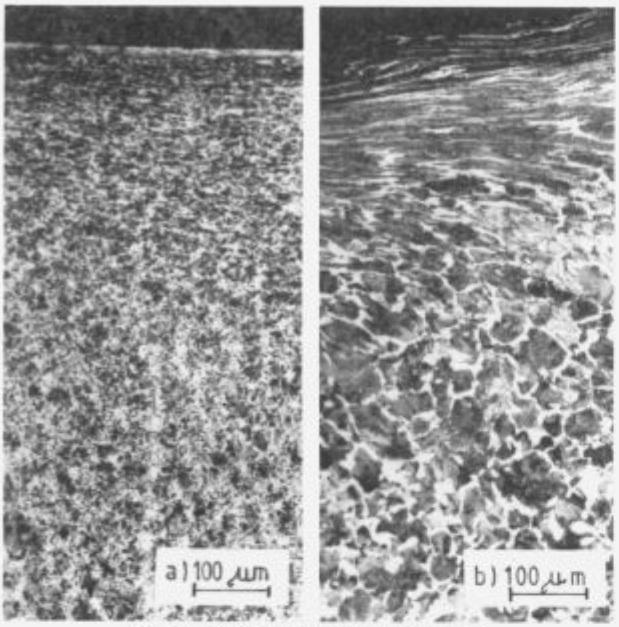

Figure 3: Microstructure of a rail section
a) Pr. 10 - high friction moment; more than 10 Nm
b) Pr. 5 - low friction moment; about 6 Nm

Slika 3: Mikrostruktura preseka tirnice
a) Pr. 10 - visok moment trenja; preko 10 Nm
b) Pr. 5 - nizek moment trenja; okoli 6 Nm

Figure 5: Damaged running surface - parts of oxides, stickers of metals... (unsurfaced running wheel)

Slika 5: Poškodovana tekalna površina - delci oksidov, nalepi kovine... (nenavarjeno tekalno kolo)

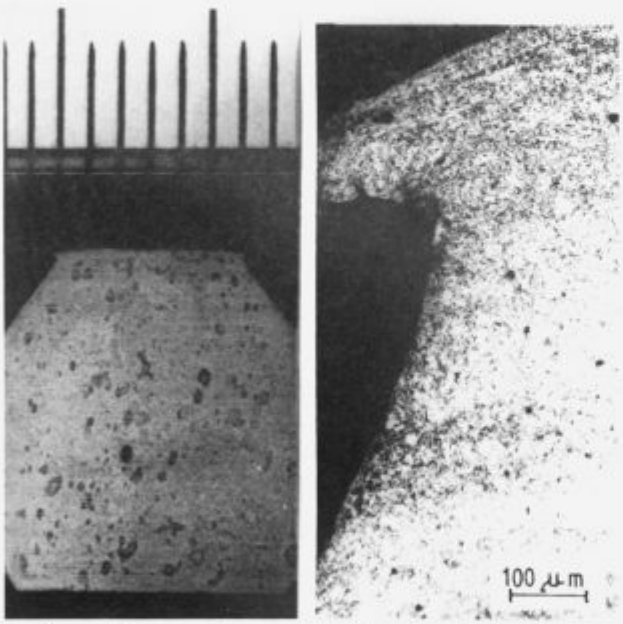

Figure 4: Appearance of an unsurfaced running wheel section and its microstructure

Slika 4: Izgled preseka nenavarjenega tekalnega kolesa in njegova mikrostruktura

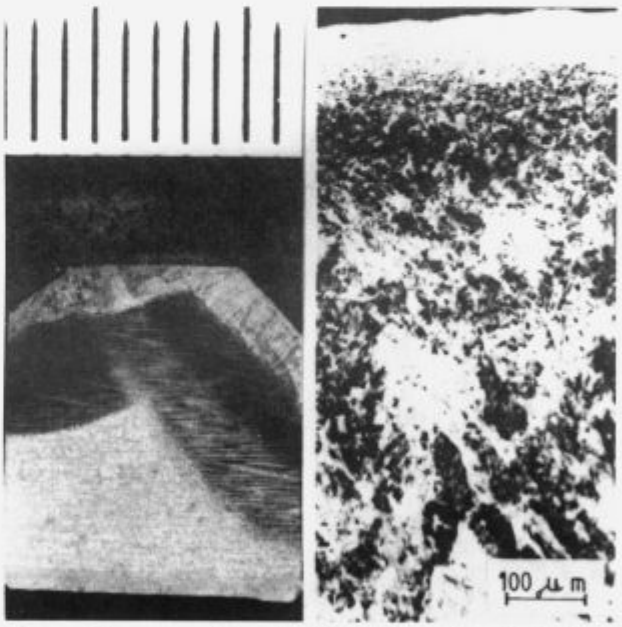

Figure 6: Appearance of a surfaced (0-7 SM) running wheel section and its microstructure.

Slika 6: Izgled preseka navarjenega (0-7 SM) tekalnega kolesa in njegova mikrostruktura

eration with a lower friction moment, and consequently result in a weaker heating of the contact surfaces in sliding friction as well as in rolling friction.

Heating of the contact surfaces, which is particularly strong with high friction moments, results, in the case of strong loads, in a considerable deformation of the surface layers of the rail **(Fig.3)** and of the running wheels **(Fig.4)** if they have not been surfaced, i.e. refined with a hard cladding. Plastic deformation is accompanied also by crystalline modification of the surface layer if the latter heats above 555°C due to rolling friction[15]. If heating during rolling, which strongly depends on friction moment, is very intensive, the crystalline modification zone can extend also beyond the deformation zone **(Fig.3)**. The deformation zone in rails goes approximately 0.4 mm deep, while the crystalline modification zone, in the case of high friction moments, goes even 2 mm deep **(Fig.3)**.

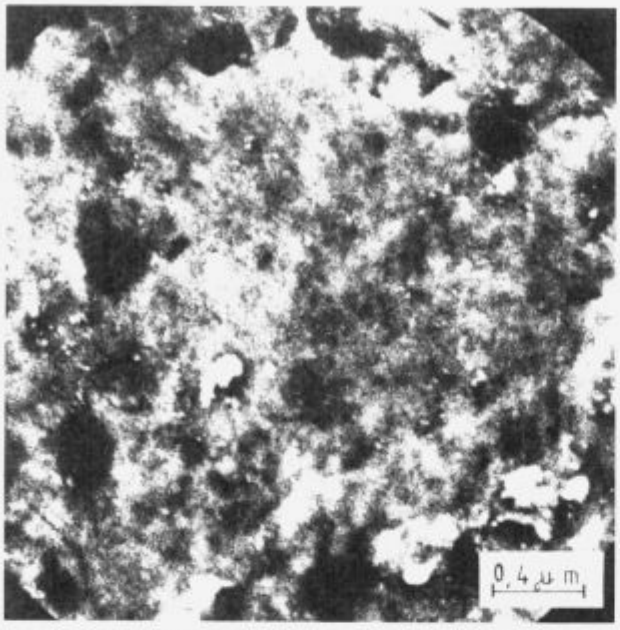

Figure 7: Damaged running surface - parts of oxides, stickers of metals... (surfaced running wheel; 0-7 SM).

Slika 7: Poškodovana tekalna površina - delci oksidov, nalepi kovine... (navarjeno tekalno kolo; 0-7 SM)

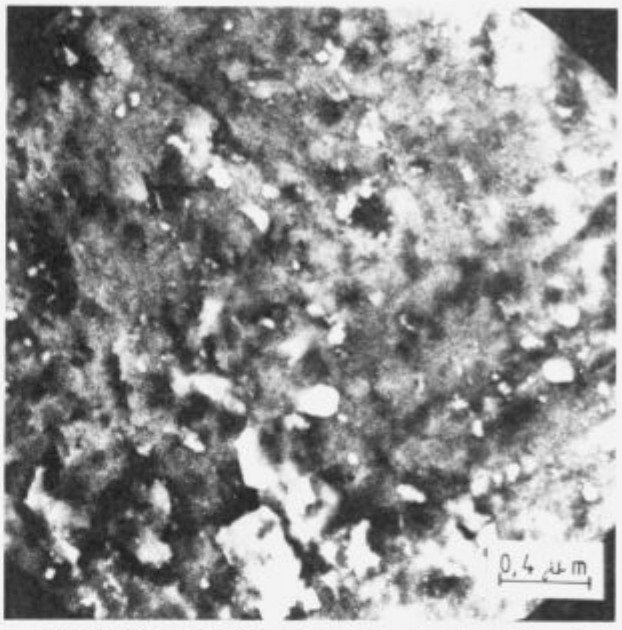

Figure 9: Damaged rolling surface - parts of oxides, stickers of metalls... (surfaced rolling wheel; BM-2)

Slika9: Poškodovana tekalna površina - delci oksidov, nalepi kovine... (navarjeno tekalno kolo; BM-2)

A distinct deformation and oxidation of the surface due to intensive heating of the contact surfaces during rolling results in damages to the running wheel surface **(Fig. 5)**.

Submerged-arc surfacing itself with alloyed agglomerated flux "0-7 SM" highly improves wear resistance of the running wheel. Deformation of the surface layer is considerably weaker. The contact surface increases, due to wear and plastic deformation, only by 15 % **(see Fig. 6)**. With the unsurfaced sample, the contact surface has increased by even 30 % during testing. Also the deformation depth with the surfaced sample is only 80 to 100 µm **(see Fig. 6)**, which is easy to understand since the surfaced-layer has martensitic-bainitic structure while with the unsurfaced sample (**Fig. 4**, deformation depth 200-250 µm), the surface layer has ferritic structure.

With the surfaced samples of the running wheels, deformation and oxidation cause damages to the contact surface, i.e. folded metal and stickers of metals and oxides **(Fig. 7)**. These are, however, essentially weaker than those to the unsurfaced samples (cf. **Figs. 5 and 7**).

Even weaker deformation and lesser damages of the running surface occurred with the samples which were submerged-arc surfaced with high-alloyed welding fluxes "U-Mo 1" and "BM-2" **(see Fig. 9)**. After tribologic testing, the surface layer has been very little deformed **(Fig. 8)**. Increase of the contact surface due to deformation and oxidation of the surface **(Fig. 8)** is insignificant too (around 5 %).

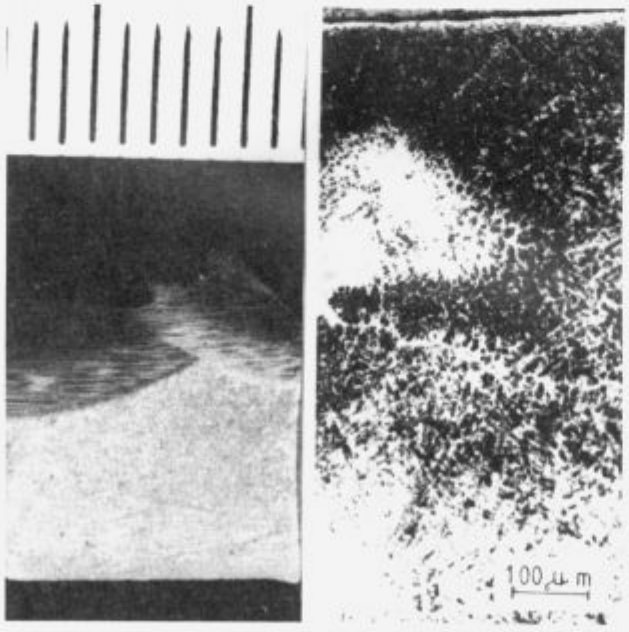

Figure 8: Appearance of a surfaced (BM-2) running wheel section and its microstructure.

Slika 8: Izgled preseka navarjenega (BM-2) tekalnega kolesa in njegova mikrostruktura

4. Conclusion

Wear resistance of running wheels can be improved by surfacing. The very submerged-arc surfacing of the wheels with alloyed wire "EPP Cr 6" and with fused flux somewhat improves their wear resistance with regard to that of unsurfaced wheels. An even more distinct improvement of wear resistance of the wheels can be achieved if running wheel surfaces are submerged-arc surfaced with alloyed agglomerated fluxes or high-efficiency alloyed thick-coated electrodes to obtain higher-alloyed and harder claddings. These filler materials permit us to surface structural unalloyed steels in one layer with high-alloyed claddings.

Testing of wear resistance of the surfacings has shown that the alloyed agglomerated welding flux "0-7 SM" in combination with the unalloyed wire "EPP 2" is quite a suitable substitute to be applied for submerged-arc surfacing of the running wheels with alloyed wire "EPP Cr 6" and fused flux.

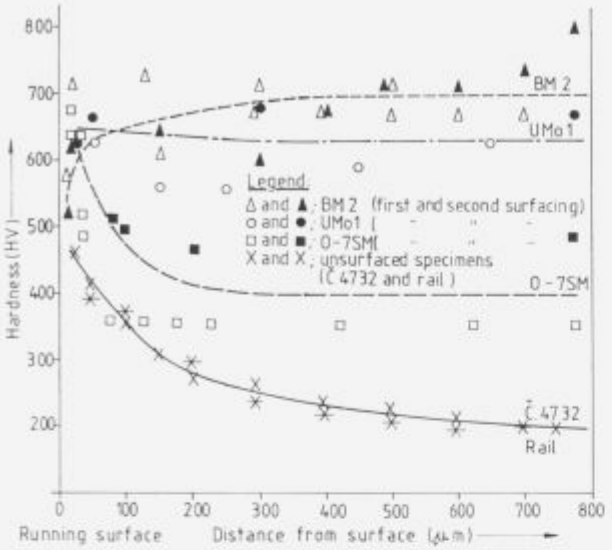

Figure 10: Hardness of sections of unsurfaced and surfaced specimens
Slika 10: Trdote na prerezu nenavarjenega in navarjenih tekalnih koles

High wear-resistance of the claddings which were submerged-arc surfaced on the running wheel with alloyed-agglomerated flux "0-7 SM" is resulting from surface hardening (600-700 HV; **Fig. 10**) due to deformation of the surface layer. The claddings which were submerged-arc surfaced with high-alloyed agglomerated fluxes "U-Mo 1" and "BM-2", however, are hard (around 700 HV; **Table 2**) right after surfacing; therefore, they practically neither deform nor harden during tribologic testing. In the case when the wear resistant cladding was made by submerged-arc surfacing with high-alloyed agglomerated flux "BM-2", stress and heating of the running surface resulted even in stress relieving and insignificant decrease of hardness immediately upon the surface (**Fig. 10**, upper curve).

Wear of the wheels surfaced with higher-alloyed claddings is insignificant. It is only the wear of the rail which becomes important and which increases with the increased hardness of the running wheel surface (which itself depends on alloying of the cladding surfaced). Hard running wheel surfaces are of interest most of all with higher stresses because they make possible operation with a lower friction moment; and consequently result in a weaker heating of the contact surfaces in sliding friction as well as in rolling friction. Wear resistance of the running crane wheels can be considerably improved by surfacing and by appropriate selection of filler materials without essentially influencing the wear of the rail.

References

[1] L. Föppl: *Beanspruchung von Schiene und Rad beim Anfahren und Bremsen*, Munchen 1963.

[2] K. H. Kloos, E. Broszeit, M. Koch: *Eigenspannungesänderungen beim Überrollen von gehärtetem Wälzlagerstahl 100 Cr 6"*. Institut für Werkstoffkunde, Darmstadt.

[3] H. Poritsky, N. Y. Schenectady: *Stresses and defletions of cylindrical bodies*, New York 1949.

[4] Dr. Marko Kos: *Raziskava trajnostne meje tekalnih koles in tirnice*, Ljubljana 1972.

[5] J. Vižintin, A. Vesel: Popis napetostnega stanja na tekalnem kolesu in tirnici. *Poročilo ZRMK Ljubljana za RP 03–2663-227–88*, Delovni stroji, strojni elementi in konstruiranje, Ljubljana, 1988, 88/106.

[6] A. Vesel, R. Kejžar, J. Vižintin, M. Anželj: Tribološki parametri navarjenih tekalnih koles žerjavov. *Poročilo ZRMK Ljubljana za URP C2-1528-227-89*, Konstruiranje delovnih strojev in motorjev, Ljubljana, 1989, 30/52.

[7] R. Kejžar: Hardfacing by Submerged Arc Welding", *Proceedings of the 2nd International conference on Tooling: Neue Werkstoffe und Verfahren für Werkzeuge*, Bochum, 1989, 301/314.

[8] R. Kejžar: Izdelava in obnavljanje orodij z navarjanjem, *Strokovne informacije 17, Materiali in sodobna izdelava*, Ljubljana, 1991, 117/136.

[9] R. Kejžar: Oplemenitenje površin z navarjanjem in metalizacijo. *Kovine zlitine tehnologije*, 26 (1992), 1/2, 79–84.

[10] R. Kejžar: Perspektive aglomeriranih varilnih praškov, *38. Posvet o metalurgiji in kovinskih gradivih*, Portorož/Ljubljana 1987, 87–98.

[11] R. Kejžar: Legirani aglomerirani praški za posebna navarjanja, *Rudarsko-metalurgki zbornik*, Ljubljana 38 (1991), 2, 275/290.

[12] R. Kejžar: Navarjanje močno legiranih nanosov na konstrukcijska jekla, *Varilna tehnika* 41 (1992), 4, 96–101.

[13] R. Kejžar, J. Vižintin, L. Kosec, J. Cankar, P. Žmitek: Tribološke lastnosti površinsko oplemenitenih jekel – tekalno kolo žerjava. *Poročilo ZRMK Ljubljana URP C2-1528*. Konstruiranje delovnih strojev in motorjev, Ljubljana, 1990, 91 in 92.

[14] R. Kejžar, M. Hrženjak, V. Živkovič, J. Vižintin, L. Kosec, J. Cankar: Izbira dodajnega materiala in tehnologije navarjanja tekalnega kolesa žerjava. *Kovine zlitin tehnologije* 27 (1993) 3, 267.

[15] Ahlert: Erkenntnisse und Entwicklungen der Thermit – Schweisstechnik, *ETR – Eisenbahntechnische Rundschau* 12 (1969) 105.

INŠTITUT ZA KOVINSKE MATERIALE
IN TEHNOLOGIJE p.o.

INSTITUTE OF METALS
AND TECHNOLOGIES p.o.

61000 LJUBLJANA, LEPI POT 11, POB 431,
SLOVENIJA

Telefon: 061/1251-161, Telefax: 061 213-780

VACUUM HEAT TREATMENT LABORATORY

Vacuum Brazing

Universally accepted as the most versatile method of joining metals. Vacuum Brazing is a precision metal joining technique suitable for many component configurations in a wide range of materials.

ADVANTAGES

- Flux free process yields clean, high integrity joints
- Reproducible quality
- Components of dissimilar geometry or material type may be joined
- Uniform heating & cooling rates minimise distortion
- Fluxless brazing alloys ensure strong defect free joints
- Bright surface that dispense with expensive post cleaning operations
- Cost effective

Over five years of Vacuum Brazing expertise at **IMT** has created an unrivalled reputation for excellence and quality.

Our experience in value engineering will often lead to the use of Vacuum Brazing as a cost effective solution to modern technical problems in joining.

INDUSTRIES

- Aerospace
- Mechanical
- Electronics
- Hydraulics
- Pneumatics
- Marine
- Nuclear
- Automotive

QUALITY ASSURANCE

Quality is fundamental to the **IMT** philosophy. The choice of process, all processing operations and process control are continuously monitored by **IMT Quality Control Department**.

The high level of quality resulting from this tightly organised activity is recognised by government authorities, industry and International companies.

Kovine, zlitine, tehnologije / letnik 28 / 1994 / številka 4 / strani 595 do 600

Cockcroft-Latham Fracture Criterion and Bulk Formability of Copper Base Alloys

Cockroft-Lathamov kriterij loma in masivna preoblikovalnost bakrovih zlitin

B. Ule*, V. Leskovšek, B. Breskvar, Institute of Metals and Technology, Ljubljana, Slovenia
K. Kuzman, D. Švetak, Faculty for Mechanical Engineering, Ljubljana, Slovenia
F. Kofol, Kolektor, Idrija, Slovenia

The ductility of metalic materials is generally defined as the ability to deform plastically without fracture. It is usually expressed as a measure of the strain at fracture in a simple tension test[1]. However, the percentage elongation in a tensile test is often dominated by the uniform elongation, which is dependent on the slope of the stress/strain curve. The end of uniform elongation coincides with the onset of plastic instability accompanied by voids nucleation, their growth and coalescence. It appears that the elongation value is too complex to be regarded as a fundamental property of a material and it seems reasonable to assume that any criterion of fracture will be based on some combination of stress and strain rather than on either of these quantities separately. Two grades of copper base alloys used for the production of commutators for electrical motors were tested in compressing and stretching. The bulk formability of these alloys were projected using the Cockcroft-Latham criterion[2,3], based on the tensile strain energy density at fracture. This criterion emphasizes the importance of tensile stresses in fracture and can be applied to a variety of cold working processes.

Key words: ductility, formability, fracture, Cockcroft-Latham fracture criterion, copper base alloys

Duktilnost kovinskih materialov je v splošnem definirana kot sposobnost, da se plastično deformirajo brez pojavljanja razpok. Običajno jo izrazimo z lomno deformacijo pri enostavnem nateznem preiskusu[1]. V odstotkih izmerjen celokupni raztezek pri nateznem preiskusu je dokaj odvisen od enakomernega raztezka, to je od strmine krivulje napetost-deformacija. Konec enakomernega raztezanja sovpada s pojavljanjem plastične nestabilnosti, ki jo spremlja nastajanje por, njihova rast in združevanje. Zdi se, da je raztezek preveč kompleksen in ga ne moremo smatrati kot osnovno materialno lastnost. Zato je smiseln privzetek, po katerem bo moral lomni kriterij temeljiti prej na neki kombinaciji napetosti in deformacij, kot le na eni posamični količini. Za tlačno in natezno preiskušanje smo izbrali dve bakrovi zlitini za izdelavo kolektorjev pri elektromotorjih. Masivno preoblikovalnost teh zlitin smo opredelili s Cockcroft-Lathamovim kriterijem[2,3], ki temelji na gostoti natezne deformacijske energije. Ta kriterij poudarja pomen nateznih napetosti pri lomu in ga lahko uporabitmo pri različnih procesih preoblikovanja v hladnem.

Ključne besede: duktilnost, preoblikovalnost, lom, Cockcroft-Lathamov kriterij loma, bakrove zlitine.

1. Introduction

The evolution of ductile damage within the deforming body is considerably influenced by the stress state in the material. It was suggested by Siebel[4] that the cracking in metalworking is associated with induced tensile stresses, even in processes such as forging that are predominantly compressive. The importance of tensile stresses is indirectly confirmed by the large increase in ductility when the materials are deformed under hydrostatic pressure[5]. Pugh and Green[6] demonstrated that superimposing a hydrostatic pressure in the extrusion process greatly enhanced reductions could be achieved in ductile materials, and that even some brittle materials could be extruded without difficulty. In a tensile test of a cylindrical test specimen the stresses at the minimum section of the neck can be calculated in different ways[5,7-11] and may be considered to be the sum of two parts. One part, the equivalent stress, is equal to the current yield stress and is constant across the cross-section. The other part, a hydrostatic tension, varies from zero at the periphery to a peak value at the centerline. As stated by Cockcroft and Latham[1], that the use of the criterion based on total plastic work per unit volume at the fracture point, which would take into account only the equivalent stress i.e. the current yield stress, is not a proper solution.

* Dr. Boris ULE, dipl. inž.,
IMT Ljubljana, Lepi pot 11, 61000 Ljubljana

The current yield stress, unlike the peak stress, is not influenced by the shape of the necked region. Consequently, the neck shape should have no effect on the fracture strain, a conclusion which is contrary to experimental facts[1]. Therefore Cockcroft[2] and Cockcroft and Latham[3] proposed a criterion based on the tensile strain energy density where the magnitude of the highest normal stress is taken into account. At tensile testing this would be the stress acting in the centerline where fracture is initiated.

As an outgrowth of experimental evidence of the influence of stress state on ductile fracture, several other criteria were also suggested for the prediction of fracture in complex stress states. A modification of the Cockcroft-Latham criterion which includes a hydrostatic-pressure term was suggested by Brozo et al.[12]. Other criteria of importance were proposed by Oyane[13], Clift[14] Hoffmanner[15] and Osakada[16]. Such criteria were successfully applied by a number of investigators to a variety of cold working operations[17-21].

2. Fracture criterion

With the Cockcroft and Latham tensile ductility approach, the fracture is predicted when

$$\int_0^{\bar{\varepsilon}_f} \bar{\sigma} \left(\sigma^* / \bar{\sigma} \right) d\bar{\varepsilon} = C \tag{1}$$

where $\bar{\varepsilon}$ is equivalent i.e. effective strain, $\bar{\varepsilon}_f$ is equivalent strain at fracture, $\bar{\sigma}$ is equivalent i.e. effective stress, σ^* is the highest tensile stress, $(\sigma^*/\bar{\sigma})$ is a non-dimensional stress-concentration factor representing the effect of the highest tensile stress, σ^*, and C is a material constant. If there is no tensile stress operating but only a compressive stress, $\sigma^* = 0$ and fracture does not occur[1].

The expression (1) has the dimensions of work per unit volume ($N/m^2 = Nm/m^3 = J/m^3$). The reduced form

$$\int_0^{\bar{\varepsilon}_f} \sigma^* \, d\bar{\varepsilon} = C \tag{2}$$

is used for calculation. The correction for necking and projections for σ^* could be obtained by different approaches[5,7-11]. Wright and coworkers[18], for instance, successfuly used the equations of Davidenkov and Spiridonova[7], whereas the equations of Bridgman[5] were used in our experiments.

Fig. 1 illustrates the geometry at the necked region and the distribution of axial stress by this localized deformation. In accordance to Bridgman[5], the variation of the stresses in a minimum section of a necked bar in tension is given as

$$\sigma_{av} = \bar{\sigma} \left(1 + 2\rho / R \right) ln \left(1 + R / 2\rho \right) \tag{3a}$$

$$\sigma_{rr} = \sigma_{\varphi\varphi} = \bar{\sigma} \; ln \; \frac{R^2 + 2R\rho - r^2}{2R\rho} \tag{3b}$$

$$\sigma_{zz} = \bar{\sigma} + \sigma_{rr} \tag{3c}$$

where σ_{av} is the average stress on the minimum section of the neck (load divided by minimum neck area), R is the radius of the minimum cross section at the neck, r' is the so called "strained length" ($r' \equiv r \, R/R_0$), R_0 is the radius of initial cross section ($R_0 = 5$ mm) and ρ is the radius of curvature of the neck profile. In the centerline of the necked region, where $r = r' = 0$, $z = 0$ the stress component σ_{zz} reaches the highest value $\sigma_{zz,\,max} = \sigma^*$

$$\sigma^* = \bar{\sigma} + \bar{\sigma} \; ln \; \frac{R + 2\rho}{2\rho} \tag{4}$$

Considering the strain hardening, the flow curve can be approximated by several constitutive equations. The most common are proposed by Hollomon[22], Ludwik[23], Swift[24] and Voce[25]. The most simple one is the Hollomon power low relation:

$$\bar{\sigma} = K \bar{\varepsilon}^n \tag{5}$$

where n is the strain-hardening exponent and K is the strength coefficient of the material. Both constants could be determined simply by the values of 0.2% offset yield strength and fracture stress[18] or by computer least-squares fits by plotting $ln \; \bar{\sigma}$ against $ln \; \bar{\varepsilon}$, where n and K are the slope and intercept respectively. However, the strain-hardening exponent n, and the strength coefficient, K, could be also evaluated from the tensile test data by applying the criterion of instability at the onset of necking, $d\sigma/d\varepsilon = \sigma$. From this, it can be shown that at necking, where the ultimate tensile strength is measured, the strain-hardening exponent is given as

$$\bar{\varepsilon}_u = n \tag{6}$$

Once the strain-hardening exponent is known, the strength coefficient K in the Eq. (5) can be easily determined by means of ultimate tensile strength σ_{uts}, as

$$K = \sigma_{uts} \left(2 \cdot 71828 / n \right)^n \tag{7}$$

From the results of Eq. (5), a relationship of σ^* to $\bar{\varepsilon}$ can be determined by using Eqs. (3a) and (4) and assuming that the

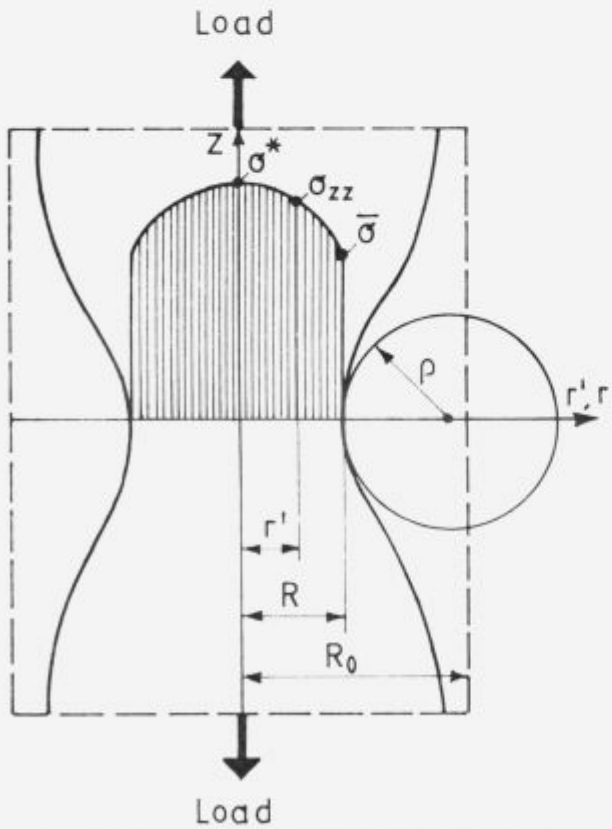

Figure 1: The geometry at the necked region and the distribution of axial stress σ_{zz}.

Slika 1: Geometrija vratu in porazdelitev aksialne napetosti σ_{zz}.

necking is initiated at the ultimate tensile strength σ_{uts}, when $\sigma_u = \sigma_{uts}$ and when $\bar{\varepsilon}$ achieves n (Eq. 6), assuming also that σ^* increases linearly with equivalent strain (**Fig.2**). Considering the hatched areas on **Fig. 2**, the integral (2) can be separated as follows

$$C = \int_0^{\bar{\varepsilon}_f} \sigma^* \, d\bar{\varepsilon} = \int_0^{\bar{\varepsilon}_u} \bar{\sigma} \, d\bar{\varepsilon} + \int_{\bar{\varepsilon}_u}^{\bar{\varepsilon}_f} \sigma \, d\bar{\varepsilon} \qquad (8)$$

By substituting the known function $\bar{\sigma}$ vs. $\bar{\varepsilon}$ and using a trapezoidal formula for the second integral, we finally get

$$C = \frac{K}{n+1} \bar{\varepsilon}_u^{n+1} + \frac{\sigma_{av.u} + \sigma_f^*}{2} \left(\bar{\varepsilon}_f - \bar{\varepsilon}_u \right) \qquad (9)$$

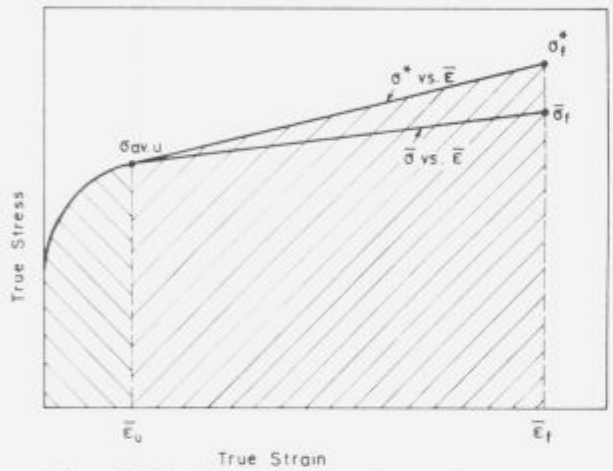

Figure 2: Effective stress, $\bar{\sigma}$, and peak stress, σ^*, versus effective strain at tensile testing (schematically).

Slika 2: Ekvivalentna napetost $\bar{\sigma}$ in maksimalna napetost σ^* v odvisnosti od ekvivalentne deformacije pri natezanju (shematsko).

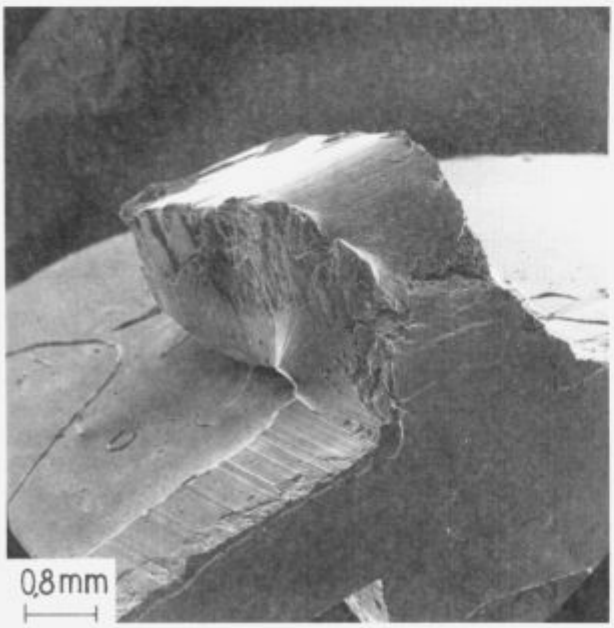

Figure 3: Cracks on commutator segments occured at cold bending.

Slika 3: Razpoke, nastale na krakih kolektorja pri upogibanju v hladnem.

3. Experimental methods

Two copper base alloys declared as CuAg0.2 (OF) and CuAg0.2 respectively were selected for the present study. Both alloys, commercially available as one-half inch diameter wires, contain 0.2 wt. % Ag. This type of copper base alloys has good creep strength at elevated temperatures and high softening temperature and is used for instance for the production of commutators for electrical motors.

The experimental CuAg0.2 alloy contained 0.01 wt. % O and 0.005 wt. % P whereas the CuAg0.2 (OF) alloy i.e. oxygen free alloy contained < 0.005 wt. % O and 0.002 wt. % P. However, the bulk workability of CuAg0.2 alloy with higher oxygen content was essentially worse than that of oxygen free alloy. As shown on **Fig. 3**, a ductile damage occured at cold bending of commutator segments from such oxygen containing CuAg0.2 alloy. On the contrary, the bulk formability of experimental oxygen free alloy was excellent as it didn't present any problems in metalworking processes.

The microstructure of both alloys is shown in **Fig. 4** and **5**. The microstructure of oxygen containing CuAg0.2 alloy (**Fig. 4**) consisted of relatively small grains with twinned areas, whereas the microstructure of oxygen free CuAg0.2 alloy (<0.005 % O) (**Fig. 5**) is characterized by somewhat larger, equiaxed grains

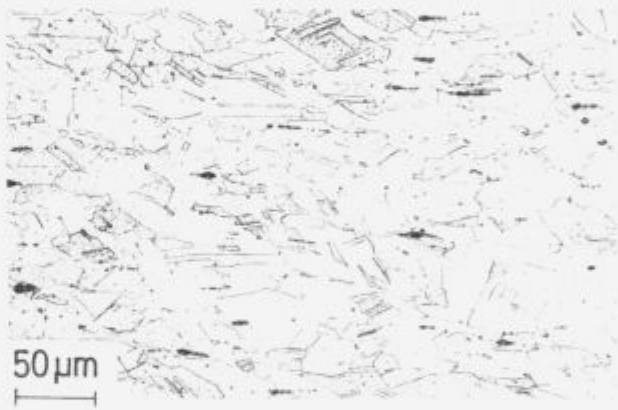

Figure 4: Microstructure of oxygen containing CuAg0.2 alloy, showing relatively small grains with some twinned areas.

Slika 4: Mikrostruktura kisik vsebujoče zlitine CuAg0.2. Razmeroma drobna kristalna zrna s posameznimi področji dvojčenja.

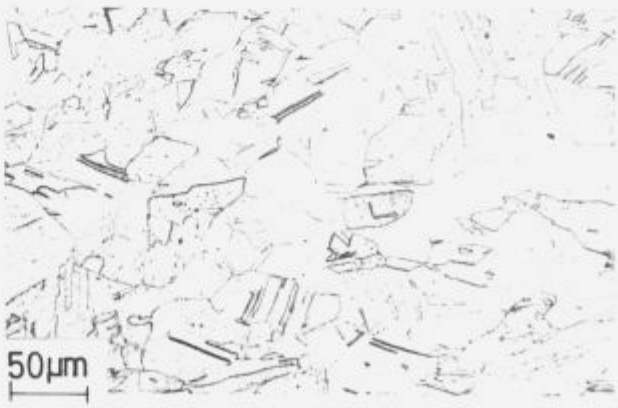

Figure 5: Microstructure of oxygen free CuAg0.2 alloy, showing equiaxed grains with irregular boundaries. Some grains contain twinned areas.

Slika 5: Mikrostruktura kisika proste zlitine CuAg0.2. Enakoosna kristalna zrna z iregularnimi mejami in dvojčki v posameznih zrnih.

with irregular boundaries and twinned areas. The microstructure of both alloys is typical for the as annealed state where only a slight cold reduction was applied at the calibration drawing.

Tensile flow curves were obtained using an Instron machine by pulling standard tensile specimens with gauge sections of 10 mm diameter and 100 mm length at a cross-head speed of 1 mm/min. The neck profile radius was established from the photographs of the necked region using an appropriate geometrical aproximation. A discontinuous compression testing was carried out on a instrumented hydraulic press on specimens with 10 mm in diameter and initial height of 12 mm. In order to minimize the frictional constraints, teflon was used on contact surfaces and constant friction coefficient of 0.024 was achieved. Cumulative height reductions reached 86 %. The strain rate at compression testing was comparable with that at the uniform tension and remained nearly constant over most of the strain range. Load-displacement data obtained were fed into a computer by points for stress-strain analysis. A correction factor for the adequate compensation of friction was also incorporated into the computer program.

4. Results

Fig. 6 are the plots of load vs. elongation at tensile test of both experimental alloys. The values obtained at testing are listed in **Table I**. The yield stress at tensile testing was determined as 0.2 % Offset Yield Stress. The yield stress measured at compression testing is also included in the table (values in parenthesis). As already mentioned, the radius of the minimum cross section of the neck R, and the radius of curvature of the neck profile r, of the tensile specimens were measured too. By the CuAg0.2 alloy (0.01 % O) the neck profile radius was 2.20 mm, the minimum cross section radius was 2.85 mm, whereas at oxygen free CuAg0.2 alloy (<0.005 % O), where more a rupture than a fracture was observed, the neck profile radius was only 0.15 mm and the minimum cross section radius was 1.80 mm.

In **Table II** the values of Hollomon constants calculated from the compression- and tensile tests data are listed. The constants, obtained from tensile test data were determined by various methods of analysis, because the high percent error in $\bar{\varepsilon}_u$ makes sometimes the Eq. (6) unacceptable. However, n is the exponent of an empirical equation (5) and it is not surprising that this equation cannot accurately describe the stress-strain curves in the whole strain range. Man et al.[26] described the tensile curves

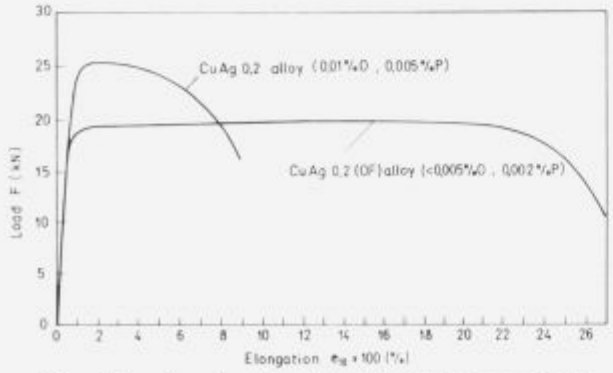

Figure 6: Load vs. elongation at tensile test of both experimental alloys.

Slika 6: Odvisnost med obremenitvijo in raztezkom pri nateznem preiskušanju obeh eksperimentalnih zlitin.

Table I: Tensile test results

Tabela I: Rezultati nateznega preizkušanja

	Yield stress* σ_{y_2} (MPa)	Tensile strength σ_{us} (MPa)	Uniform elongation e_u x 100 (%)	Total elongation e_{10} x 100 (%)	Reduction in area Z x 100 (%)
CuAg0.2 alloy (0.01 % O)	306 (321)	323	2	9	68
CuAg0.2 (OF) alloy(<0.005%O)	232 (248)	258	14.2	27	87

* The values in parenthesis were obtained by compression testing

Table II: Comparison of Hollomon constants by various test methods

Tabela II: Primerjava Hollomonovih konstant dobljenih pri različnih metodah preizkušanja

	Strength coefficient K (MPa)	Strain-hardening exponent n	Correlation coefficient r
Compression Test			
CuAg0.2 alloy (0.01 % O)	397	0.090	0.977
CuAg0.2 (OF) alloyσ (< 0.005 % O)	379	0.139	0.993
Tension test			
CuAg0.2 alloy (0.01 % O)	431	0.087*	
CuAg0.2 (OF) alloy (< 0.005 % O)	385	0.133**	

*Calculated from the true stress-true strain tensile test data

**Calculated from the uniform elongation /Eq. (6)/

Table III: Values of the material constants

Tabela III: Vrednosti materialnih konstant

	σ_{y_2} (MPa)	$\sigma_{av.u}$ (MPa)	$\bar{\varepsilon}_u$	$\bar{\sigma}_f$ (MPa)	$\bar{\varepsilon}_f$	σ^* (MPa)	C/Eq(9)/ (MJ/m^3)
CuAg0.2 alloy (0.01 % O)	306	330	0.019	435	1.124	652	548
CuAg0.2(OF) alloy (<0.005 % O)	232	288	0.129	423	2.040	1246	1499

of copper using two equations of Hollomon type[22]. This kind of analysis is based on the assumption that a change in deformation mechanism occurs during the deformation.

The collection of final results is given in **Table III** where 0.2 % offset yield stress, σ_{y_2}, average ultimate stress, $\sigma_{av.u}$, and fracture stress, σ_f, with corresponding strains, $\bar{\varepsilon}_u$ and $\bar{\varepsilon}_f$ respectively, the highest tensile stress σ^* as well as the material constant C are shown. The value of C, i.e. the value of tensile strain energy density of oxygen free CuAg0.2 alloy (<0.005 % O) is extremely large. This alloy with low oxygen content exhibited

more a rupture than a fracture at tensile testing resulting in adequate small radius of curvature of the neck profile while the tensile stress in necked region strongly increased. In spite of the fact that the original Bridgman[5] analysis and the similar analysis of Davidenkov and Spiridonova[7] give the best approximate procedure for the calculation of stress distribution in the necked region, nowadays, more accurate numerical solutions can be obtained with FEM.

5. Discussion

Using the fracture criterion based on the model of Cockcroft and Latham[2,3], the tensile strain energy density at fracture for two copper base alloys was calculated. The calculation utilized the results of tensile and compression tests. When the constant crosshead-speed is used at tensile test, the strain rate decreases slighty during the homogenous deformation and then rises rapidly as necking occurs. The rise in strain rate during the necking results in an anomalous rise in flow stress and restricts the usefulness of the data obtained by strains smaller than those prevailing during the onset of the necking[27]. Probably some discrepancies between the tensile and the compression test results (see **Table II**) could be explained also with Bauschinger effect and with the assumption that a change in deformation mechanism occurs during tensile deformation. Zankl[28] and Schwink and Vorbrugg[29] found these kind of stages also in the tensile curves of annealed nickel and copper at low strains. Furthermore, Mishra at al.[30] proposed that in the range of uniform strain the Hollomon law overestimates the flow stress in the initial stages and underestimates it in the final stages. It seems therefore, that the tensile test data of experimental copper base alloys should fit better with double-n method which uses the two Hollomon equations. Kleemola and Nieminen[31] found out that the use of the Hollomon equation for pure copper in an annealed state and after 40 pct deformation gives a misleading picture of the strain-hardening properties of the material because the strain-hardening exponent n is not equal to the correct $\bar{\varepsilon}_u$ value. The same was also observed in our CuAg0.2 experimental alloy with 0.01 % oxygen where computer least-squares fits by plotting tensile test data had to be used instead of Eq. (6). In opposition to tensile test data, the compression test data are obtained from a much larger strain range and it is therefore assumed that the use of the simple Hollomon power law relation is justified. The regression analysis of compression test data also gives satisfactory high linear correlation coefficients (0.98 and 0.99 respectively).

The data presented in **Table III** (C-values) shows that at oxygen free CuAg0.2 alloy the integral of the maximal tensile stress over the plastic strain path /Eq. (9)/ reaches a value of approx. 1500 MJ/m^3, which is nearly three times larger than that of CuAg0.2 alloy with 0.01 % oxygen (C approx. 550 MJ/m^3). However, the reduction in area at tensile test of oxygen free CuAg0.2 alloy is only for one quarter larger than that of CuAg0.2 alloy with 0.01 % oxygen. It seems that a considerable increase in ductility may result by an only relatively low improvement in the reduction-in-area value, so that such way of expressing the ductility shows little discrimination in very ductile metals. Namely, once the necking develops, a "negative feedback" effect occurs, which tends to prevent the exhibition of really large ductility values[3]. At the onset of necking, the stress system changes and a component of hydrostatic tensile stress is generated which is superimposed on the axial stress. The hydrostatic tensile stress increases as the neck becomes deeper, with the result that the fracture is more likely to occur. This situation leads to a stabilizing effect and an increase in ductility causes a deeper neck to be formed, hence higher local stresses are developed and a greater possibility of fracture occurs. The Cockcroft-Latham criterion of ductile fracture is therefore a much more reasonable criterion than the criterion based simply on reduction-in-area value at tensile test. However, it should be noticed that at the neck profile which is characteristic for rupture instead of fracture, the extremely high value of tensile stress σ^*, and high tensile strain energy density C, are somewhat doubtful. The equations of Bridgman[5] /(3a,b and c) and (4)/ and equations of Davidenkov and Spiridonova[7] becomes questionable at very low radius of curvature of the neck profile typical for the rupture and when asymptotic continuum mechanics analyses could not be applied for the description of stress state due to local singularity.

The excellent bulk formability of the experimental CuAg0.2 oxygen free alloy with regard to the verification based on the Cockcroft-Latham criterion is not surprising. This criterion has the desirable feature for homogenous compression, in which case the tensile stress σ^* is zero and no fracture limit is predicted. This coincides well with the experimental results at homogeneous (frictionless) compression. However, following the theoretical analysis of Kuhn et al.[1], it is possible to relate the C-value calculated from tensile test data /Eq. (9)/ and the principal tensile and compressive surface strains, i.e. the circumferencial and axial strains measured on the barreled equatorial free surface at fracture in upset test. It was also experimentally confirmed that there is a linear relationship between the tensile and compressive surface strains at fracture by upsetting by rolling and by bending. Consequently, the representation of fracture data as a plot of tensile versus compressive strains at fracture became a useful form for the analysis of the fracture in cold forming processes resulting in a "forming limit diagram concept". The Cockcroft-Latham tensile strain energy fracture criterion is consistent with this concept[1].

6. Conclusions

The Cockcroft-Latham tensile strain energy density criterion was used for a reliable evaluation of the ability of two copper alloys to metalworking operations. This criterion implies that the fracture depends both on the stresses imposed and on the strains developed and it could be described as "fracture will occur when the plastic work of the largest tensile stress, per unit volume, reaches a characteristic critical value".

It was demonstrated that there is a good qualitative agreement between the prediction of formability under bulk metalworking conditions based on this criterion and the observed behaviour in the production of commutators for electical motors. The plastic work done per unit volume by oxygen free CuAg0.2 alloy with excellent bulk formability is nearly three times larger than that done by the oxygen containing CuAg0.2 alloy (0.01 % O), while, the difference in the tensile reduction of area of both alloys was much smaller. Consequently, the reduction-in-area value at tensile test cannot be appreciated in general.

References:

[1] Kuhn, H. A., Lee, P. W., Erturk, T.: *Trans. ASME*, 1973, 213-218.

[2] Cockcroft, M. G.: *Ductility*, American Society for Metals, Metals Park, Ohio, 1968, 199-226.

[3] Cockcroft, M. G., Latham, D. J.: *Journal of the Institute of Metals*, 96, 1968, pp. 33-39. [4] Siebel, E.: *Steel*, 93, 1933, 17, 37.

[5] Bridgman, P. W.: *Studies in Large Plastic Flow and Fracture*, McGraw-Hill, New York, 1952.

[6] Pugh, H. L. D., Green, D.: The Effect of Hydrostatic Pressure on the Plastic Flow and Fracture of Metals, *Proc. Inst. Mech. Eng.*, 179, 1964, No. 1.

[7] Davidenkov, N. N., Spiridonova, N. I.: *Proc. Amer. Soc. Test. Mat.*, 46, 1946, 1147.

[8] Chen, W. H.: *International Journal for Solids and Structures*, 7, 1971, 685-717.

[9] Needleman, A.: *Journal for Mechanics and Physics of Solids*, 20, 1972, 111-127.

[10] Norris, D. M. jr., Moran, B., Schudder, J. K., Quinones, D. F.: *Journal for Mechanics and Physics of Solids*, 26, 1978, 1-17.

[11] Saje, M.: *Int. J. Solids Structures*, 15, 1979, 731-742.

[12] Brozzo, P., Deluca, B., Rendina, R.: A new method for the prediction of the formability limits of metal sheets, *Proceedings of 7th Biennial Congr. of Int. Deep Drawing Research Group*, 1972 (from Dood, B. and Bai, Y.: Ductile Fracture and Ductility, Academic Press inc., London, 1987, 205.)

[13] Oyane, M.: *Bull. JSME*, 15, 1972, 1507-1513.

[14] Clift, S. E.: Identification of defect locations in forged products using the finite element method, *Ph.D.-Thesis*, Univ. of Birmingham, U.K., 1986.

[15] Hoffmanner, A. L.: *Metal Forming - Interrelationship Between Theory and Practice*, A. L. Hoffmanner, ed., Plenum Press, New York, 1971, 349-391.

[16] Osakada, K., Koshijima, J., Sekiguchi, H.: *Bull. JSME*, 24, 1981, 534-539.

[17] Bolt, P. J., Kals, J. A. G., Dautzenberg, J. H.: Prediction of ductile failure in forming, *Proceedings of the Second International Conference on Technology of Plasticity*, Vol. I, Stutgart, August 1987, 385-391.

[18] Wright, R. N., Kircher, T. A., Vervlied, J. R.: *Journal of Metals*, October 1987, 26-29.

[19] Dung, N. L., Mahrenholtz, O.: A Criterion for the Ductile Fracture in Cold Forging, *Proceedings of the Second International Conference on Technology of Plasticity*, Vol. II, Stuttgart, August 1987, 1013-1020.

[20] Vujović, V., Vilotić, D., Plančak, M., Trbojević, I., Francuski, P.: Strain history influence on the material formability, *Proceedings of the Fourth International Conference on Technology of Plasticity*, Vol. I, Beijing, China, September 1993, 275-280.

[21] Luo, Z. J., Ji, W. H., Guo, N. C., Xu, X. Y., Xu, Q. S., Zhang, Y. Y.: A ductile-damage model and its application to metal-forming processes, *Journal of Materials Processing Technology*, Vol. 30, 1992, 31-43.

[22] Hollomon, J. H.: *Trans. AIME*, 162, 1945, 268-290.

[23] Ludwik, P.: *Elemente der Technologischen Mechanik*, Verlag Von Julius Springer, Leiptzig, 1909, 32.

[24] Swift, H. W.: *Journal Mech. Phys. Solids*, Vol. I, 1952, 1-18.

[25] Voce, E.: *Journal Inst. Met.*, 74, 1948, 537-562.

[26] Man, J., Holzmann, M., Vlach, B.: *Phys. Status Solidi*, 19, 1967, 543-553.

[27] Rao, K. P., Doraivelu, S. M., Gopinathan, V.: *Journal of Mechanical Working Technolgy*, No. 6, 1982, 63-88.

[28] Zankl, G.: *Z. Naturforsch.*, 18a, 1963, 795-809.

[29] Schwink, Ch., Vorbrugg, W.: *Z. Naturforsch.*, 22a, 1967, 624-642.

[30] Mishra, N. S., Mishra, S., Ramaswamy, V.: *Metallurgical Transactions A*, 20A, 1989, 2819-2829.

[31] Kleemola, H. J., Nieminen, M. A.: *Metallurgical Transactions A*, 5, 1974, 1863-1866.

Kovine, zlitine, tehnologije / letnik 28 / 1994 / številka 4 / strani 601 do 608

Properties of Cu-based Alloys-powders for Brazing Prepared by Water Atomization

Lastnosti prahov-zlitin na osnovi bakra izdelanih z vodno atomizacijo

B. Šuštaršič*, B. Breskvar, V. Leskovšek, A. Rodič, Institute of Metals and Technologies, Ljubljana, Slovenia

Cu based alloys-powders are currently used as solder and brazing agents in many fields of application. Cu-Ag based alloys-powders are the most common brazing agents used in electrical engineering and electronics. Similarly, Au-Cu based alloys-powders find many applications in electrical engineering and electronics as well as in jewellery. Vacuum brazing of tool and high speed steels as well as hard metals (cemented carbides) on the structural steel base with Cu-Ni or Cu-Cr base alloys-powders is also increasingly used in many fields of application. Fluid and centrifugal atomization are the most frequent and therefore the most important manufacturing methods for the production of Cu based alloys-powders. Among the fluid atomization processes, gas and water atomization are the most common and the most important ones. The stream of liquid metal is disintegrated by high pressure jets of inert gas (N_2, Ar or He) or water. Gas atomization makes it possible to produce high quality, on the surface non-oxidized spherical powder particles. Water atomization is a simpler and cheaper powder manufacturing method. The metal powder produced by water atomization usually has irregularly shaped particles which are coated with a thin oxide film. In spite of that, the gas atomized powders could be replaced by water atomized powders in many fields of application. We therefore investigated the applicability of water atomization for the preparation of Cu based alloys-powders. The present article introduces the morphological and microstructural characteristics of prepared Cu-based alloys-powders and possibilities for their application.
Key words: powder manufacturing, powders for brazing, water atomization, properties of Cu-based alloys-powders.

Prahovi-zlitine na osnovi bakra se uporabljajo na mnogih področjih kot sredstva za mehko in trdo spajkanje. V elektrotehniki in elektroniki so najpogostejše spajke na osnovi Cu-Ag. Podobno se zlitine na osnovi Au-Cu uporabljajo v elektrotehniki, elektroniki in tudi zlatarstvu. Vakuumsko spajkanje orodnih jekel ali karbidnih trdin na osnovo iz konstrukcijskega jekla s prahovi-zlitinami na osnovi Cu-Ni ali Cu-Cr se tudi vse bolj uveljavlja v praksi. Prahovi-zlitine na osnovi Cu se najpogosteje izdelujejo s tekočinsko in centrifugalno atomizacijo. Med postopki tekočinske atomizacije se najpogosteje uporabljata plinska in vodna atomizacija. Curek raztaljene kovine pri teh postopkih razpršimo v hitro strjene delce prahu s pomočjo visokotlačnih curkov inertnega plina (He, Ar ali N_2) ali vode. Plinska atomizacija omogoča izdelavo visoko kakovostnih neoksidiranih prahov krogličnе oblike. Vodna atomizacija je enostavnejši in cenejši postopek, vendar so tako izdelani kovinski prahovi običajno površinsko oksidirani in imajo zato tudi nepravilno oblikovane delce. Kljub temu bi lahko vodno atomizirani prahovi na mnogih področjih zamenjali dražje plinsko atomizirane prahove. Zato smo raziskovali možnost uporabe vodne atomizacije za izdelavo kovinskih prahov-spajk na osnovi Cu. V pričujočem delu so predstavljene morfološke in mikrostrukturne značilnosti izdelanih prahov ter posledično možnosti njihove praktične uporabe.
Ključne besede: izdelava kovinskih prahov, prahovi za trdo spajkanje, vodna atomizacija, lastnosti prahov zlitin na osnovi Cu.

1. Introduction

Metal powders are used extensively as filler material in the brazing and soldering industries[1]. Powders offer the most convenient method of applying filler metal to parts which have to be joined (bonded) together, although alternative filler metal forms (wire, rod, sheet, foil, etc.) are also used. Filler metals (alloys) for brazing have liquidus temperature above 450°C and below the solidus of the base metal, and filler metals for soldering have liquidus temperature below 450°C and below the solidus of the base metal. For brazing and soldering applications metal alloys-powders either as pure powder without additions or in flux-powder paste form are used.

Cu based alloys-powders are currently used as brazing agents (filler material) in many fields of application. Cu-Ag based alloys-powders are the most common brazing agents used in electrical engineering and electronics. Similarly, Au-Cu based alloys-powders find many applications in electrical engineering and electronics as well as in jewellery. Vacuum brazing of tool and high speed steels (HSS) as well as hard metals (cemented carbides) on the structural steel base with Cu-Ni or Cu-Cr as well

* Mag. Borivoj ŠUŠTARŠIČ, dipl. inž.,
IMT Ljubljana, Lepi pot 11, 61000 Ljubljana

as Ni-Cr base alloys-powders is also increasingly used in many fields of application[2,3].

Fluid and centrifugal atomization are the most frequent and therefore the most important manufacturing methods for the production of Cu based alloys-powders. Among the fluid atomization processes, gas and water atomization are the most common and the most important ones[4,5]. The stream of liquid metal is disintegrated either by high pressure (commonly 10 - 30 bars) jets of inert gas (N_2, Ar or He) or by high pressure (commonly 100 - 300 bars) jets of water. **Fig. 1** represents schematically a gas atomizer and the disintegration of a free falling molten metal stream by high pressure jets of inert gas.

Gas atomization makes it possible to produce high quality, on the surface non-oxidized spherical powder particles. Water atomization is a simpler and cheaper powder manufacturing method. **Fig. 2** shows schematically the production of metal powder by water atomization.

The metal powder produced by water atomization usually has irregularly shaped particles which are coated with a thin oxide film. In spite of that, the gas atomized powders could be replaced by water atomized powders in many fields of application. We therefore investigated the applicability of water atomization for the preparation of Cu based alloys-powders.

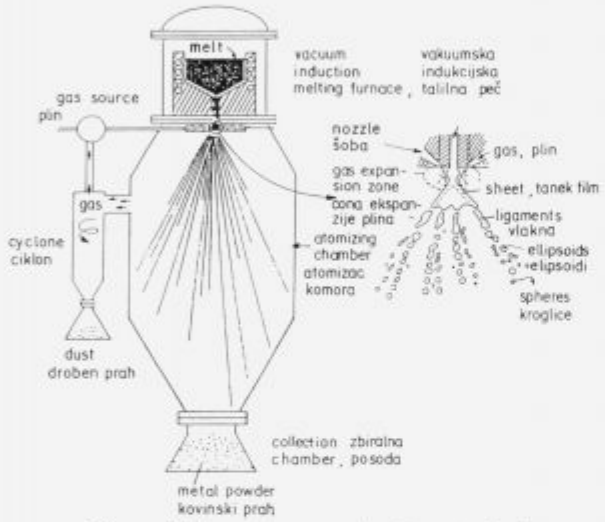

Figure 1: Schematic presentation of gas atomizer[4]

Slika 1: Shematični prikaz postopka plinske atomizacije[4]

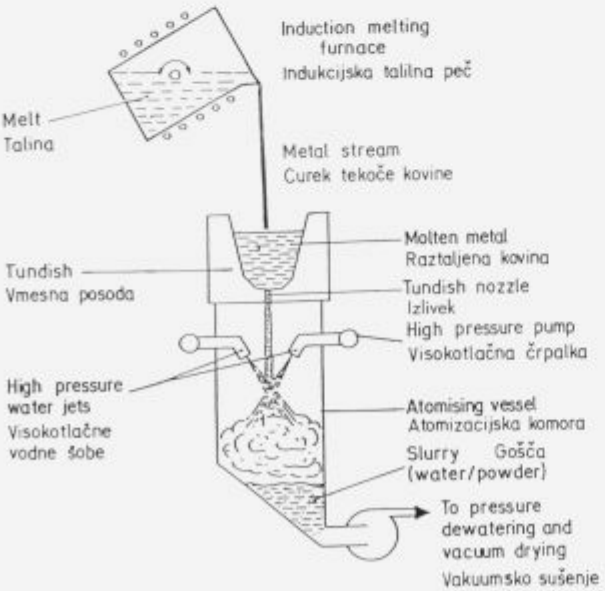

Figure 2: Schematic presentation of water atomization[6]

Slika 2: Shematični prikaz postopka vodne atomizacije[6]

2 Experimental procedure

Most of the experiments and investigations have been done at the Institute of Metals and Technologies, Ljubljana.

Two different vacuum brazing alloys (Cu with 2% of Ni and Cu with 1,5% of Cr) and two typical Cu-Ag based brazing alloys (L-Ag15P and L-Ag40Cd) were selected for our experiments and investigations. For the comparison some other types of alloys-powders (Ni and Co-based powders for welding, HSS powders, Alnico hard magnetic powders) of previous investigations[7,8,9,10] were also used. The powders of selected alloys were prepared by water atomization (pilot atomizer Davy McKee, type D5/2) installed at IMT Ljubljana (see **Fig. 3**).

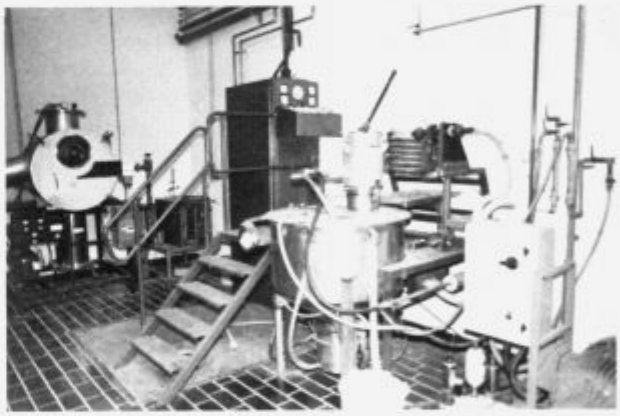

Figure 3: PM&RST laboratory at the IMT Ljubljana with water atomizer in the foreground.

Slika 3: PM&RST laboratorij na IMT Ljubljana z vodnim atomizerjem v ospredju.

Table 1: Chemical compositions of prepared Cu-Ag based water atomized powders in comparison with ASTM standardized[1] brazing alloys-powders.

Tabela 1: Kemične sestave z vodno atomizacijo pripravljenih prahov na osnovi Cu-Ag v primerjavi z zlitinami standardiziranimi po ASTM standardih[1]

Material	B CuP-5	L Ag15P	B Ag-2	L Ag40 Cd
	nominal	IMT	nominal	IMT
Elements	(mass %)			
Cu	≥79,85	balance	26,0	19,0
Ag	15,00	14,9-15,60	35,0	40,0
P	5,00	6,0-6,20	–	–
Zn	–	–	21,0	21,0
Cd	–	–	18,0	20,0
Other elements	0,15max.	not determined	0,15max.	not determined

Table 2: Process parameters of water atomization for the preparation of Cu-2%Ni and Cu-Ag based alloys-powders.

Tabela 2: Procesni parametri postopka vodne atomizacije za pripravo kovinskih prahov Cu-2%Ni in Cu-Ag.

Process parameter (water atomizer D5/2 Davy McKee	Cu-2%Ni alloy	Cu-Ag alloys	Remarks
Temperature of superheating (°)	1230±20°C	810±30°C	pyrometer
Tundish temperature (°)	1210±20°C	850±30°C	Pt-PtRh 13
Tundish nozzle diameter (mm)	∅4,0/4,5	∅4,0/4,5	fused quartz
Metal flow rate (kg/min.)	4,5-5,5	5,6-7,3	
Water nozzle diameter (mm) two (2) main nozzles two (2) side nozzles	 1,2 x 1,05 1,1 x 0,85	 1,2 x 1,05 1,1 x 0,85	 1503 type 1502 type
Jet apex angle (°) between main water streams between side water streams	 50 40	 50 40	 original manifold
Water/metal ratio	11–12	7,3–9,6	
Water pressure range (bar)	120	180–215	manometer
Protective atmosphere (nitrogen)	0,6m³/h	0,65m³/h	flow meter

The initial chemical compositions (ingots for melting) as well as the final chemical compositions of prepared powders were determined and controlled by classical chemical analysis. No significant difference between initial and final compositions was observed. In **Table 1** the chemical compositions of selected Cu-Ag brazing alloys are presented.

The process parameters of water atomization are water pressure, tundish nozzle diameter, apex angle and diameter of water jets, superheating of the melt, etc. The main influent powder particle size parameter of these is water pressure[11] and water velocity, respectively. In the first stage of our experiments the process parameters of water atomization were established and optimized in order to get an optimal mean particle size and optimal particle size distribution. For brazing, first of all the powder fractions between 45 and 125 µm are commonly used. In **Table 2** the main controlled process parameters of water atomization during our experiments are presented.

All prepared powders were then sieved and their main morphological properties (particle shape, particle size distribution, mean particle diameter, apparent density and flowability) were determined. Besides the chemical composition of the alloy, these powder properties are the main applicability criteria of metal powders for brazing.

3 Results and discussion

All prepared powders were examined by optical and scanning electron microscopy (SEM). The micrographs show microstructures which strongly depend on the particle size and the cooling rate. **Fig. 4** and **5** show the typical microstructure of prepared powders. Some internal porosity of powder particles was noticed. **Fig. 6** shows the SEM micrograph of a water atomized Cu-2%Ni alloy-powder with nearly spherical particles. **Fig. 7** shows internal porosity of a water atomized Cu-Ag (L Ag15-P) based alloy-powder. Particularly Cu-Ag based alloys-powders show a large amount of powder particles with internal porosity.

The standard sieving analysis, as well as the Silas Alcatel laser granulometry of powders were also performed[4,5,12]. The powders have a regular and partially irregular particle shape. The mean particle diameter of prepared powders strongly depends on the water pressure used. The portion of irregularly shaped particles raises with increasing water pressure (increased collision between droplets of molten metal as well as partially solidified particles during atomization). The relatively high portion of regularly shaped particles confirms the sometimes forgotten fact[6] that water atomization can also produce nearly spherical powders, which is a condition for high apparent density and good flowability of powders.

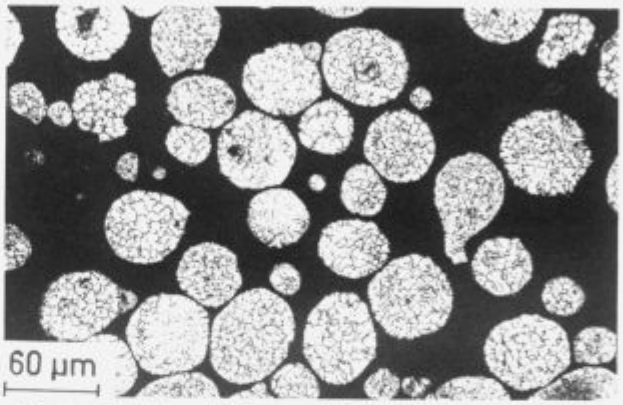

Figure 4: Cellular solidification of Cu-2%Ni alloy-powder particle.

Slika 4: Celična strjevalna mikrostruktura delca Cu-2%Ni prahu.

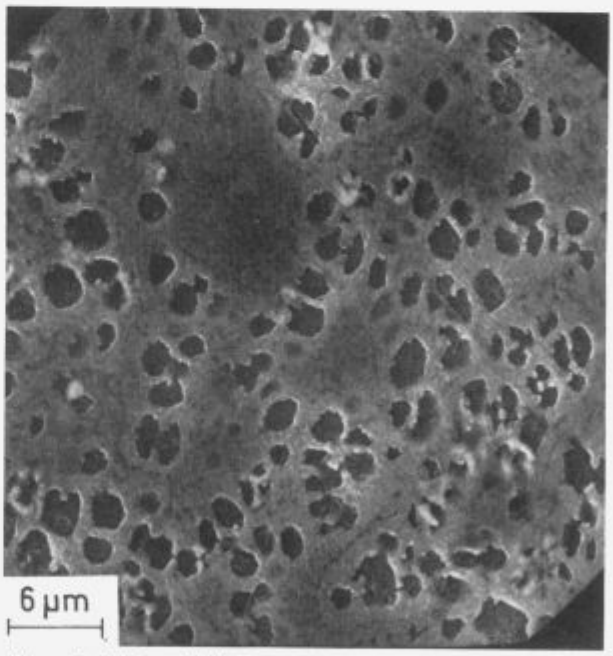

Figure 5: Cellular solidification of Cu-Ag (L Ag15-P) alloy-powder particle.

Slika 5: Celična strjevalna mikrostruktura delca Cu-Ag prahu (L Ag15-P).

The mean particle diameter of prepared Cu-2%Ni powders is approximately 50 µm at atomizing pressure 120 bars with a relatively regular particle shape and narrow particle size distribution (standard deviation $\sigma = 2,2$). The mean particle diameter of the prepared Cu-1,5%Cr powders is approximately 55 µm at atomizing pressure 150 bars with a higher amount of irregularly

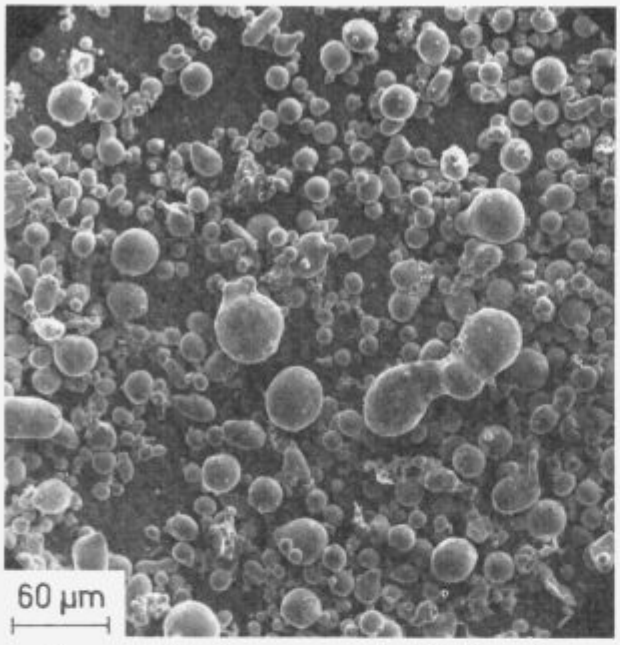

Figure 6: Particle shape of prepared Cu-2% Ni alloy-powder.
Slika 6: Oblika delcev pripravljenih Cu-2% Ni prahov.

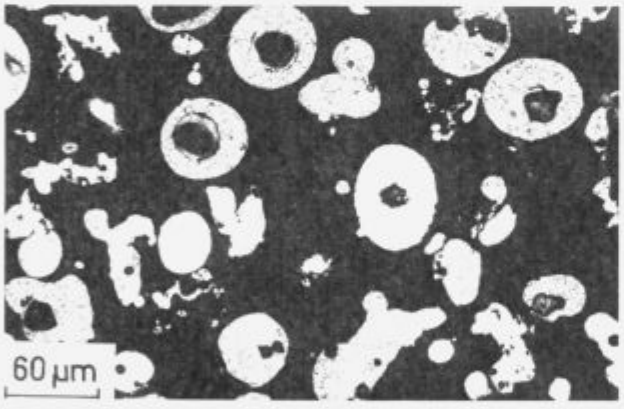

Figure 7: Internal porosity of nearly spherical Cu-Ag alloy-powder particles.
Slika 7: Notranja poroznost delcev Cu-Ag prahov.

shaped particles (high melting point Cr oxide formation) in comparison with Cu-Ni powders but a relatively narrow particle size distribution (σ = 2,1) is obtained. The preparation of Cu-Ag based powders was performed at considerably higher atomizing pressures (180 to 220 bars) in order to get a higher amount of particle size fractions below 125 µm. The mean particle diameter of the prepared Cu-Ag powders is approximately 70 µm at 180 bars and approximately 45 µm at the atomizing pressure 215 bars with a higher amount of irregularly shaped particles (increased collision) in comparison with Cu-Ni powders and a relatively narrow particle size distribution (σ = 2,25) is also obtained. Two informative atomizing experiments for the preparation of Au-Cu based alloys-powders (alloy with 58 mass % of Au - 14 carat gold and alloy with 75 mass % of Au - 18 carat gold) were also

Figure 8: SEM micrograph of Au-Cu water atomized powder with irregularly shaped (tear drop and ligamental) particles.
Slika 8: REM posnetek vodno atomiziranega prahu na osnovi Au-Cu z delci nepravilne (vlaknaste in kapljičaste) oblike.

performed. The mean particle diameter of the prepared Au-Cu powders is approximately 55 µm at atomizing pressure 140 bars with a relatively high amount of irregularly shaped particles (see **Fig. 8**).

Unfortunately our pilot water atomizer is too large (15 kg/batch) for the preparation of small quantities of the very expensive Au-Cu based alloys-powders which are normally used in practice. For these types of alloys-powders a small atomizer with the capacity of up to 0,5 kg/batch max. is suitable. We therefore decided to give up further experimental work until we purchase a small gas/water atomizer suitable for the preparation of these alloys-powders.

For other constant process parameters of atomization, the relationship between water pressure and the mean particle size shows a good, from the literature[4,5,6,11] well known exponential correlation ($D_{50} = k \cdot P_{H2O}^{n}$) for all prepared powders. The constants **k** and **n** depend on the alloy composition, the geometry of the atomizer and other process parameters of atomization. For the Cu-Ag based alloy (L Ag15-P type) the constants are estimated as **k** ≈ 8900 and **n** ≈ -0,96 for the tundish nozzle diameter 4,0 mm and the other process parameters of atomization given in **Table 2**. **Fig. 9** shows the experimental correlation: mean parti-

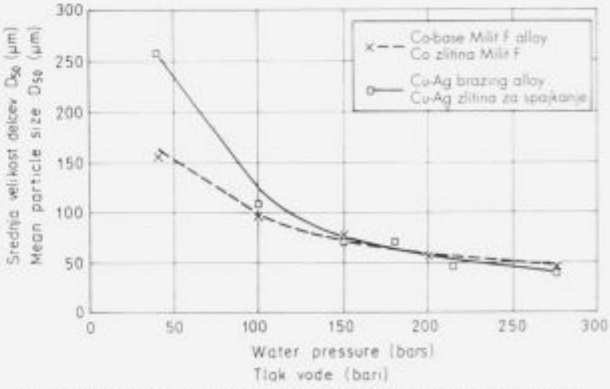

Figure 9: Mean particle size vs. water pressure for Cu-Ag brazing-alloy powder and Co-based welding-alloy powder.
Slika 9: Povprečna velikost delcev v odvisnosti od tlaka vode za prahove na osnovi Cu-Ag in prahove za navarjanje na osnovi Co.

cle size vs. water pressure for the Cu-Ag brazing alloy-powder and the Co-based welding-alloy powder. The influence of chemical composition is evident.

All prepared powders have the bimodal particle size distribution with two maxima at approximately 40 to 60 μm and approximately 100 to 180 μm virtually independent of the applied water pressure and other parameters of water atomization. This confirms the statement[13] that the disintegration of the molten metal stream during water atomization is carried out in two steps (the so-called primary and secondary disintegration). **Fig. 10** presents the sieving analysis of Cu-Al powders with noticeable bimodal particle size distribution and the influence of chemical composition. **Fig. 11** shows the bimodal particle size distribution of prepared Co-based water atomized powders determined by laser granulometry[9]. Bimodal particle size distribution with two maxima is clearly evident.

In the Wösthoffs apparatus the oxygen content of prepared powders was determined. The prepared water atomized powders have a relatively high oxygen content in spite of the fact that for pure metals (Cu, Ag, Ni and Au) Gibbs free entalphy for the reaction $Me+H_2O=MeO+H_2$ is positive[6,14] and therefore theoretical possibility for oxidation of pure metals with water steam is relatively low. Obviously, the alloying elements and impurities with higher affinity to oxygen (Cr, Mn, Cd, Zn, P, etc.) have an important influence on thin oxide film formation on the surface of powder particles as well as other factors which can increase oxygen content (discussed later in the article). **Fig. 12** shows that from the theoretical point of view, for some pure metals as well as alloys smaller oxygen contents in water atomized powders could be expected, and vice versa. In spite of that a rough estimation of oxygen content in water atomized powders is possible from this diagrammatic presentation. The diagram is based on literature[6] as well as our own experimental data.

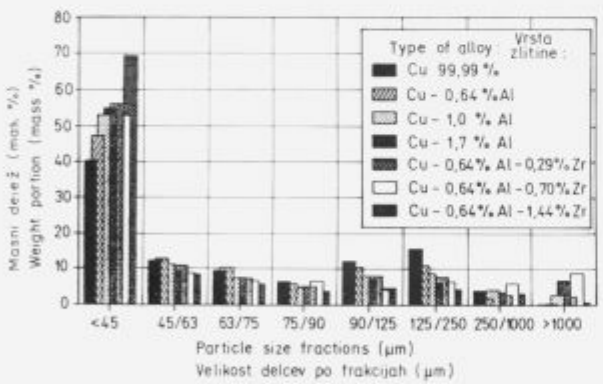

Figure 10: Sieving analysis histograms of Cu-Al water atomized powders.

Slika 10: Histogrami sejalnih analiz Cu-Al vodno atomiziranih prahov.

The plot oxygen content vs. particle size fractions exhibits, for most powders, the minimum oxygen content for particle fractions between 60 and 90 μm. The explanation of this phenomenon is in the combination of the effects of the particle size and the cooling rate (specific surface area - degree of oxidation) of particles during water atomization[1]. Exceptionally, powders with a high degree of particle shape irregularity exhibit a direct proportional increasing degree of oxidation with increased specific surface area of the powder[1]. **Fig. 13** shows the plot oxygen content vs. particle size fractions of different prepared powders with

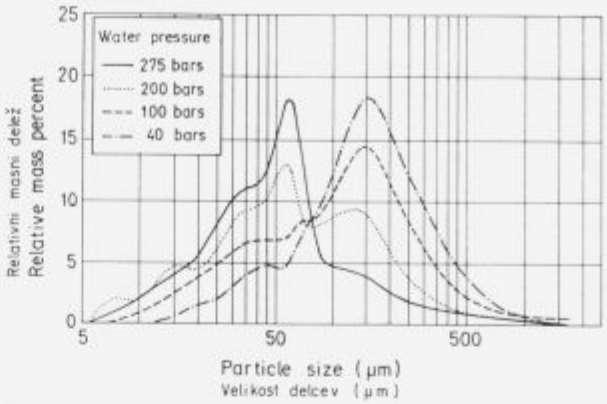

Figure 11: Bimodal particle size distribution of Co based welding alloy-powders performed by laser granulometry.

Slika 11: Dvogrba velikostna porazdelitev delcev prahov za navarjanje na osnovi Co dobljena z laserskim granulometrom.

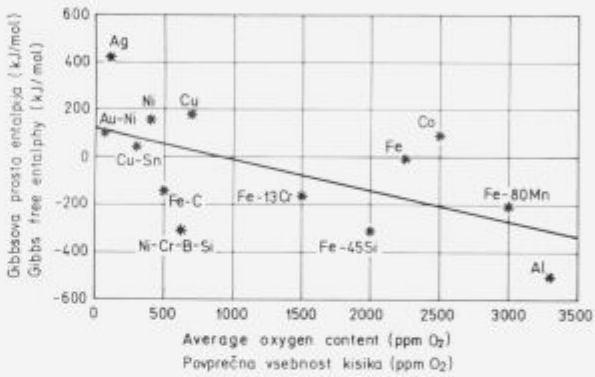

Figure 12: Gibbs free entalphy for the reaction $Me+H_2O=MeO+H_2$ vs. oxygen content for different water atomized alloys-powders.

Slika 12: Gibbsove proste entalpije za reakcije $Me+H_2O=MeO+H_2$ v odvisnosti od vsebnosti kisika za različne vodno atomizirane prahove–zlitine.

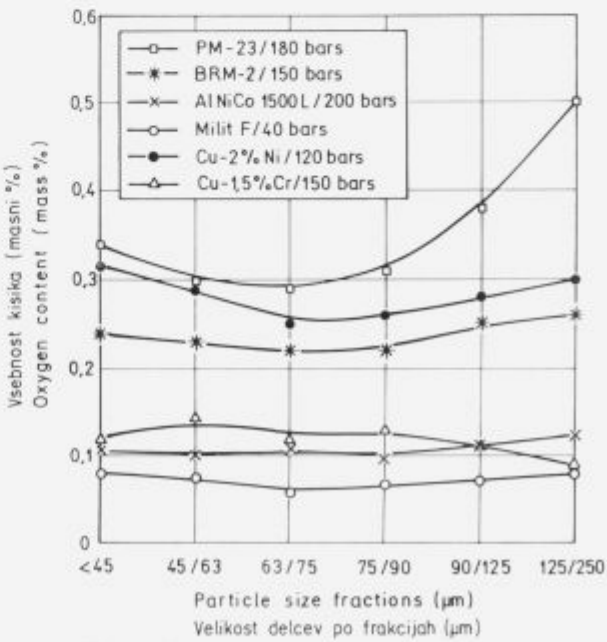

Figure 13: Oxygen content of prepared powders.

Slika 13: Vsebnost kisika v izdelanih prahovih.

the minimum oxygen content for particle size fractions between 60 and 90 μm.

The average oxygen content of prepared Cu-2%Ni powders is 0,23 mass % O_2, for Cu-1,5%Cr powders 0,15 mass % of O_2 and for Cu-Ag powders 0,15 mass % of O_2. Our opinion is that a considerable reduction of these values is possible by an additional optimization of water atomization (melting time reduction, superheating temperature as low as possible, inert gas blowing or protective slag used during melting, reduced water/powder particle interconnecting time, etc.). For example, the average oxygen content 0,075 mass % for Cu-Ag alloy-powder was already obtained during our experiments.

The relatively high oxygen content found in prepared Cu-based alloys-powders requires the consideration in what forms the oxygen can be found in powder particles. It is usually found in metal particles in the following forms: dissolved oxygen, surface oxides, surface adsorbed molecular oxygen and discrete oxides. The Ni and Cu-based powders can contain several thousand ppm of dissolved oxygen if not adequately deoxidised prior atomization[18]. The free energy for the reaction of Ni and Cu with water steam is positive, which suggests that the amount of surface oxides present in the Cu-Ni based powders is insignificant. The origin of discrete oxides is usually slag and refractory particles. The surface adsorbed molecular oxygen, which results from powder handling after the atomization, must not be neglected, either. In our future experiments, it would therefore be necessary to determine precisely the individual contribution of the above mentioned oxides to the total oxygen content of Cu-Ni powders.

The flowability and the apparent density of powders were determined with the Hall's apparatus[12]. The flowability raised with increased sphericity of powders. The fractions between 45 μm and 125 μm of all prepared powders have relatively good flowability but the particle size fraction below 45 μm has no flowability, except Cu-2%Ni and Cu-Ag powders prepared at the lowest (120 bars) water pressure. **Fig. 14** shows the correlation: flowability of prepared powders vs. particle size fractions. The powder fractions between 63 μm and 125 μm have the best flowability. The prepared Cu-2%Ni powders have the best flowability in comparison with other prepared powders. This is in accordance with the highest amount of regular (spherical) powder particles obtained for this type of alloy.

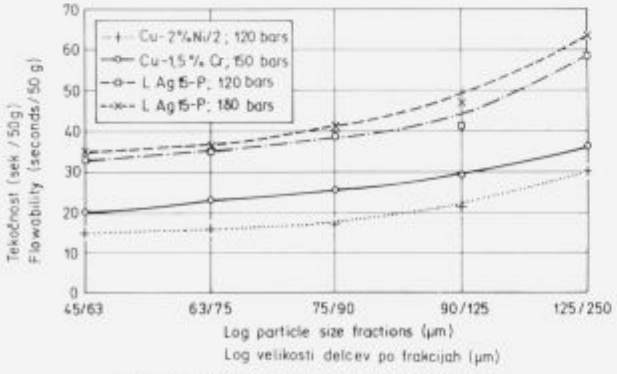

Figure 14: Flowability of prepared powders.
Slika 14: Tekočnost izdelanih prahov.

Fig. 15 shows the correlation: apparent density of prepared powders vs. particle size fractions. The highest apparent as well as tap densities are obtained for the finest fractions of powders. In accordance with high amounts of internal particle porosity of prepared L Ag15-P alloy-powders a relatively poor apparent as well as tap density of these powders is obtained.

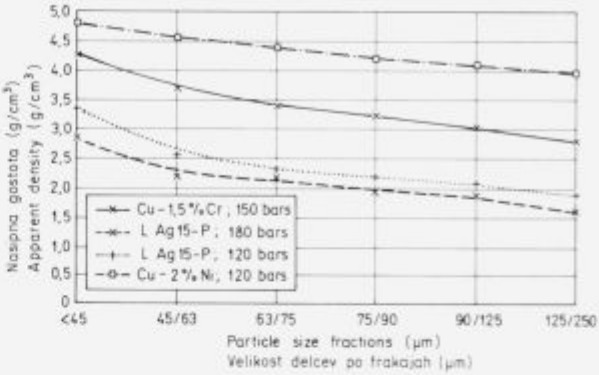

Figure 15: Apparent densities of prepared powders.
Slika 15: Nasipne gostote izdelanih prahov.

The determined morphological properties of prepared alloys-powders show that water atomized powders could be useful for different brazing applications, where relatively high oxygen content is not harmful (vacuum brazing, brazing in reductive atmosphere, brazing with alloy additions of deoxidizers or fluxes that produce light low melting point protective slags). Therefore we also made some brazing experiments[2,15,16]. Vacuum brazing of high speed steel (circular saw segments and paper knifes) on the structural steel base with a Ni-Cr based alloy (Nicrobraz Wall Colmonoy type 30 and LM filler metals) as well as with the prepared Cu based brazing alloy-powder gives high strength, non porous and other defect free, well diffusion bonded joints. **Fig. 16** shows a high temperature vacuum brazed high speed steel (circular saw segments) on the structural steel base with simultaneous heat treatment performed at IMT Ljubljana. **Fig. 17** shows the microstructure of a high temperature vacuum brazed tool steel/structural steel joint produced at IMT Ljubljana with a Cu-based brazing powder.

Vacuum brazing of sharp edged WC-Co particles on the steel plate also gives good results. **Fig. 18** shows vacuum brazing of sharp edged WC-Co particles on a steel plate (grinding wheel)

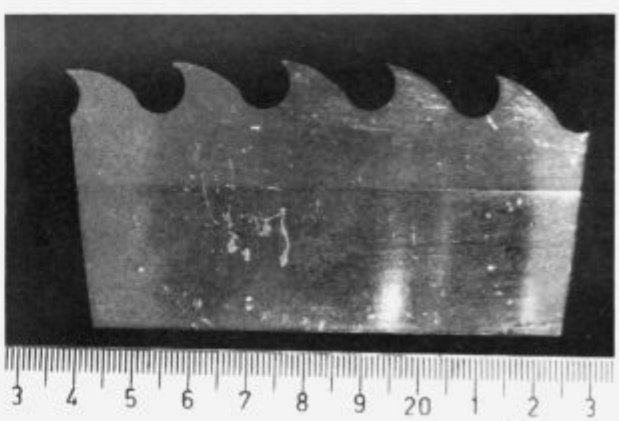

Figure 16: Vacuum brazing of high speed steel (circular saw segments) on the structural steel base.
Slika 16: Segment krožne žage iz orodnega jekla vakuumsko spajkan na osnovo iz konstrukcijskega jekla.

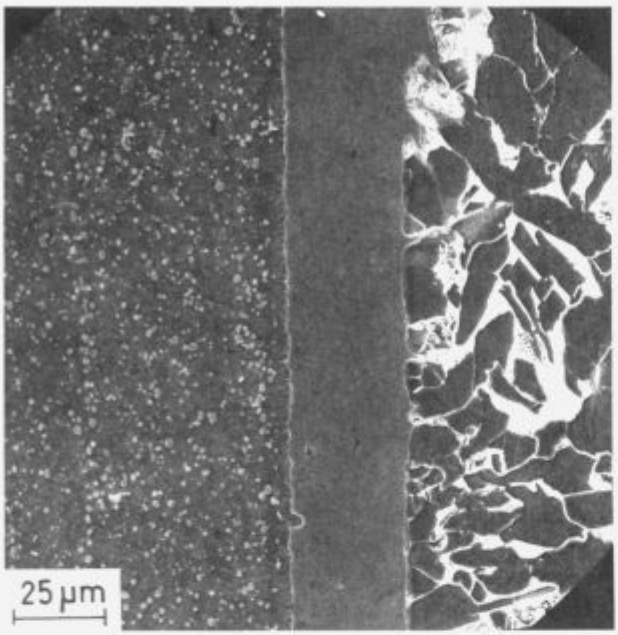

Figure 17: Microstructure of high temperature brazed tool steel/structural steel joint.

Slika 17: Mikrostruktura vakuumskega spoja orodnega in konstrukcijskega jekla.

with a prepared Cu-2%Ni brazing alloy-powder performed at IMT Ljubljana. Cu-Ag based alloys-powders also give good brazing results and the above mentioned brazing alloys are already produced on the level of small scale production for Slovenian electrical engineering industry (ISKRA Autoelektrika Nova Gorica, Metalflex Tolmin, etc.). **Fig. 19** shows industrial vacuum brazing of heating elements on the steel plate carrier performed at IMT Ljubljana. **Fig. 20** shows electrical components industrially brazed with water atomized Cu-Ag based alloys-powders.

4 Conclusions

The preparation of Cu based brazing alloys-powders by water atomization was investigated. The main morphological properties of prepared powders were then determined. The determined morphological properties of prepared alloys-powders, as well as practical brazing experiments show that water atomized powders could be successfully used in many brazing applications, especially where relatively high oxygen content in water

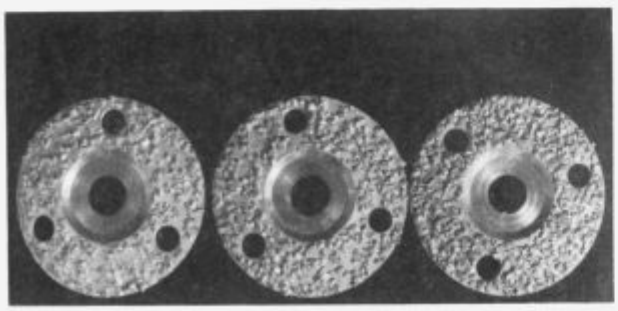

Figure 18: Vacuum brazing of WC-Co particles on the steel plate.

Slika 18: Vakuumsko spajkanje ostrorobih delcev karbidne trdine na jekleno osnovo.

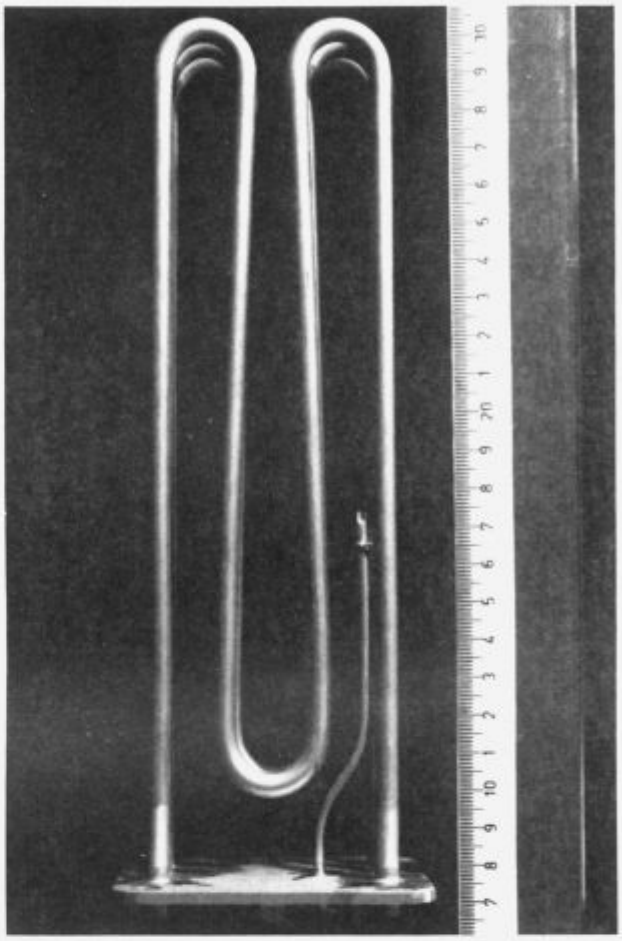

Figure 19: Vacuum brazing of boiler heating elements on the steel plate carrier.

Slika 19: Vakuumsko spajkanje grelnih elementov na jekleno nosilno osnovo.

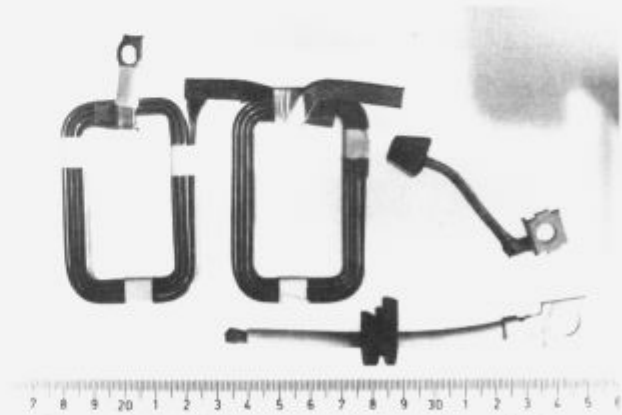

Figure 20: Electrical components for automotive applications industrially brazed with water atomized Cu-Ag based alloys-powders manufactured at IMT Ljubljana.

Slika 20: Električni sestavni deli za avtomobilsko industrijo spajkani z vodno atomiziranim Cu-Ag prahom izdelanem na IMT Ljubljana.

atomized powders is not harmful. However, practical brazing experiments supported by metallographical and mechanical investigations of each individual brazing application are always necessary in order to confirm the usability of the selected water atomized Cu based alloy-powder.

An important fact that has to be considered is the yield of usable metal powder (fraction +45 -125μm up to +45 -75μm) for brazing applications. Water and gas atomization give approximately the same but relatively poor powder yield (=25÷35%). Centrifugal atomization gives a better yield (= 40%) but seems to present some practical difficulties in engineering and reliability[17]. Therefore, from this point of view, it can be concluded that water atomized powders for brazing are comparable with gas atomized powders.

References

[1] E. Klar et al.: Part 3: Production of Metal Powders and Part 7: Powder Systems and Applications - Metal Powders Used for Brazing and Soldering, Metal Handbook, 9th edition, Volume 7, *Powder Metallurgy*.

[2] V. Leskovšek, D. Kmetič, J. Gnamuš, G. Rihar: High Temperature Vacuum Brazing of HSS on Construction Steel with Simultaneous Heat Treatment, *Vuoto*, 20, 1990, 2, 515-518.

[3] M. Stöck, K. Hack: Thermochemical Aspects of Multiphase Diffusion during Brazing of Hard Metal, *Z. Metallkd.* 84, 1993, 11, 759-766.

[4] R. M. German: *Powder Metallurgy Science*, Metal Powder Industries Federation (MPIF), Princeton, New Jersey, 1984.

[5] F. V. Lenel: *Powder Metallurgy* - Principles and Applications, MPIF, Princeton, New Jersey, April 1980.

[6] J. J. Dunkley: The Production of Metal Powders by Water Atomization, *Powder Metallurgy International*, Vol. 10, No. 1/78.

[7] B. Šuštaršič, S. Beseničar, J. Holc, Z. Lengar, S. Tašner: Water Atomized Fe-Co-based Powders for AlNiCo magnets, *8th International Conference on Powder Metallurgy in Czechoslovakia*, October 1992, Pieštany, ČSFR, Conference Proceedings Vol. 3, pp. 261-264.

[8] M. Torkar, B. Šuštaršič: Microstructural Characteristics of Water Atomized Powder of Ni-superalloy, *Praktische Metallographie*, Sonderbände 24, Carl Hansen Verlag, München-Wien, pp. 79-85.

[9] B. Šuštaršič, A. Rodič, M. Torkar, F. Vodopivec: Preparation of Cobalt Based Powders by Water Atomization, *Metallurgy*, 33, 1994, 4, 147-150; Croatian Metallurgical Society, Faculty of Metallurgy Sisak, University of Zagreb.

[10] B. Šuštaršič, M. Torkar: Manufacturing of High Speed Steel Powders by Water Atomization (Slovenian language), *VAKUUMIST* - Slovenian Society of Vacuum Technology, Ljubljana, May 1991, No. 23-24, 1991/2-3, 9-15.

[11] J. J. Dunkley, J. D. Palmer: Factors Affecting Particle Size of Atomized Metal Powders, *Powder Metallurgy International*, 29, 1986, 4.

[12] MPIF: *Standard Test Methods for Metal Powders and Powder Metallurgy Products*, Metal Powder Industries Federation, Edition 1985/1986, Princeton, New Yersey.

[13] M. Bürger, E. V. Berg, S. H. Cho, A. Schatz: Fragmentation Processes in Gas and Water Atomization Plants for Process Optimization Purposes, I. Discussion on the Main Fragmentation Processes, *Powder Metallurgy International*, 21, 1989, 6, 10-14.

[14] C. Jörgensen, I. Thorngren: *Thermodynamic Tables for Process Metallurgists*, Almqvist & Wiksell, Stockholm, 1969.

[15] D. Kmetič et al.: *Bonding of Tool Steels with Structural Steels in Vacuum Heat Treatment Furnace*, IMT Ljubljana R&D reports (Slovenian language), November 1988, No. MI 87-032.

[16] D. Kmetič et al.: *High Temperature Brazing with Simultaneous Heat Treatment in Vacuum*, IMT Ljubljana R&D reports (Slovenian language), November 1991, No. IMT 89-064.

[17] J. J. Dunkley: The Atomisation of Electronic Grade Solder Powder, *Powder Metallurgy World Congress PM'94, Paris*, Conference Proceedings Vol. 2, 353-356.

[18] J. J. Dunkley: The Factors Determining the Oxygen Content of Water Atomized 304L Stainless Steel Powder, *Reprint of Paper Presented at the National PM Conference*, Philadelphia, U.S.A., May 1981, Davy-Loewy R&D Centre.

Kovine, zlitine, tehnologije / letnik 28 / 1994 / številka 4 / strani 609 do 611

Use of a Mathematical Model GPRO to Describe Complex Gas - Metal Reactions

Uporaba matematičnega modela GPRO pri opisovanju kompleksnih reakcij med plinsko in kovinsko fazo

B. Koroušić*, Institute for Materials and Technologies, Ljubljana, Slovenia

The knowledge of the thermodynamics in complexe systems consists of gases and metal shoud be valuable for the control of industrial processes. The Gibbs energy minimization model has been implemented in the software program GPRO and associated with a powerfull reliable database. This computer package can perform computation of the equilibrium composition in very complex chemical and metallurgical systems. Some examples in this paper illustrate the simplicity of the computation and use of the program in the field of typically metallurgical applications which have been traditionally assigned to specialists.
Key words: Equilibrium reactions, active gas-atmospheres, decarburisation of non-oriented electrical steels

Poznavanje termodinamičnih odnosov v kompleksnih sistemih plin - kovina ima lahko izreden pomen za kontrolo industrijskih procesov. Gibbsov model o minimizaciji energije je implementiran v programsko opremo GPRO, ki mu služi kot osnova močna baza verificiranih termodinamičnih podatkov. Programska oprema omogoča izračunavanja ravnotežnih sestav v zelo kompleksnih kemijskih in metalurških sistemih. Navedeni primeri v tem članku ilustrirajo enostavnost izračunavanj in način uporabe programa na področju metalurških aplikacij, ki jih večinoma izvajajo strokovnjaki na tem področju.
Ključne besede: Ravnotežne reakcije, aktivne plinske atmosfere, razogljičenje neorientirane elektro pločevine.

Introduction

The application of thermodynamics to a system gas/solid enables to calculate the composition at equilibrium and the direction and extent of change which can take place under specified conditions. In this paper an attempt is made to demonstrate the use of a personal computer software program as an elegant and sensitive method for numerous metallurgical applications especially for analysis of gas-metal systems.

It is expected, that user of this method will be in good position to go more deeply into learning thermodynamic correlations.

Principles of the Gibbs method

In the fields of heat treatment of metals as annealling, carburizing, steel decarburizing, nitrocarburizing and many other operations, the metallurgist is concerned not with pure gases but with mixtures of various components (gases and solids) which form the atmosphere in the furnace.

Description of used method for the complex equilibrium conditions

Several excellent software programs for general studing and calculating of equilibria reactions by high temperatures have been developed in the last two decades (e.g. SOLGASMIX, THERMOCALC, FACT, CHEMSAGE ...)[2,3].

However, most of them are designed and written in complex form requiring very strong computer units, few others are intented simply as a tool to be applied for the purposes of solving real problems.

Therefore, it seemed worthwhile to develop a program which will take some midway path between these two computer program designs. The new software program, called GPRO is based on the method of free energy minimization and extended to systems containing numerous gaseous and condensed phases mainly in accordance with SOLGASMIX-principles[5-8].

Thermodynamical approaches to the Gibbs-method

The advantage of Gibbs method energy minimization is based on his simplicity for description of chemical reactions in complex systems and its ability to facilitate determination of the effect of a change in the external influences on the equilibrium state. In the GPRO software program the user needs only to specify the type, the components present in the system and the conditions (for example: temperature and chemical composition of the system) for the calculation.

The program will perform automatically the equilibrium thermodynamic computions typically associated with complex

* Prof. dr. Blaženko KOROUŠIĆ.
IMT Ljubljana, Lepi pot 11, 61000 Ljubljana

chemical equilibria from a defined database.

With the aid of the GPRO-program, a user is able to perform most of the following operations:

- The energy for pre-heating the initial mixture from the initial temperature T_o to the reaction temperature T,
- The heat of reaction,
- The computation of the complex chemical equilibria in gaseous mixtures and activity of solid compounds,
- Displaying and printing data of compounds and solutions at any temperatures and compositions.

Associated databases for the thermodynamic equilibrium computations

From many excellent standard treatises on thermodynamics it is known, that without reliable thermodynamic data most of the equations are ineffective and numerical answers will be wrong.GPRO software program is based on use of both formula for calculations of the standard Gibbs energies of the formation of the phase:

1. in the form:

$$\Delta G_T^\circ = \frac{A}{T} + B + CT + DT^2 + ET^3 + FT\ln T \qquad (a)$$

2. over the enthalpy ΔH_T° entropy ΔS_T° and heat capacity $C_p(T)$:

$$\Delta G_T^\circ = \Delta H_{298}^\circ + \int_{To}^{T} C_p(T)\,dT - TS_{298}^\circ - T\int_{To}^{T}\frac{C_p(T)}{T}\,dT \qquad (b)$$

$C_p(T) = A + BT + CT^2 + DT^{-2}$

Both methods used from the database involve a search for a minimum value of the free energy G of a system and give equivalent results. However the second method considering the enthalpy H, entropy S and heat capacity Cp has more advantages by combining heat and equilibrium calculation. Typical example is the determination of the adiabatic flame temperature, where enthalpy of reaction serves as the criterion of the heat balance.

Exploiting the GPRO-program for heat and standard free enthalpy calculations

Traditionally the concept of heat enthalpy and standard free enthalpy as a state function are introduced by considering the behaviour and properties of many chemical and metallurgical reactions.

Since the equilibrium state has been obtained, the heat generation or the total heat of process can be computed, using the thermodynamical functions .E.g. the energy necessary for preheating the initial mixture from the initial temperature T to the reaction temperature T, H - H_o, (taking into the account the transition values within the actual temperature interval T - T_o added to the heat of reaction - H_o), gives the H_o - total total heat of the system.

Example No.1

Statement of the problem

A mixture of Fe, (O_2), SiO_2 present in the molar ration 2 : 1 : 1 is adiabatically heated from 298 K to 1173 K. Calculate H_o - H_{298} and G_o for the reaction:

$$2\langle Fe\rangle + (O_2) + \langle SiO_2\rangle = \langle Fe_2SiO_4\rangle \qquad (1)$$

where:

<> = solid, () = gas

Compare the obtained results with results from literature for the Gibbs free energy of the fayalite formation[3]:

$$\Delta G_T^\circ = -555504 + 135{,}23T\,(J.mol^{-1})\,(900...1478K) \qquad (2)$$

$$\Delta G_T^\circ = -505263 + 101{,}32T\,(J.mol^{-1})\,(1478...1508K) \qquad (3)$$

Since the end temperature is higher then 1773 K all transition and latent heats of the reactants and products must be considered:

1. $Fe(\alpha \rightarrow \beta) = 1033K, \Delta H^\circ_{\alpha\rightarrow\beta} = 5024\,(J.mol^{-1})$.
2. $Fe(\beta \rightarrow \gamma) = 1183K, \Delta H^\circ_{\beta\rightarrow\gamma} = 921\,(J.mol^{-1})$.
3. $Fe(\gamma \rightarrow \delta) = 1674K, \Delta H^\circ_{\gamma\rightarrow\delta} = 879\,(J.mol^{-1})$.
4. $Fe(T_m) = 1809K, \Delta H^\circ_{Tm} = 13860\,(J.mol^{-1})$.
5. $Fe_2SiO_4\,(T_m = 1493K), \Delta H^\circ_m = 9210\,(J.mol^{-1})$.

Solution :

Fig. 1 shows a plot of G_o versus T for the reaction (1). There is a change of the entalpy due to melting Fe_2SiO_4 at T = 1492 K and calculated values for G_o over Cp - expression and from a formels (2) and (3).

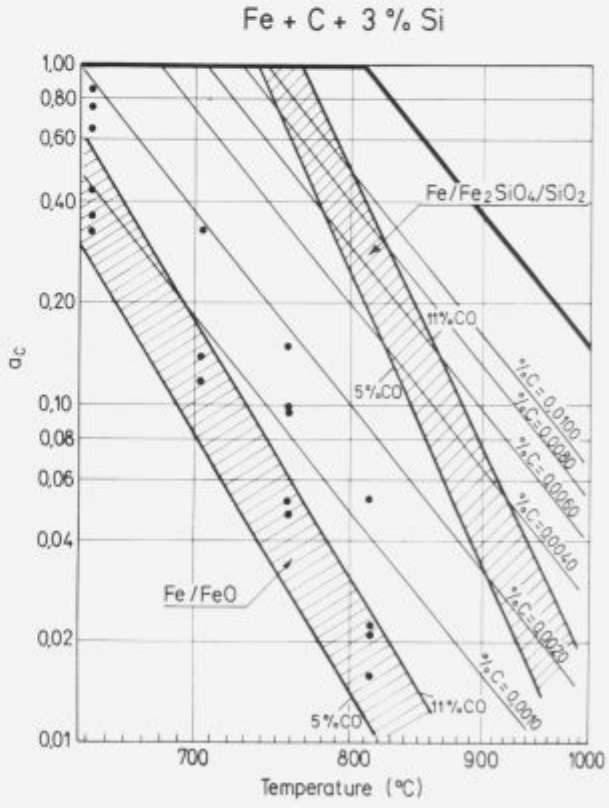

Figure 1: Plot of thermodynamical data for Fe_2SiO_4 as a function of temperature calculated with GPRO-program. (Model) and (Lit.) using data from Richardson and Jeffes[3]

Slika 1: Diagram termodinamičnih podatkov za Fe_2SiO_4 kot funkcija temperature izračunano s programom GPRO.

Exploiting the GPRO-program for complex equilibria calculations

In this chapter, some examples of work performed in our laboratory on the application of the computer-based model GPRO will be reviewed. The accuracy of the gaseous atmosphere control in steel decarburizing furnaces has been remarkably improved owing to the application of computer control systems and the development of new measuring techniques (for example: oxygen and/or carbon sensors).

Gaseous active atmospheres

There is relatively little emphasis in the literature about use of the thermodynamical models on the field of active atmospheres. Such mixtures containing both gaseous and condensed components (for example: Fe + C + O + H + N are extremly complicated for the numerical calculations). Detailed experimental studies are difficult and also thermodynamical results are mostly presented in the graphical form, which are very useful in research work but of little effectivness in searching solutions for a current practical operation.

To obtain equilibrium compositions in the real gaseous mixtures by high temperatures, taking into account both energy and material balances, development of new approaches are strongly required.

Example No. 2

Statement of the problem

The use of gaseous atmosphere with a well-defined oxygen potential for decarburisation of low carbon iron-silicon steels in the continuous furnace can be simulated by use of thermodynamical model.

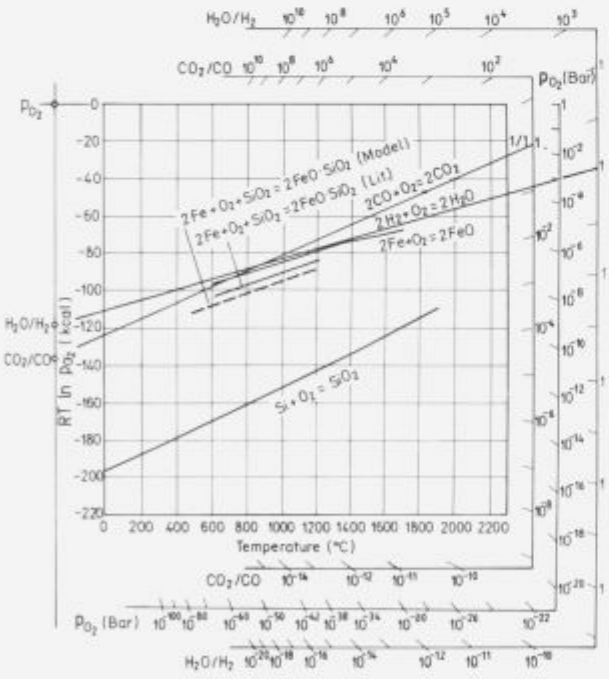

Figure 2: Equilibrium behavior of different oxide phases during the decarburization of Fe-C-Si alloys in active gas atmosphere ($CO + CO_2 + H_2 + H_2O + N_2$)

Slika 2: Ravnotežni odnosi različnih oksidnih faz, ki nastajajo med razogljičenjem jekel Fe-C-Si v aktivni plinski mešanici ($CO + CO_2 + H_2 + H_2O + N_2$)

Equilibrium calculations and practical measurements show that solubility and carbon activity in Fe-C-Si steels depend on the gaseous atmosphere, temperature and steel composition.

The thermodynamic analysis permit on the base of thermodynamical data to predict the equilibrium carbon contents in electrical steels **(Fig. 2)**.

Concluding Remarks

One of the widely known methods for chemical and metallurgical equilibrium calculations by the high temperatures is Gibbs energy minimization method. Based upon these principles and implementing some algorithms from computer program SOLGASMIX, the new user-friendly computer program called GPRO was developed.

GPRO-software program is designed as a system which can perform equilibria thermodynamic computations in systems containing gaseous and stoichiometric and/or non-stoichiometric condensed phases.

The computer program lists options as menu and the user is slowly directed through the program, choosing one option at a time. Before using the level of the main menu, user must create the relevant thermodynamic data file which contains the reliable thermodynamic data as heat capacity, enthalpy, entropy with respect to a chosen references state.

In this paper some typical examples are presented to illustrate the simplicity of the computation in the complex chemical and metallurgical systems at high temperatures for typical industrial applications.

Reference

[1] Gaskel, D. R.: *Introduction to Metallurgical Thermodynamic* McGraw - Hill Book Company, (Washington, D.C), (1973)

[2] Christopher, W. B., G. Erriksson: *Metallurgical Thermochemical Databases* - a review, Canadian Metallurg. Quat. Pergamon Press, (Oxford) 29, 1990, 2, 105–132.

[3] Eriksson, G., K. Hack: ChemSage - A Computer Program for the Calculation of Complex Chemical Equilibria. *Metallurgical Transactions B*, (Materials Park, OH) 21B, 1990, 1013–1023

[4] Richardson, F. D., J. H. E. Jeffes: *J. Iron Steel Inst.*, (London) 160, 1948, 261–270

[5] Koroušić, B.: Computerized thermodynamical expression of gas-metal reactions in industrial application of carburizing with in situ produced atmosphere process. *Journal of Heat Treating, JHTRDR*, (Franklin, WI) to appear

[6] Koroušić, B.: Študij ravnotežnih reakcij v plinskih mešanicah I.del: Varovalne atmosfere. *Rudarsko-metalurški zbornik*, 40, 1993, 1–2, 5–17

[7] Koroušić, B., J. Langerweger., E. Kolb: Fortschritte in den Optimierungsrechnungen des Entkohlungsprozesses von Silizium-legierten Stahlen, *HTM* (1994) (to appear)

[8] Koroušić, B., A. Rosina: Contributions to the computer predictions of the homogeneous and heterogeneous equilibrium compositions for the gas atmospheres. *Veitsch - Radex Rundschau* (1994), 1–2, 523–530.

INŠTITUT ZA KOVINSKE MATERIALE
IN TEHNOLOGIJE p.o.

INSTITUTE OF METALS
AND TECHNOLOGIES p.o.

61000 LJUBLJANA, LEPI POT 11, POB 431,
SLOVENIJA

Telefon: 061/1251-161, Telefax: 061 213-780

VACUUM HEAT TREATMENT LABORATORY

Vacuum Heat Treatment

Vacuum Heat Treatment is recognised as a high quality cost effective and ultra clean method for processing a wide range of components and materials currently in use in today's industry. The range of our equipment enables us to heat treat most sizes of load, from small batches to work up to 350 mm diameter, 910 mm high, and weight up to 380 kg.

ADVANTAGES

- Clean, bright surface finish
- Minimal distortion
- Minimal post treatment operations, e.g., grinding or polishing

Five years of continual investment has ensured that **VHTL** maintains it position as market leader in the field of high quality sub-contract metal processing.

We operate the latest generation of IPSEN VTTC furnace capable of processing components up to 350 mm in diameter, which in addition to our high pressure, rapid quenching facilities increases the range of materials suitable for Vacuum Heat Treatment.

TYPICAL APPLICATIONS

- Bright Annealing
- Bright Stress Relieving
- Hardening/Tempering
- Brazing/Hardening/Tempering
- Solution Treatment
- Demagnetisation
- Degassing
- Diffusion Treatments
- Sintering

QUALITY ASSURANCE

Quality is fundamental to the **IMT** philosophy. The choice of process, all processing operations and process control are continuously monitored by IMT Quality Control Department.
The high level of quality resulting from this tightly organised activity has been acknowledged by government authorities. industry and International companies.

Kovine, zlitine, tehnologije / letnik 28 / 1994 / številka 4 / strani 613 do 617

Protection of Carbon/Carbon Composites against Oxidation

Zaščita kompozitov tipa ogljik/ogljik pred oksidacijo

Borchardt G.,* Institut für Allgemaine Metallurgie, Technische Universität Clausthal, Deutschland

R. Turk, S. Javorič, V. Nardin, Oddelek za metalurgijo in materiale, FNT, Univerza v Ljubljani, Slovenia

A mayor problem of carbon/carbon composites is use in oxidative environments. Protective coating in this study consists of SiC outer and B4C inner coating and offer efficient protective of composites against oxidation. Because of cracks and erosion of microstructure as a result of oxidation oxidized samples have lower mechanical properties.
Key words: carbon/carbon composites, oxidation, protective coatings, mechanical properties of oxidized composites.

Največji problem kompozitov tipa ogljik/ogljik je njihova uporaba v oksidativnih atmosferah. Ugotavljali smo učinkovitost večplastne zaščite grafita pred oksidacijo, sestavljene iz zunanje SiC in notranje B4C plasti. Rezultati kažejo, da je takšna zaščita učinkovita v temperaturnem intervalu 600–1000°C. Zaradi razpok in erozije strukture grafita, ki so posledica oksidacije, so mehanske lastnosti oksidiranih kompozitov slabše.
Ključne besede: kompoziti tipa ogljik/ogljik, oksidacija, zaščitne plasti, mehanske lastnosti oksidiranih kompozitov.

1. Introduction

Carbon fibers and carbon/carbon (C/C) composites are attractive materials because of strength-to-weight properties superior to those of any other materials.

Potential uses range from those in aircraft, autoindustry to medical and sport applications (boat making, fishing rod...).

C/C composites consist of carbon fibers set in a graphite matrix. Mechanical properties of C/C composites depend on fibers, which exhibit high Young's modulus E (E = 250–500 GPa) compared to the graphite matrix (Ey = 30 GPa).[1]

Strong bonding between the matrix and the fibers results in high shear strength while weak bonding increases the toughness, so that crack propagation in the matrix can be arrested at the fiber surface.

High tensile strength is a consequence of very strong covalent bonds between carbon atoms and high anizotropic crystalline fibers.[2]

2. Protection of C/C Composites against Oxidation

The most obvious advantage of using C/C composites in aerospace application is their high relative strength compared with low weight.

A mayor problem is using such materials in oxidizing environments (hot flowing gases). Carbon rapidly reacts with oxygen at temperatures as low as 500°C, forming gaseous products (CO, CO_2). Gasifications leads to a rapid degradation of the composite. This oxidation process results in the erosion of the structure and in the degradation of the mechanical properties which the material originally posessed.

Many protective coatings are being considered to prevent contact between oxygen and carbon. Most of these coatings rely on oxide films formed during oxidation as oxygen diffusion barriers.

2.1. Protective Coatings

The most important 1934 U.S. patent[3] in work on protection against oxidation for C/C composites describes a coating system for graphite materials composed of a SiC and vitreous overlay coatings.

Work on oxidation protection for C/C composites started in 1970's. The coating system was very similar to that in the 1934 patent and was composed of a SiC conversion layer and silicate glaze overlay.

Any coating material used to protect the composite from oxidation must prevent the invard diffusion of oxygen, and has low volatility to prevent erosion. Coating issues associated with oxidation protection are coating erosion, spallation and oxygen permeation of the intact coating system.

Erosion resistance requires the use of outer coatings that have low vapor pressures. The high thermal expansion coefficient is a strong negative factor because the large differences in thermal expansion behavior often results intension–induced coating cracks.

* Prof. dr. GÜNTHER BORCHARDT,
Inst. für Allgemeine Metallurgie,
Tehn. Universität Maustal, Deutschland

In the presence of an oxide film on the surface, the oxygen has to diffuse through it to reach the substrate/oxide surface. Oxide film acts as a diffusion barrier. The oxidation of a substrate involves five steps, shown schematically in **Figure 1**:[4]

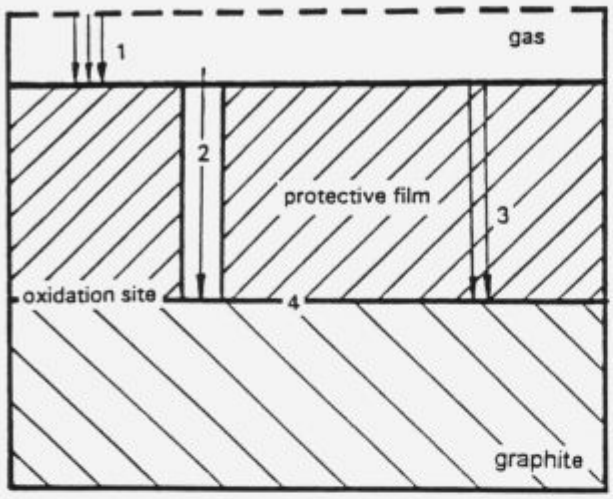

Figure 1: The oxidation of a protected graphite
Slika 1: Oksidacija zaščitenega grafita

1. gas phase diffusion across the boundary layer;
2. oxygen diffusion through cracks: if the oxide film is cracked, (oxygen diffuse through it to the substrate/oxide film interface);
3. condensed phase diffusion (if the oxide film is nonporous);
4. reaction at the interface substrate/oxide;
5. counter diffusion of gas products back to atmosphere.

Oxides have usualy higher thermal expansion coefficients than corresponding carbides. For this reason it is advantageous to start with a nonoxide outer coating that converts to an appropriate oxide upon exposure. Such deposition reduce diferences between thermal expansion behaviour of coating and substrate.

Studies have shown the utility of borate glasses for protecting C/C composites from oxidation. Current coating system for protecting C/C composites are composed of an outer coating of SiC and an inner B_4C coating. Due to oxidation SiC is converted to SiO_2 which acts as primary oxygen barrier.[5]

Oxidation of the inner B_4C coating through cracks in the SiC outer coating produces a borate glass B_2O_3. Above the melting point of B_2O_3 it flows to fill cracks present in the inner and outer coatings.

3. Mechanical Properties of Oxidized C/C Composites

Oxidation of the graphite leads to pitting, degradation and porosity of C/C composites. Gasification appeared to lead progressively to the formation of pores in the matrix, followed by propagation of longitudinal channels along the fiber axes.

Cracks, which appears under loading, leads to a loss in strength of the composite. One of the most oxidized and loaded fibers rupture and this leads to crack initiation and propagation of transversional cracks because of shear stresses.[7] Strength of oxidized composites is reduced because of cracks and microstructure erosion.

Bending strains for oxidized C/C composites are much lower than that for unoxidized ones.

4. Experimental Procedure

Graphite EK 986 used in this study were supplied by Ringsdorf, Germany. The average density was 1.85 g/cm^3 and open porosity 8%. Graphite samples were cut in approximately cube form, side 0.7 +- 0.01 mm.

Multilayer coating was composed of an outer coating of SiC and of an inner B_4C coating.

SiC and B_4C coatings various thicknesses were deposited by Physical Vapor Deposition (PVD) process with High Frequency (HF) Sputtering.

Samples were sputtered in vacuum at 2-3 x 10^{-5} mbar, frequency 10 MHz and voltage 1kV. 80 min of sputtering was sufficient to deposit a B_4C film of 0.30 µm and 75 min to deposit a SiC film of 0.70 µm on the surface of the samples. Some graphite samples were only B_4C coated.

Measurements of the oxidation kinetics of all graphite samples were carried out in a vertically open–ended furnace in stagnant air, between 600 and 1200°C.

Mass changes of the specimens were measured by Thermo Gravimetry Analyses (TGA) using an automatic "SARTOTIOUS M 25 D-V" thermobalance (sensitivity +-0.001 mg) which was connected with computer.

All kinetics data were collected and approximated with Computer operated data on line acquisition system. Samples were cooled down in air and were observed using Scanning Electron Microscope (SEM), Jeal JSM - 35.

C/C composites materials BB 7655 used in this study were made from SCHUNK, Germany. Samples were preprotected with Si, which was deposed into the graphite matrix ("Kapillarziliziert").[8]

Samples with average dimensions 20 x 20 x 1.7 mm, the average density 1.64 g/cm^3 and the average porosity 8.2% were oxidized between 400° and 800°C.

Oxidized samples were cooled down in air and tensioned by GLEEBLE 1500 (DUFFERS SCIENTIFIC) at room temperature in air at a rate of 0.1 mm/sec.

5. Results and Discussion

5.1 Oxidation behaviour of uncoated graphite

Oxidation of the graphite appeared to occur at specific active sites, leading to pitting, degradation and porosity at the surface.

Figure 2 shows the relative weight loss for oxidized samples per unit of calculated geometric area (dm/A_0) as a function of time at 600°C and 1000°C.

Due to the presence of porosity, the effective surface area over which reaction can occur is possibly 10 to 100 times higher than the geometric area. This is consistent with the high porosity of the C/C composites.

Oxidation process of graphite results in the erosion of the structure **(Figure 3)**. Because of higher erosion the oxidation rate for uncoated graphite samples **(Figure 2.b-A)** at 1000°C is higher than rate at 600°C **(Figure 2.a-A)**.

The low temperature rate - limiting step is probably a surface reaction - desorption of oxidation products (CO, CO_2) from the carbon network.

At higher temperatures the release of the oxidation products becomes easier and leaves defects in the carbon network. The rate is then probably controlled by oxygen diffusion into pores.

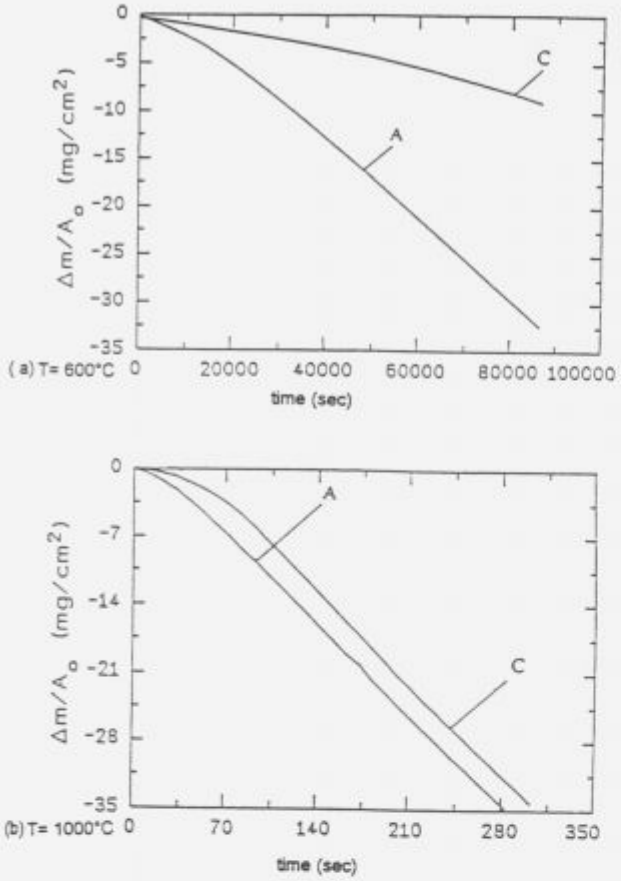

Figure 2: Relative weight loss per unit of calculated geometric area (dm/A_o) as a function of time at 600°C(a) and 1000°C(b).
A ... uncoated graphit
C.... graphit, coated with SiC and B_4C protective coating

Slika 2: Relativna izguba mase na enoto izračunane geometrične površine (dm/A_o) kot funkcija časa pri 600°C(a) and 1000°C(b).
A ... nezaščiten grafit
B ... grafit, zaščiten s SiC in B_4C zaščitno plastjo

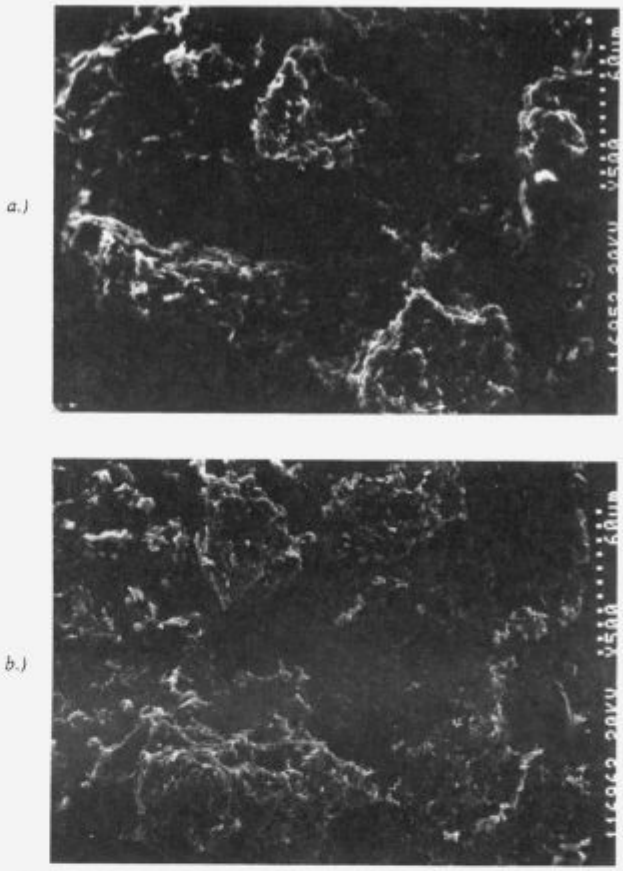

Figure 3: Surface of uncoated graphite after oxidation at 600°C (a) and 1000°C (b)

Slika 3: Površina nezaščitenega grafita po oksidaciji pri 600°C (a) in 1000°C (b)

With continued oxidation the porosity and active surface area increased resulting in the increase in the oxidation rate.

An important question is whether oxidation of C/C composites proceeds more readily along the carbon fiber axes or in the less well crystallized matrix of the composite.

Because of the higher incidence of reactive edge sites, amorphous carbons tend to be more susceptile to gasification than crystalline graphite.

Oxidation of the graphite occured simultaneously at specific active sites (vacancies, pores). Burn off of oxidation products leads progresively to formation of pores in the matrix **(Figure 4.a)**, followed by the propagation of longitudinal channels along the fiber axes **(Figure 4.b)**. Facile oxygen diffusion along such channels allowed a rapid excavation of material and growth of larger pores between the fiber bundles.

Gasification also occured rapidly at the exposed ends of the fibers, leading to diffusion of oxygen along the fiber axes.

5.2 Oxidation behaviour of coated graphite

In the temperature range 600°C–1000°C samples covered with SiC and B_4C coating **(Figure 2.a,b-C)** showed better oxidation resistance and reduction in the oxidation rate compared with uncovered graphite samples **(Figure 2.a,b-A)**.

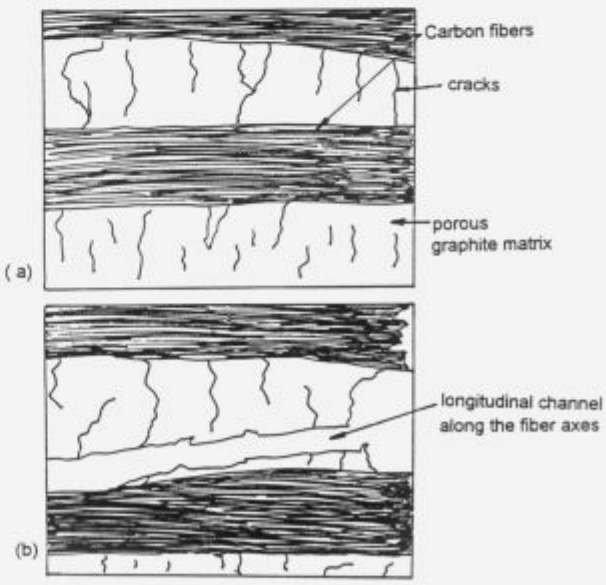

Figure 4: Oxidation of the graphite occured simultaneously at specific active sites, appeared to lead progressively to the formation of pores in the matrix (a), followed by the propagation of longitudinal channels along the fiber axes (b) and growth of larger pores between the fiber bundles (c).

Slika 4: Oksidacija grafita prične simultano na specifičnih aktivnih mestih, kar vodi do tvorbe por v matrici (a), podolžnih kanalov vzdolž osi vlaken (b) in rasti večjih por med vlakni (c)

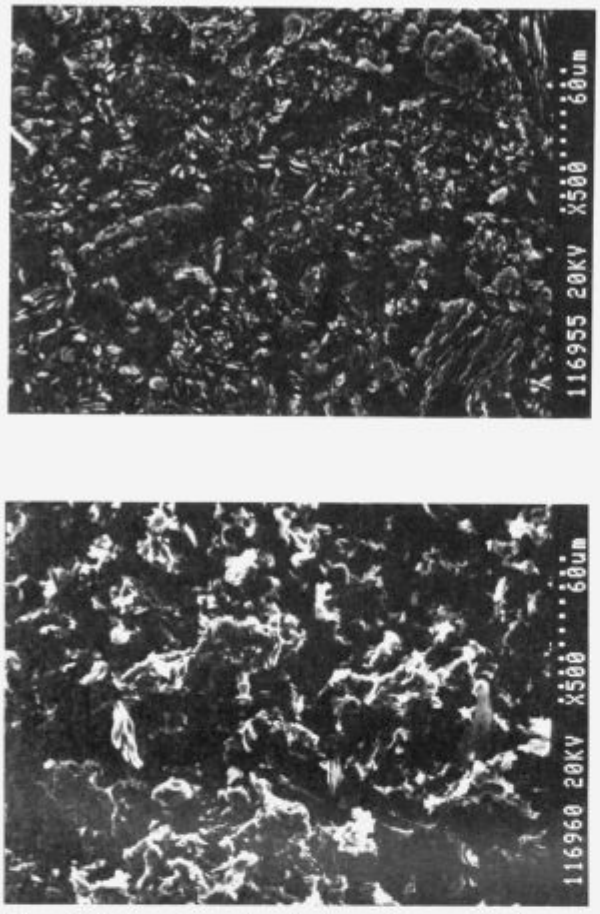

Figure 5: Surface of coated graphit after oxidation at 600°C (a) and 1000°C (b)

Slika 5: Površina zaščitenega grafita po oksidaciji pri 600°C (a) in 1000°C (b)

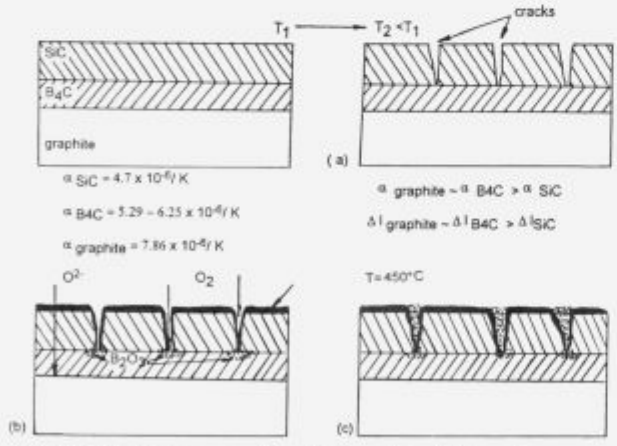

Figure 6: Cooling composite leads to cracking in the coating as a result of thermal expansion mismatches (a). Oxygen diffuse through cracks and causes oxidation of underlying carbon (b). B_2O_3 flows to fill thermal expansion mismatch cracks in the outher SiC coating and in the matrix (c).

Slika 6: Pri ohlajanju kompozita se v zaščitnih plasteh pojavijo razpoke zaradi razlik v temperaturni raztežnosti zaščitnih plasti grafita (a). Kisik difundira skozi razpoke in povzroča oksidacijo spodaj ležečega ogljika (b). B_2O_3, ki se tvori med oksidacijo, zapolni razpoke v SiC plasti in v grafitni matrici (c)

Oxide films formed during oxidation prevent direct contact between oxygen and underlying graphite and reduce numbers of specific active sites and presence of porosity over which oxidation can occur **(Figure 5)**.

Examination of the B_4C plus SiC coated specimen on removal from the furnace suggested that oxidation was initiated at the corners and edges of the sample.

Bonding of the coating at these sites was probably poorer than on the faces and that local mismatches caused microcracking in these regions.

SiC prevent direct oxygen attack on the carbon matrix. Cooling composite from relatively high deposition temperatures leads to cracking in the coating as a result of thermal expansion mismatches **(Figure 6.a)**.

Upon exposure to oxygen SiC becomes an oxide SiO_2 which is an excelent oxygen barrier so oxidation by diffusion through SiO_2 layer is not the limiting factor.

Porous structure of SiC and cracks in the coating degrades the oxidation resistance of graphite. Oxygen diffuse through cracks and causes oxidation of underlying carbon. **(Figure 6.b)**. That is the reason why SiC coating offered only limited protection of oxidation.

The use of B_4C gave good protection at temperatures up to 1000°C. B_4C forms borate glass B_2O_3 on oxidation which has surface energies less than 100 mJ m^{-2} for carbon wetting and viscosities of 10^4 to 10^2 dPa s (in the 600 to 1100°C range).

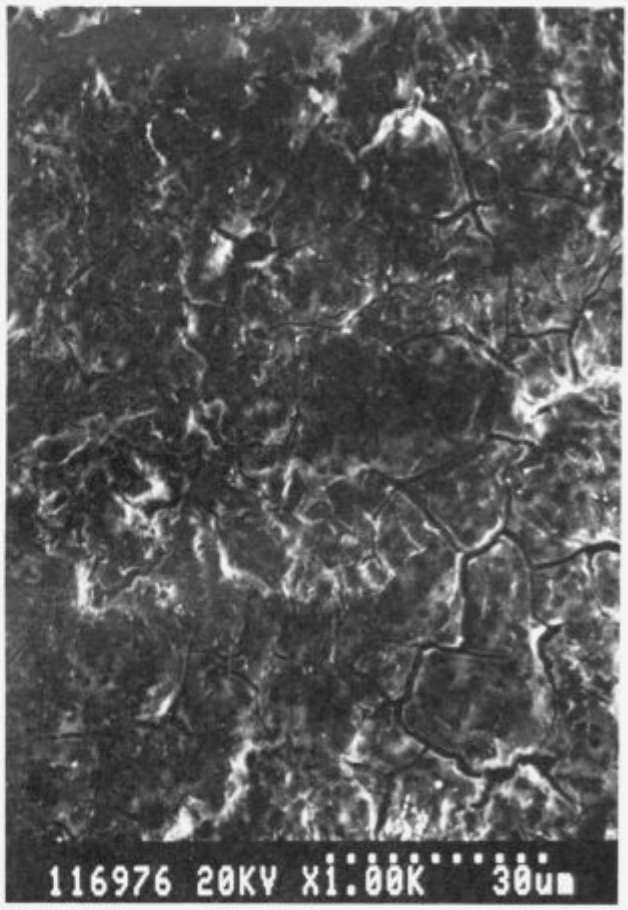

Figure 7: After removal from the furnace we noticed that B_4C plus SiC coating resignate from graphite matrix and cracked.

Slika 7: Po oksidaciji smo ugotovili, da je zaščitna plast B_4C plus SiC odstopila od grafitne matrice in razpokala.

Above the melting point of B_2O_3 (450°C) it flows to fill thermal expansion mismatch cracks in the outher SiC coating and in the matrix **(Figure 6.c)** providing a diffusion barrier in the composite. B_2O_3 is segregated in clusters at the active sites on the graphite surface where oxidation normally occured and blocks this active sites.

The use of borate coating is limited by the volatility of the borate. Volatization of the coating leaves the underlying material exposed. Rapid oxidation and a 250% volume increase at the conversion of B_4C to B_2O_3 are essential features of these coatings.

After removal from the furnace we noticed that B_4C plus SiC coating resignate from graphite matrix and crack **(Figure 7)**. Hydrolysis of B_2O_3 produces orthoboric acid and a 125% volume increase:

$B_2O_3 + H_2O = 2B_2O_3 + H_2O = B_2O_3 + H_3BO_3$

Heating releases water and produces a mixture of boric oxide and metaboric acid. Under dry conditions the complete conversion H_3BO_3 back to B_2O_3 completed at about 450°.

5.3 Mechanical properties of oxidized C/C compozites

Because of cracks and erosion of microstructure of C/C composites oxidized samples have lower mechanical properties.

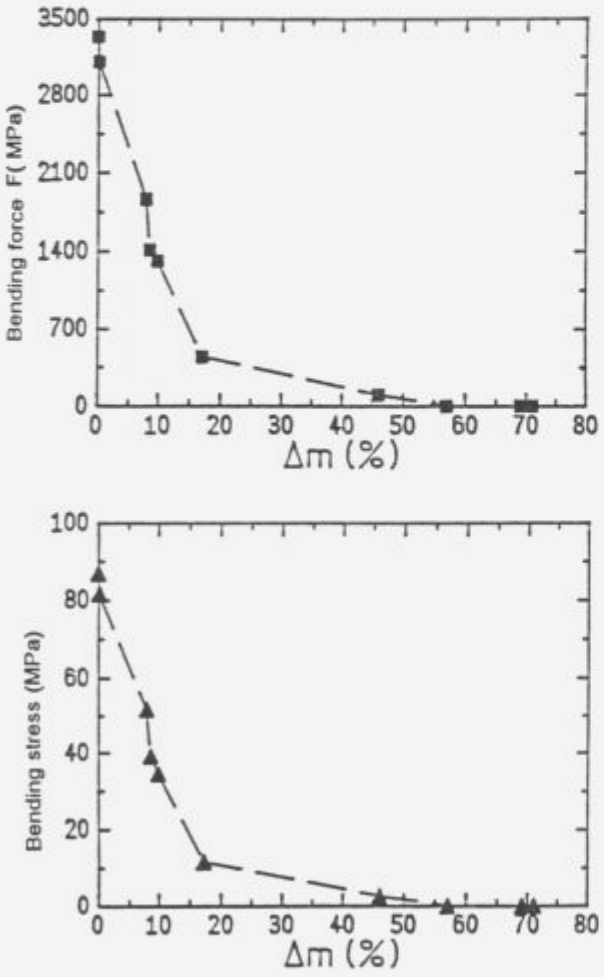

Figure 8: Bending forces and breaking stresses (up to 90 MPa) for less oxidized C/C composites as for well oxidized samples (minimal bending forces and stresses).

Slika 8: Pri manj oksidiranih C/C kompozitih so za porušitev potrebne manjše upogibne sile (do 3300 N) oz. napetosti kot pri zelo oksidiranih vzorcih, kjer so potrebne minimalne upogibne sile oz. napetosti.

Figure 8 shows that bending forces (up to 3300 N) and stresses (up to 90 MPa) for less oxidized C/C composites (at 0.036% mass loss) are much higher than those for well oxidized samples (minimal bending forces and stresses).

Relationship between breaking force (F) and mass loss (C) can be represented as following equation:

$F = a + b(sqr(C))^2$,

where coefficients are a = 58.2238 and b= - 7.1752.

6. Conclusions

1. The main problem for C/C composites is use of such materials in oxidizing environments (hot flowing gases). Carbon rapidly reacts with oxygen at temperatures as low as 500°C, forming gaseous products (CO, CO_2). Gasifications leads to a rapid degradation of the composite.
2. Many protective coatings are being considered to prevent oxygen from reaching carbon. Most of these coatings rely on oxide films formed during oxidation as oxygen diffusion barriers. Coatings with less permeability for oxygen and temperature expansion coefficient similar to those of substrat shows efficient protection of oxidation, so layers could be mechanically stable during cooling and heating processes.
3. Graphite samples in approximately cube form, side 0.7+-0.01 mm were covered with multilayer protective coating, which was composed of an outer coating of SiC and of an inner B_4C coating.
4. SiC and B_4C coatings of various thicknesses were deposited by Physical Vapor Deposition (PVD) process with High Frequency (HF) Sputtering.

   Measurements of the oxidation kinetics of all graphite samples were carried out in a vertically open - ended furnace in stagnant air, between 600 and 1200°C.
5. Comparison between uncovered graphite and graphite, covered with SiC and B_4C protective coating shows reduction in the oxidation rate resulting from protective coating.
6. After removal from the furnace we noticed that B_4C plus SiC coating resignate from graphite matrix. Because of cracks and erosion of microstructure shows oxidized C/C composites lower mechanical properties. Bending forces (up to 3300 N) and stresses (up to 90 MPa) are much higher for less oxidized C/C composites (at 0.036% mass loss) than those for well oxidized samples (minimal bending forces and stresses).

Reference:

[1] J. L. Figueiredo et al: Carbon Fibers Filaments and Composites *NATO ASI series*, 177, 1989

[2] H. V. Johnson: *US Patent 1*, 948,382 (1934)

[3] M. S. Dresselhaus: *Graphite Fibers and Filaments*, Springer Verlag, London 1988, Chapter 1-5

[4] K. Luthra: *Carbon* 26, 1988, 52, 217–224

[5] J. E. Sheehan: *Carbon*, 27, 1989, 5, 709–715

[6] T. M. Wu, C. Wei, S. E. Hsu: *Ceramics International*, 18, 1992, 167–172

[7] G. C. Grimes: *ASTM*, 10, 1992, 1120

[8] V. Nardin: Izdelava, lastnosti in oksidacija ogljikovih kompozitov, *Diplomsko delo*, Univerza v Ljubljani, 1992

[9] L. E. Jones, P. A. Thrower: *Carbon*, 29, 1991, 522, 251–269

[10] T. M. Wu, W. C. Wei, S. E. Hsu: *Carbon*, 29, 1991, 8, 1257-1265

[11] S. M. Gee, J. A. Little: *Journal of Material and Science*, 26, 1991, 1093–1100

[12] D. W. McKee, C. L. Spiro, E. J. Lamby: *Carbon*, 22, 1984, 6, 507–511

[13] D. W. McKee: *Carbon*, 25, 1987, 4, 551–557

[14] W. J. Tomlinson, J. C. Whitney: *Ceramics International*, 18, 1992, 207–211

SLOVENSKE ŽELEZARNE

IZŠLA JE KNJIGA

SLOVENSKA JEKLA

Naj vam jo na kratko predstavimo:

Knjiga je zbir vseh jekel, litin in specialnih zlitin, ki jih izdelujejo v družbah Slovenskih železarn.

Deli se v tri dele; v prvem delu je seznam jekel razvrščen po rastoči oznaki materiala W.NR., ki je osnovni ključ za iskanje. V tem delu lahko najdete vse ostale podatke o jeklu, kot npr. proizvajalca, vrsto jekla, kemijsko sestavo, oznake po evropskih in ameriških standardih, dobavne oblike in namen uporabe.

V drugem - indeksnem delu so po abecedi razvrščene oznake slovenskih proizvajalcev ter nacionalne in mednarodne oznake primerjane z W:NR:

V tretjem delu so jekla, razvrščena glede na vrsto - uporabo.

Knjiga obsega 300 strani, velikega formata in je prva tovrstna knjiga v Sloveniji, kjer so na enem mestu zbrani podatki o jeklih, litinah in specialnih zlitinah. V pomoč bodo proizvajalcem, predelovalcem, kupcem, prodajalcem, tehnologom, konstrukterjem, razvojnikom, skratka vsem, ki imate opravka z jekli. Je štirijezična (v slovenskem, angleškem, nemškem in francoskem jeziku), tako da jo lahko s pridom uporabite, ko boste kontaktirali s tujimi partnerji.

ŽELIMO VAM, DA BI VAM BILA KNJIGA V POMOČ IN KORIST PRI VAŠEM DELU.

Pokličite na naš telefon ali pa nam pošljite izpolnjeno naročilnico.

RAVNE
STANDARD

ŽELEZARNA RAVNE
STANDARDIZACIJA IN DOKUMENTACIJA
62390 Ravne na Koroškem,
Tel.: 0602 21 131 int. 5622
Fax: 0602 23 013 - STANDARDIZACIJA

NAROČILNICA

Naročamo SLOVENSKA JEKLA po ceni 3.900 SIT

število izvodov _____

Firma
Ime in priimek
Kraj in poštna številka

podpis žig

Kovine, zlitine, tehnologije / letnik 28 / 1994 / številka 4 / strani 619 do 622

Influence of the Scaling upon the Heating Process of Steel Slabs in a Pusher-type Furnace

Utjecaj ogorine na proces zagrijavanja čeličnih slabova u peći potisnog tipa

M. Kundak, J. Črnko, Metalurški fakultet Sisak, Croatia

In the frame of this paper an existing and a proposed more optimal temperature regime for heating of steel slabs in a pusher-type furnace is analysed. The influence of steel oxidation upon the heating process and its influence upon the optimal temperature regime calculation is also investigated.
Key words: pusher-type furnace, scaling, heating of steel.

U okviru ovog rada analiziran je postojeći i predloženi optimalniji temperaturni režim zagrijavanja čeličnih slabova u peći potisnog tipa. Također je istražen utjecaj oksidacije čelika na proces zagrijavanja i njezin utjecaj pri proračunu optimalnog temperaturnog režima.
Ključne besede: peć potisnog tipa, zagrijavanje, oksidacija.

1. Introduction

The intensity of oxidation of the heated steel generally depends on the affinity of the basic material, i.e. of iron and alloying elements towards oxygen, on gas composition above the heated steel, on the temperature of furnace space and the time of exposure to high temperatures. Oxidation doesn't depend solely on the presence of free oxygen in the furnace atmosphere. Aqueous vapour, carbon and sulphuric dioxide also appear as reactants. Results achieved regarding the influence of these factors on steel scaling revealed differences, the cause of which has not been explained adequately so far. Quantitive values regarding the extent of the scaling achieved during the investigation stated in references, are given as medium values of several repeated investigations. Such data can be useful for determining the influence scale has on steel heating, especially due to the changes in scale composition throughout the depth of the scale layer, as stated in references, the layer may significantly influence the coefficient of heat conductivity. However, it should be taken into consideration that iron oxidation in the course of steel heating also introduces heat into the process. Yet, exploitation of such heat is insignificant, as the oxygene necessary for iron oxidation is brought from the furnace surroundings, i.e. with the air required for fuel combustion, therefor a corresponding quantity of nitrogen is present, which is heated to the temperature of waste gases. A part of the heat produced by iron oxidation is lost by this heating. Formation of scale diminishes utilization of heat from waste gases inside the furnace, as the heat source on the steel surface decreases the possibility of heat transfer from the waste gas to steel, and due to the low coefficient of conductivity, heat conductivity is limited as well. The latter indicates the importance of defining the thickness of the scale layer on the surface of the heated steel semiproduct. The thickness of the scale layer in relation to the one obtained by calculation from referential data may be checked by means of plant investigations in actual process conditions of given steel heating. This paper also presents the research results regarding the influence of scale layer thickness on the time required for the low carbon steel heating in a pusher-type furnace of a nominal capacity of 67 t/h.

2. A pusher-type furnace and the research results

To study the influence scaling has on the rate of charge heating, in other words the temperature regime of the furnace, a temperature profile of the wall and of the upper surface of the charge lengthways of the pusher-type furnace is determined by an optical pyrometre and presented by a diagram in **Fig. 1**. The length of the furnace from the slab charging line up to the front wall is 26,5 m, and the furnace length covered with slabs is 24,4 m. The inside width of the furnace is 4,6 m. A schematic presentation of the furnace profile and of its main dimensions is given in **refer-**

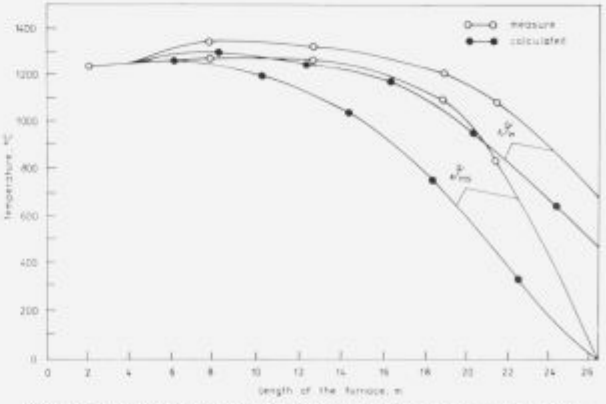

Figure 1: Temperature profile of the wall and of the upper charge surface along a pusher-type furnace

Slika 1: Temperaturni profil zida i gornje površine uloška po dužini peći potisnog tipa

* Doc. dr. Mijo KUNDAK,
Metalurški fakultet Sisak, Aleja narodnih heroja 3, 44103 Sisak, Croatia

ence 1. In the course of determining the temperature profile slabs of the St 12 (per DIN) quality, with dimensions of 430x190x3800 mm and mass of 2500 kg were heated. The furnace capacity was 31,4 t/h. To be able to estimate the value of the determined temperature regime, due to low furnace productivity, a numerical method was used to obtain an optimal temperature regime in such conditions. The numerical method[2] starts by dividing the calculation into several sections within which variables may be considered constant with regard to temperature. While the material was passing along the section length, the charge was considered motionless and its heating was calculated as such as in a hearth furnace of the same temperature, the temperature flow of the flue gas was determined on the basis of the section heat equilibrium.

According to this, a preheating and heating zone was divided into five sections, the soaking zone itself consisted one of the sections. The calculation presumes that heating effects from below were equal to those from above in the heating and preheating zone which was confirmed during determination of the temperature regime. The calculation starts with the required final temperature of the material and is successively carried out for each section up to the beginning of the preheating zone. The initial temperature was always the final temperature of the material of the preceding section. The calculation was considered to be completed when the obtained initial temperature of the material in the first preheating zone section was app. 20°C. If, however, the initial temperature of the material differed considerably from the one stated, the calculation would be repeated. **Table 1** presents values for some calculated variables and the results of the temperature regime calculation for a 31,4 t/h productivity of the pusher-type furnace. The wall temperature and the charge temperature along the furnace during heating were obtained by calculating on optimal temperature regime that is presented in a diagram form in **Fig. 1**.

Table 1: Some variables and the results of the pusher-type furnace temperature regime calculation

Number of section	Length of a section (mm)	Θ_g °C	h W/m²K	k W/mK	N_u	τ	c_g kWs/kgK	Θ_{sr} °C	Θ_{sr} °C	$\Delta\Theta_{sr}$ °C	Θ_s °C
1.	4066	1300	269	29,2	8,88	0,74	0,71	1225	1228	4	1230
2.	4066	1450	308	29,2	1,03	0,73	0,71	1260	1270	18	1303
3.	4066	1400	292	27,4	1,01	0,73	0,71	1171	1200	37	1260
4.	4066	1350	252	26,8	0,90	0,75	0,71	1004	1050	70	1190
5.	4066	1200	198	33,9	0,55	0,84	0,62	713	760	64	975
6.	4066	800	91	51,3	0,17	0,97	0,51	318	330	15	650

Due to the effect of the furnace atmosphere an oxide film (scale), consisting of the Fe_2O_3, Fe_3O_4 and FeO bound more or less tightly onto the iron base, is formed on the white hot steel surface. On the basis of the accepted steel scale composition: consisting of 5% Fe_2O_3, 10 % Fe_2O_3 and 85 % FeO[3,4] and density ranging from 5200 kg/m³, 5100 kg/m³ for Fe3O4 and 5900 kg/m³[3,5], a correspoding scaling density of 5785 kg/m³ is determined. The density and the scale composition enable the calculation of the percentage of steel burn off in regard to the heated charge. **Fig. 2** shows diagrams of the dependence of the scale layer thickness in regard to the percentage of steel burn off and slabs thickness heated both sidedly in a pusher-type furnace.

The amount of burn off steel per unit of steel charge surface may be calculated according to the temperature and duration of detainment at that temperature, as stated in **reference 6, 7, 8** when fuels of higher heating values (coke-oven gas, natural gas

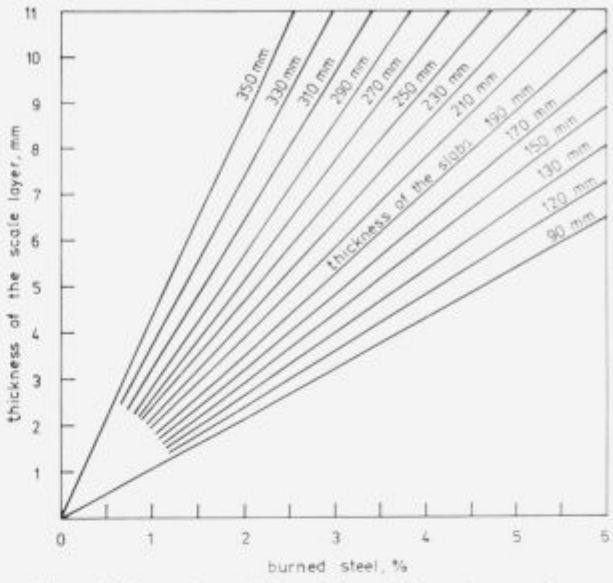

Figure 2: Dependence of the scale layer thickness in regard to percentage of steel burned off and the slabs thickness during heating from both sides

Slika 2: Odvisnost debljine sloja ogorine od postotka čelika koji odgori i debljine dvostrano zagrijavanog uloška

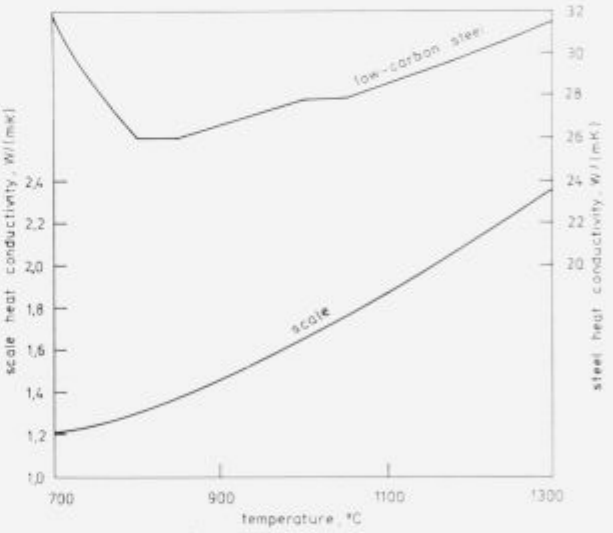

Figure 3: Scale heat conductivity and low-carbon steel in regard to temperature

Slika 3: Toplinska vodljivost za ogorinu i niskougljični čelik u ovisnosti od temperature

and heavy fuel oil) are used the generated flue gases have a similar effect upon the formation of scale. The quantity of the steel burn off per unit of the heated charge surface is presented in the references quoted in a form of a table and diagram in regard to various air factors during fuel combustion, i.e. from 0,6 to 1,1.

Fig. 3 shows diagrams regarding the dependence of scale heat conductivity and low-carbon steel to temperature[4]. From the determined relation it can be seen that the scale heat conductivity is more than ten times lower than that of low-carbon steel, therefor it acts as an isolating layer on the heated steel charge surface. Based on this data a specific heat resistance, depending on the thickness of the scale layer formed during 190 mm thick slabs

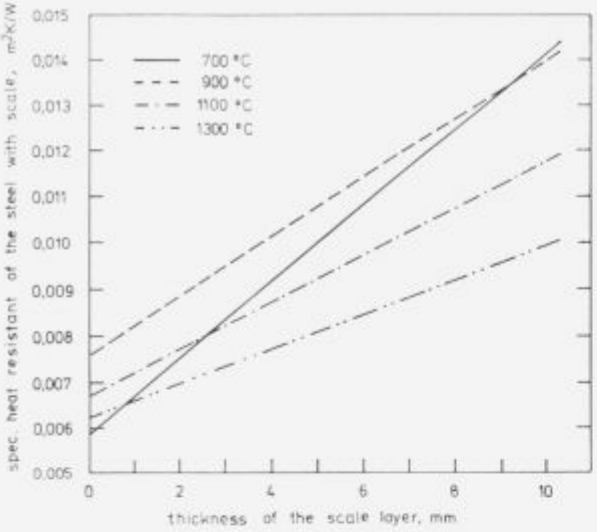

Figure 4: Specific heat resistance of low-carbon steel covered with a scale layer in regard to scale thickness and temperature for 190 mm thick slabs

Slika 4: Specifični toplinski otpor niskougljičnog čelika sa slojem ogorine u ovisnosti od debljine ogorine i temperature za uložak debljine 190 mm

were heated and their temperature, as this is the most common charge of a pusher-type furnace (over 70%), was determing and is presented in a form of a diagram in **Fig. 4**.

However, for the operating conditions investigated, first average temperatures of the charge surfaces in single sections of the furnace were defined from the diagram presented in **Figure 1**, the calculated optimal temperature regime was determined on the basis of data from **Table 1** regarding for the temperature of the charge surface at the end of a single section an average temperature of two neighbouring sections was taken. On the basis of these temperatures and the time of charge detention in single sections along the furnace the parametres regarding scale, as well as the extra time required for charge heating due to scale, were calculated. Natural gas used as fuel (Hu 37300 kJ/m^3), the air factor was 1.1, data and methods stated in **reference 8** were used for the calculation. The results of calculation regarding the scaling of the steel St 12 are presented in **Table 2**.

Table 2: Calculation results in regard to steel scaling during charge heating in a pusher-type furnace

Length of a section (mm	For operating conditions					For calculated conditions				
	ϑ_{sr} (°C)	Burned steel (kg/m^2)	%	Layer (mm)	Δt (%)	ϑ_{sr} (°C)	Burned steel (kg/m^2)	%	Layer (mm)	Δt (%)
4066	350	–	–	–	–	–	–	–	–	–
4066	950	0,719	0,09	0,12	2,2	545	–	–	–	–
4066	1150	1,872	0,26	0,32	5,0	905	0,420	0,06	0,07	0,7
4066	1200	2,650	0,36	0,45	7,0	1125	0,907	0,12	0,16	2,5
4066	1230	3,600	0,49	0,61	9,5	1235	2,430	0,33	0,42	6,3
4066	1230	4,372	0,60	0,75	11,0	1249	3,318	0,45	0,57	8,5

Measurements of the scale layer thickness were carried out in the working plant, after the charge was pushed out of the furnace and adequately cooled, data on thickness of the scale layer formed in different working conditions of the furnace with regard to the delays in the working of the furnace due to war circumstances in the country were obtained. **Table 3** shows the results of the measurements of scale layer thickness on slabs with dimensions of 430x190x3800 mm, steel grade St 12, during continuous and discontinuous furnace operation when the slabs were kept too long in the furnace[9].

Table 3: Results of measurements of the scale layer thickness on the surface of steel St 12 during continuous and discontinuous operation of a pusher-type furnace

Working conditions of the furnace	Continuous working of the furnace	Discontinuous working of the furnace			
		Heating	16 h	12 h	–
		Blind firing	8 h	12 h	60 h
Layer thickness	1,0 mm		4,8 mm	7,0 mm	10,0 mm

Slabs were kept in the furnace for 264 min. The calculated optimal temperature regime not only improved the heat flow of the slabs in the initial period, but also shortened the period of slab detention at higher temperatures and reduced scale loss, the growth of the furnace floor and the heat energy consumption.

3. Discussion of the results

In addition to disadvantages that scaling causes such as are reduction of charge mass and defects in products, scale also behaves as an isolating layer on the heating surface of a charge, therefor more energy is required for its heating as the heating capacity of a pusher-type furnace decreases. **Figure 1** shows data aquired from a pusher-type furnace during operation regarding the temperature regime and the calculated optimal temperature regime at a productivity of 31,4 t/h in a diagram form. The influence of the scale layer thickness upon the heating of a charge could be studied and necessary corrections in the optimal temperature regime calculation could be applied from these data. Generally, on the basis of the scale layer thickness, slabs thickness and heating procedures (one or both sidedly), a percentage of steel burn off can be predicted. From the diagram in **Fig. 2** it may be seen that for the scale layer of thickness 2 mm, which does not differ with slab thicknesses in a corresponding furnace atmosphere, the steel burn off at the charge thickness of 350 mm is 0,45 % and at the charge thickness of 90 mm is 1,75 %. As such the percentages of steel burn off increase or decrease in regard to increase or decrease of charge thickness, the specific heat resistance also increases or decreases. From the expounded it may be noted that the oxidation atmosphere of the furnace space contributes a great deal to a formation of scale on the charge surface, and the increase of specific heat resistance was larger when thinner charges were heated.

To what degree scale behaves as an isolating layer can be seen from the diagram in **Fig. 3**. The coefficient of scale heat conductivity, in regard to the temperature level, is more than ten times lower than that of steel. In **Fig. 4** specific steel heat resistance for different scale layer thicknesses of a 190 mm thick charge heated in a pusher-type furnace is presented in a diagram. As the specific heat resistance increases in regard to temperature, it is necessary to correct the calculated heating time of the charge. From the diagram in **Fig. 4** it is also possible to define parametres for the charge of various dimensions when the atmosphere remains unchanged inside the furnace, as already evident in the diagram in **Fig. 2**, increase or decrease of the specific heat resistance parameter presented in diagram, **Fig. 4** for the percentage of increase or the decrease of the steel burn off for the same scale layer thickness.

Table 2 presents quantities of scale determined by calculation following the method referred to in **reference 8** during op-

eration and a calculated optimal temperature regime of a pusher-type furnace. It has been noted that scaling is greater in the temperature regime achieved during operation than that at the calculated optimal one, which can be explained by the higher surface temperature of the charge in the first temperature regime. From the data (Δt) in **Table 3** it may be ascertained that detention at certain temperature sections should be altered, i.e. in a manner that the corresponding temperatures of flue gas and of the walls inside the furnace are higher in the 5th and 6th section in regard to calculated optimal temperature regime, due to the isolating behavior of the scale. However, the temperature regime determined during operation in fact corresponds to the optimal temperature regime of the furnace with a heating capacity of 40 t/h. That increase of capacity would not have an essential influence upon the quantity of scale, as formation due to detention at higher temperatures (which is shortened due to capacity increase) has a significantly greater influence.

Research carried out in a pusher-type furnace has shown that in the operating conditions, with a heat regime obtained by continuous work, a larger quantity of scale is formed in compare with the quantity of scale determined through calculation (**Table 3**). The difference is: (1 - 0,745) 100/0,745 = 34,23 %. The increase of steel burn off may be explained due to a greater oxidation atmosphere inside the furnace due to the air sucking through the openings on the furnace. This was confirmed by additional investigations. Particular attention should be payed to the formation of scale during discontinuous work after longer periods of delay in operation brought about by war circumstances. Five-day operation of the rolling mill train with 12 hours (one and a half) shifts was followed by 60 h delay, which led to a formation of 10 mm thick scale layer on the slabs surface. By normalising of conditions the continuous work was obtained. The result of abnormal conditions was a mass loss of the charge and an increased consumption of energy, because the time necessary for the charge to be heated was more than twice as long as usually. It was noticed that scale formed when the charge was kept in the furnace for over 60 hours, consisted of many layers of probably different composition and microstructure. This might be worth while to investigate in the future due to the influence on heat conductivity and due to great loss of the charge weight.

Research carried out lit the harm that scale makes as an isolating layer on the slab surface, during its heating. A correction of calculated heating time is necessary in the case of determination of proper heating conditions (regime) or by actual heating proces analysis. They can be useful as a ground for further studies of scaling influence on the quantity of air necessary for the start of fuel combustion, or the amount of O2 in waste flue gasses at the end of the furnace.

4. Conclusion

The scale on the surface of a charge behaves as an isolating layer, which enlarged the heating time and increased energy consumption. This is much apparent in the case of thinner charges heating in an oxidating atmosphere. The heating is slower due to the influence of scale. By the determining of an optimal temperature regime is necessary to consider the influence of scale formed. Inaccuracy by the calculation of a temperature regime, due to the increase in specific heat resistance is higher than in the case if no scale is present. A case of a pusher-type furnace with 190 mm thick steel charge heated and with a correction applied in the course of optimal temperature regime calculation, contributing to a better quality of the heated charge is described.

In particular, the influence of a thicker scale layer, formed due to larger stoppage of the rolling mill, the span of the heating time and energy consumption is described. During longer stoppages in a rolling mill multi-layered scale is noticed on a charge surface. A long time a blind fired furnace probably has an influence on scale formation and on its heat conductivity, and also on other parametres connected to charge heating. These investigations may also be useful as a ground for further studies of scale influence on quantity of air required at the beginning of operation and for the determination of fuel to air rate for the automatic regulation of the burners of the pusher-type furnace.

List of simbols

c_p – specific heat of steel, Ws/(kg K)

h – heat transfer coefficient, W/(m^2 K)

k – thermal conductivity of steel, W/(m K)

N_{Bi} – Biot number,

Δt – extention of heating time, %

$\Delta\Theta_m$ – the highest temperature difference in slabs, °C

τ – coefficient for thick-wall bodies

Θ_g – temperature of flue gas, °C

Θ_{ma} – average temperature of slabs, °C

Θ_{ms} – temperature of slabs surface, °C

ϑ_{ms} – medium temperature of slabs surface, °C

Θ_w – temperature of furnace walls, °C

5. References

[1] J. Črnko: The of the Heat Energy Consumption upon the Working Intensity and the Frequency of the Isolation Maintenance of a Pusher-type Furnace, *Kovine zlitine tehnologije*, 26, 1992, 4, 239-231.

[2] M. Kundak, Ž. Acs: Analiza toplinskog režima u valjaonicama traka, gredica i bešavnih cijevi, II dio, *Metalurgija* (Sisak), 16, 1977, 1, 9-13.

[3] E. I. Kazancev: Promišlennie peči, Izdatel'stvo *Metallurgija*, Moskva, 1975.

[4] W. Lehnert: *Wärmetechnische Grundlagen für Industrieofen*, Bergakademie Freiberg, 1979.

[5] K. Ražnjević: *Termodinamičke tablice*, Izdavač "Veselin Masleša", Sarajevo, 1989.

[6] M. Čaušević: *Obrada metala valjanjem*, Izdavač "Veselin Masleša", Sarajevo, 1983.

[7] M. Kundak: Optimalizacija zagrijavanja materijala u kružnoj peći teške pruge VBC-a, *Elaborat za Valjaonicu bešavnih cijevi Željezare Sisak izrađen u Institutu za metalurgiju Sisak*, Sisak, 1982.

[8] W. Heiligenstaedt: *Wärmetechnische Rechnungen für Industrieofen*, Verlag Stahleisen M.B.H., Düsseldorf, 1966.

[9] B. Kocijančić: Analiza utjecaja potrošnje zemnog plina i stvaranje oksidnog sloja za različite varijante rada VTG-a, *Interni izvještaj Holdinga Željezare Sisak*, Sisak, 1993.

KOVINE ZLITINE TEHNOLOGIJE, 28, 1994, 1-4

1. Kronološko kazalo

Kosec Ladislav: Kompoziti ..... KZT 28 (1994) 1-2, 19-24

Malavašič Tatjana: Smeri razvoja na področju polimernih materialov ..... KZT 28 (1994) 1-2, 25-30

Marinček Miloš: Temeljne mehanske lastnosti konstrukcijskih materialov ..... KZT 28 (1994) 1-2, 31-38

Milat Ognjen, Gustaaf Van Tendeloo, Jef Van Landuyt, Severin Amelincky: Characterization of Materials by High-Resolution Electron Microscopy ..... KZT 28 (1994) 1-2, 39-44

Vodopivec Franc: Jeklo po letu 2000 ..... KZT 28 (1994) 1-2, 45-52

Šegel Jože, F. Grešovnik: Metalurške raziskave za podporo kakovosti ..... KZT 28 (1994) 1-2, 53-55

Vižintin J., E. Tomšič, F. Uranc, F. Grešovnik, J. Šegel: Primerjalno preizkušanje obrabne obstojnosti orodnih jekel ..... KZT 28 (1994) 1-2, 57-68

Velej Marjan, F. Kosel: Reologija in premiki konstrukcijskih elementov iz zlitin z oblikovnim spominom ..... KZT 28 (1994) 1-2, 69-71

Torkar Matjaž, B. Šuštaršič, J. Žvokelj: Vodna atomizacija in zgoščevanje Ni-superzlitine ..... KZT 28 (1994) 1-2, 73-78

Smolej A., M. Gnamuš, S. Vehovar: Razvoj superplastične zlitine AlZnMgCu ..... KZT 28 (1994) 1-2, 79-83

Šuštaršič Borivoj, M. Torkar, M. Jenko, B. Breskvar, V. Leskovšek, A. Rodič, F. Vodopivec: Procesi atomizacije kovinskih gradiv in konsolidacija kovinskih prahov (4. del) ..... KZT 28 (1994) 1-2, 85-90

Dretnik D., M. Iglar, A. Paulin: Predelava sekundarnih surovin z majhnim deležem plemenitih kovin ..... KZT 28 (1994) 1-2, 91-94

Kejžar Rajko: Platiranje konstrukcijskih jekel z navarjanjem ..... KZT 28 (1994) 1-2, 95-100

Bratina Janez, A. Rozman: Optimalna raba energentov v obločni peči ..... KZT 28 (1994) 1-2, 101-104

Godec M., M. Jenko, F. Vodopivec, M. Ambrožič, \. Mandrino, L. Kosec, M. Lovrečič Saražin: Določanje teksture z metodo jedkalnih figur ..... KZT 28 (1994) 1-2, 105-109

Medved J., A. Rosina, J. Ilievski: Raziskave električne prevodnosti žlinder pri postopku EPŽ ..... KZT 28 (1994) 1-2, 111-113

Vehovar Leopold, I. Zakrajšek, F. Mlakar: Raziskava korozijske odpornosti visokolegiranih jeklenih litin s silicijem v močno oksidacijskih midijih ..... KZT 28 (1994) 1-2, 115-119

Bricelj Erika, V. Marinković, F. Vodopivec: Nastajanje izločkov med deformacijo ..... KZT 28 (1994) 1-2, 121-123

Steiner D., M. Jenko, F. Vodopivec, L. Kosec: Rast rekristaliziranih zrn v razogljičenem jeklu z 1,8 % Si in 0,025% Sb ..... KZT 28 (1994) 1-2, 125-129

Križman Alojz, I. Anžel, L. Gusel: Vpliv parametrov pri kontinuirnem litju na mehanske lastnosti zlitine Cu-Cr-Zr ..... KZT 28 1994) 1-2, 131-134

Gliha V., D. Toplak: Primerjava lastnosti toplotno vplivanega področja večvarkovnega zvara na jeklu Nionicral 70 pri dveh različnih vnostih toplote ..... KZT 28 (1994) 1-2, 135-140

Rak Inoslav, M. Kocak, S. Yao, K. Seifert, H. Lampe: Lomnožilavostne lastnosti toplotno vplivanega področja mikrolegiranega jekla tipa StE 355Ti za zahtevne konstrukcije ..... KZT 28 (1994) 1-2, 141-146

Saje B., S. Kobe-Beseničar, Z. Samardžija, D. Kolar, A. E. Platts, I. R. Harris: Mikrostruktura in magnetne lastnosti zlitin v sistemu Sm-Fe-Ta ..... KZT 28 (1994) 1-2, 147-151

Jenko Monika, F. Vodopivec, M. Godec, D. Steiner, B. Praček, L. Kosec: AES karakterizacija površinske segregacije antimona v neorientirani elektro pločevini ..... KZT 28 (1994) 1-2, 153-157

Šegel Jože, A. Vučko, L. Ranc: Vodenje tehnoloških procesov v jeklarni s pompčjo mreže osebnih računalnikov ..... KZT 28 (1994) 1-2, 159-162

Šarler Božidar, A. Košir: Modeliranje prenosa toplote in snovi pri kontinuiranem ulivanju - modela ACRONI Jesenice in IMPOL Slovenska Bistrica ..... KZT 28 (1994) 1-2, 163-167

Štok B., B. Bukovec, B. Koroušič: Matematično modeliranje termičnih stanj pri strjevanju ..... KZT 28 (1994) 1-2, 169-174

Dretnik D., R. Ozimic, M., Girth: Uporaba kisika v proizvodnji svinca ..... KZT 28 (1994) 1-2, 175-177

Doberšek M., A. Osojnik, I. Kosovinc: Vpliv Cu' in cinka na preoblikovalne lastnosti belega zlata ..... KZT 28 (1994) 1-2, 179-182

Vojvodič Gvardjančič Jelena, B. Ule, S. Ažman: Razvoj in uvajanje visokotrdnih drobnozrnatih mikrolegiranih jekel za uporabo v procesni industriji in gradbeništvu ..... KZT 28 (1994) 1-2, 183-187

Breže Borivoj: Orientacijski izračun za sestavo nosilnega endo plina in plinske atmosfere za nikotriranje ..... KZT 28 (1994) 1-2, 189-193

Horvat S., L. Kosec, V. Gontarev, D. Kmetič: Prenos ogljika v reži med dvemi jekli ..... KZT 28 (1994) 1-2, 195-197

Rodič Jože, K. Habijan, J. Dolenc, A. Rodič, D. Sikošek, I. Kos, K. Zalesnik: Specialni dodajni materiali in elektrode ..... KZT 28 (1994) 1-2, 199-202

Rodič Jože, K. Habijan, J. Dolenc, A. Jagodic, A. Rodič: Kobaltove zlitine v lesni industriji ..... KZT 28 (1994) 1-2, 203-208

Plimon G., L. Kosec, F. Mlakar: Utrujenost valjev za valjanje kovin v vročem ..... KZT 28 (1994) 1-2, 209-212

Bizjak M., L. Kosec, A. Smolej: Mikrostruktura zlitin aluminija z veliko koncentracijo železa izdelanih po postopku hitrega strjevanja ..... KZT 28 (1994) 1-2, 213-217

Gontarev V., J. Lamut, M. Pirnat, M. Purg: Vpliv kakovosti katranske smole za fizikalne lastnosti anod ..... KZT 28 (1994) 1-2, 219-221

Vasevska Trajanka: Vpliv toplotne predelave in specifične deformacije na preoblikovalno trdnost zlitine AlMg3 pri predelavi v hladnem stanju ..... KZT 28 (1994) 1-2, 223-226

Spruk S., L. Koller, M. Jenko, A. Rodič, L. Kosec: Mikrostruktura laserskih zvarov kovin in zlitin za elektroniko ..... KZT 28 (1994) 1-2, 227-230

Obal M., S. Rozman, A. Osojnik: Pasivni postopek saniranja kislih izcednih voda ..... KZT 28 (1994) 1-2, 231-235

Košir A., B. Šarler: Modeliranje strjevanja pri kontinuiranem ulivanju z dvojno recipročno robno integralsko metodo ..... KZT 28 (1994) 1-2, 237-243

Šalamun Igor, A. Stritar, B. Šarler: Spremljanje parametrov kontinuiranega ulivanja na osebnem računalniku - II ..... KZT 28 (1994) 1-2, 245-250

Uršič Vito, I. Surina, S. Semenič, M. Tonkovič-Prijanovič: Razvoj in preiskava domačih kompleksnih cepiv za sivo litino z lamelastim grafitom ..... KZT 28 (1994) 1-2, 251-255

Kolenko Tomaž, M. Hodošček, T. Šuštar, B. Glogovac: Uvajanje programske opreme za procesno vodenje na potisno peč ..... KZT 28 (1994) 1-2, 257-262

Glogovac Branimir, T. Kolenko, B. Sicherl, F. Pavlin: Celotna toplotna prestopnost na vložek pri ogrevanju plošč v potisni peči ..... KZT 28 (1994) 1-2, 263-265

Žnidaršič Andrej, M. Drofenik: Nova generacija Mn-Zn feritov za močnostne aplikacije ..... KZT 28 (1994) 1-2, 267-270

Šoba J., A. Eleršek, H. Mikuž, F. Golčman, R. Grabner: Rezultati poskusne monolitne obzidave vmesnih ponovc pri kontinuirnem ulivanju jekla ..... KZT 28 (1994) 1-2, 271-274

Eleršek A., J. Šoba, H. Mikuž: Ognjevzdržni oblikovanci iz betona z nizko vsebnostjo cementa ..... KZT 28 (1994) 1-2, 275-277

Valant Matjaž, D. Suvorov: Mikrovalovni materiali z visoko dielektričnostjo ..... KZT 28 (1994) 1-2, 279-282

Rozman M., M. Drofenik: Hidrotermalna sinteza feritov ..... KZT 28 (1994) 1-2, 283-286

Zupančič N., D. Kolar, D. Sušnik, Z. Samardžija: Mehanizem tvorbe kalcijevega sulfoaluminata 3CaO.3Al2O3.CaSO4 in vpliv Fe2O3 na njegov nastanek ..... KZT 28 (1994) 1-2, 287-290

Kuščer Danjela, M. Hrovat, J. Holc, D. Kolar, D. Sušnik: Sinteza katodnega materiala za visokotemperaturne gorivne celice ..... KZT 28 (1994) 1-2, 291-294

Stadler Zmago: Brezazbestni torni kompoziti ..... KZT 28 (1994) 1-2, 295-297

Šventner Kosmos A., Z. Samardžija, D. Sušnik, D. Kolar: Razvoj in značilnosti grobozrnate korundne keramike ..... KZT 28 (1994) 1-2, 299-301

Žerjal B.: Mehanske in morfološke lastnosti mešanic termoplastičnega poliuretana s stiren-akrilonitrili ..... KZT 28 (1994) 1-2, 303-305

Šušterič Z.: Dinamične lastnosti mešanic elastomer/polietilen .. .. KZT 28 (1994) 1-2, 307-309

Dimitrievski Ilija, T. Malavašič: Vpliv dodatkov poliuretanskih ionomerov na vulkanizacijo matrik naravnega in akrilonitrilnega kavčuka ter vplivi matrike akrilonitrilnega vulkanizata na "in situ" poliadicije poliuretanskih ionomerov ..... KZT 28 (1994) 1-2, 311-315

Marinović Tatjana: Uporaba koagentov pri peroksidnem premreževanju etilen-propilen-dienskega kavčuka ..... KZT 28 (1994) 1-2, 317-319

Leskovšek N., L. Tušar, M. Tušar, J. Zupan: Uporaba nevronskih mrež in statističnih metod pri razvoju premaznih sredstev ..... KZT 28 (1994) 1-2, 321-325

Stropnik Č.: Polimerne asimetrične porozne membrane ..... KZT 28 (1994) 1-2, 327-331

Germič L.: Priprava membran s fazno inverzijo na osnovi difuzijskih procesov ..... KZT 28 (1994) 1-2, 333-337

Anžlovar A., I. Anžur, T. Malavašič: Prepletene polimerne mreže iz poliuretanov in poliakrilatov ..... KZT 28 (1994) 1-2, 339-343

Leben Stanko, A. Šebenik: Kopolimerizacija substituiranih acetilenov ..... KZT 28 (1994) 1-2, 345-348

Opresnik M., A. Šebenik: Radikalska fotopolimerizacija stirena in akrilatov z disulfidnimi iniciatorji ..... KZT 28 (1994) 1-2, 349-353

Šemen F., M. Huskić, A. Šebenik: Polimerizacija metil metakrilata s PVC-ksantantnim makroiniciatorjem ..... KZT 28 (1994) 1-2, 355-357

Cvelbar R., I. Emri: Analiza predhodnega pojava pri merjenju lezenja viskoelastičnih materialov ..... KZT 28 (1994) 1-2, 359-362

Žagar Ema, M. Žigon, T. Malavašič: Reakcije različnih diizocianatov z bis(hidroksimetil)propionsko kislino ..... KZT 28 (1994) 1-2, 363-366

Ulčnik M., B. Žerjal, I. Ban: Termogravimetrija - metoda za opredeljevanje lastnosti mešanic polimerov ..... KZT 28 (1994) 1-2, 367-370

Verko N., Č. Stropnik: Kemijska modifikacija polimernih membran iz polisulfona ..... KZT 28 (1994) 1-2, 371-373

Bezjak A., Č. Stropnik: Imobilizacija tripsina na površino membrane iz celuloznega acetata ..... KZT 28 (1994) 1-2, 375-377

Kastelic M., M. Žigon, T. Malavašič: Sinteza in karakterizacija poliestrskih zamreževal ..... KZT 28 (1994) 1-2, 379-382

Fajdiga B., Z. Šušterič: Ojačevalni učinek saj na kavčukove zmesi ..... KZT 28 (1994) 1-2, 383-386

Kadivec I., N. Trček, Z. Šušterič: Ugotavljanje učinkovitosti peptizatorja pri masticiranju naravnega kavčuka z gelsko propustnostno kromatografijo ..... KZT 28 (1994) 1-2, 387-390

Rozman B., T. Marinović, T. Malavašič: Obstojnost mešanice nitrilnega in polisulfidnega kavčuka v topilih ..... KZT 28 (1994) 1-2, 391-393

Lapanje Helena, I. Anžur, T. Malavašič: Sinteza poliakrilatnih disperzij z različnimi količinami zamreževala ..... KZT 28 (1994) 1-2, 395-398

Mirčeva A., T. Malavašič: Sinteza in karakterizacija blokiranih poliuretanskih vodnih sistemov ..... KZT 28 (1994) 1-2, 399-402

Keber Zlatko, I. Emri: Napetostna korozija modificiranega polistirena ..... KZT 28 (1994) 1-2, 403-406

Metlikovič P., I. Emri: Analiza procesa lezenja viskoelastičnih materialov pod vplivom strižne obremenitve ..... KZT 28 (1994) 1-2, 407-409

Pavšek V., I. Emri: Vpliv količine difundirane vlage na mehanske lastnosti polimerov ..... KZT 28 (1994) 1-2, 411-413

Gspan P.: Začetne temperature za reakcije v tankoplastnih sistemih Me/SnTe in Me/PbTe ..... KZT 28 (1994) 1-2, 415-418

Demšar A., J. Lindav, K. Nemeš, S. Cencič, M. Lukač, B. Orel: Dielectric Laser and Ar Coatings for 2,94 μm ..... KZT 28 (1994) 1-2, 419-421

Brecelj F., A. Pregelj, K. Zupan: Optimizacija sinteze magnetodielektrika na osnovi karbonilnega železa ..... KZT 28 (1994) 1-2, 423-425

Pregelj Andrej, M. Mozetič, A. Paulin: Vakuumski helijev kriostat za doseganje superprevodnosti mikrovalovnega resonatorja ..... KZT 28 (1994) 1-2, 427-430

Požun K., B. Paradiž: Tankoplastni polimerni kapacitivni senzor relativne vlažnosti ..... KZT 28 (1994) 1-2, 431-432

Belič L. I., S. Jerič: Kemizem nastanka modificirane taline pri MoMn metalizaciji ..... KZT 28 (1994) 1-2, 433-436

Maček M., F. Švegl, B. Orel: Fe2O3 Sol-gel Derived Optical Coatings for Electrochromic Device ..... KZT 28 (1994) 1-2, 437-439

Crnjak Orel Z.: Electrochemical and Optical Properties of CeO2 and Mixed CeO2/SnO2 Coatings ..... KZT 28 (1994) 1-2, 441-443

Lavrenčič-Štangar U., B. Orel: Electrochromism of Mixed Phpsphotungstic Acid - Titanium Oxide Xerogel Thin Solid Films ..... KZT 28 (1994) 1-2, 445-449

Nemanič V.: Vakuumska ploskovna izolacija - Kovinska alternativa ekološko oporečnim izolacijskim penam ..... KZT 28 (1994) 1-2, 451-455

Panjan Peter, B. Navinšek, A. Cvelbar: Kontrola čistosti površin kovin med ionskim jedkanjem ..... KZT 28 (1994) 1-2, 457-459

Mozetič M., M. Kveder, A. Zalar: Rekombinacija atomov vodika na površini polikristalinskega bakra ..... KZT 28 (1994) 1-2, 461-463

Koller L., M. Jenko, S. Spruk, D. Railič: Študij lastnosti pozlačenega kontaktnega materiala Palladec 21 v odvisnosti od obrabe in atmosfere v hermetičnem okrovu ..... KZT 28 (1994) 1-2, 465-468

Mozetič M., K. Požun, B. Paradiž, A. Paulin: Interakcija kisikove plazme s polimeri ..... KZT 28 (1994) 1-2, 469-470

Županc-Mežnar Lea: Razvoj in optimizacija postopka izdelave zaslonov z luminoforom P-53 ..... KZT 28 (1994) 1-2, 471-473

Tasevski M., K. Požun, A. Demšar: Uporaba naparjenih kovin za polprepustna zrcala za avtomobilsko smerno svetilko ..... KZT 28 (1994) 1-2, 475-478

Zupan K., F. Brecelj, E. Perman, J. Maček: Uporaba EGA metode za spremljanje sol-gel sinteze za pripravo #2-Fe2O3 .... KZT 28 (1994) 1-2, 479-482

Musil Vojko, G. Radonjič: Smeri razvoja novih materialov na podlagi polimernih mešanic in zlitin ..... KZT 28 (1994) 3, 493-495

Topolovec Ksenija, V. Musil, T. Malavašič: Raziskave mešanic polietrni termoplastični poliuretan/kopolimer stiren-akrilonitril ..... KZT 28 (1994) 3, 496-498

Vižintin Nada, M. Kovačevič: Vpliv posameznih komponent v surovinah na lastnosti mas in izdelkov v keramični industriji .... KZT 28 (1994) 3, 499-501

Breže Borivoj: Račun fizikalno-kemijskih količin nitridov Fe2-3N za temperaturi 298 in 843 K ..... KZT 28 (1994) 3, 502-505

Emri Igor, N. W. Tschoegl: Determination of Mechanical Spectra from Experimental Responses ..... KZT 28 (1994) 3, 506-511

Runovc Franc: Computer-Aided Modeling and Simulation of Fabrication Steps in Semiconductor Processes ..... KZT 28 (1994) 3, 512-515

Kejžar Rajko, B. Kejžar: Dodajni materiali na osnovi izbranih sintetičnih repromaterialov z dodatkom alkalijskih oksidov ..... KZT 28 (1994) 3, 516-519

Kosec Bojan, T. Kolenko, F. Pavlin: Temperaturno polje v valjih pri kontinuirnem litju aluminijevih trakov ..... KZT 28 (1994) 3, 520-522

Leskovšek Vojteh, A. Paulin, T. Kolenko: Razvoj indukcijsko segrevane laboratorijske peči za toplotno obdelavo v zvrtinčeni plasti ..... KZT 28 (1994) 3, 525-531

Cajner Franjo: Prilog istraživanju svojstava popuštenog martenzita i popuštenog bainita ..... KZT 28 (1994) 3, 533-538

Grozdanič Vladimir: General Solution of Heating and/or Cooling of Metallurgical Furnace Wall by Means of Jacobi #3 Function ..... KZT 28 (1994) 3, 539-541

Kaker Henrik: Napake na valjih za hladno valjanje ..... KZT 28 (1994) 3, 543-547

Legat Franc: Razvoj jekel za ladijske verige ..... KZT 28 (1994) 3, 549-551

Klinar Milan: Pregled, uporaba, primerjava in lastnosti v ognjuodpornih materialov, ki se uporabljajo za obzidavo livnih ponovc v Jeklarni Bela ..... KZT 28 (1994) 3, 553-556

Jenko Monika, F. Vodopivec, M. Godec, D. Steiner-Petrovič, H. Viefhaus, M. Lucas, M. Milun: Surface Activated Recrystallization of Antimony Alloyed Non-Oriented Electrical Steel Sheet..... KZT 28 (1994) 4, 561-565

Kobe-Beseničar S., B. Saje, G. Dražič, : Use of the HDDR Process in Preparation of Zirconia Doped Nd-Dy-Fe-B High Coercivity Powder ..... KZT 28 (1994) 4, 567-570

Vodopivec Franc, B. Ule, L. Vehovar, J. Žvokelj, V. Verbič: Macro and Micromorphology of Service Cracking and Fracture of Turbine Blades ..... KZT 28 (1994) 4, 571-577

Schlomchack G. G., I. Mamuzič, F. Vodopivec: Deformation Anomalies of Higher Order during the Plastic Extention of Rheologically Complex Materials ... KZT 28 (1994) 4, 579-587

Schlomchack G. G., I. Mamuzič, F. Vodopivec: The Role of Contact Friction and Rheology in the Deformation at Plastometric Tests of Rheologically Complex Materials ..... KZT 28 (1994) 4, 583-587

Kejžar Rajko, L. Kosec: Quality of Surfaced Running Wheels . ..... KZT 28 (1994) 4, 589-593

Ule Boris, V. Leskovšek, B. Breskvar, K. Kuzman, D. Švetak, F. Kofol: Cockroft - Latham Fracture Criterion and Bulk Formability of Copper Base Alloys KZT 28 (1994) 4, 595-600

Šuštaršič B., B. Breskvar, V. Leskovšek, A. Rodič: Properties of Cu-based Alloys - powders for Brazing Prepared by Water Atomization ..... KZT 28 (1994) 4, 601-608

Koroušič Blaženko: Use of a Mathematical Model GPRO to Describe Complexe Gas - Metal Reactions ..... KZT 28 (1994) 4, 609-611

Borchardt G., R. Turk, S. Javorič: Protection of Carbon/Carbon Composites against Oxidation ..... KZT 28 (1994) 4, 613-617

Kundak M., J. Črnko: Influence of the Scaling upon the Heating Process of Steel Slabs in a Pushe-type Furnace ..... KZT 28 (1994) 4, 619-622

2. Avtorsko kazalo

Anžlovar A., I. Anžur, T. Malavašič: Prepletene polimerne mreže iz poliuretanov in poliakrilatov .... KZT 28 (1994) 1-2, 339-343

Belič L. I., S. Jerič: Kemizem nastanka modificirane taline pri MoMn metalizaciji ..... KZT 28 (1994) 1-2, 433-436

Bezjak A., Č. Stropnik: Imobilizacija tripsina na površino membrane iz celuloznega acetata ..... KZT 28 (1994) 1-2, 375-377

Bizjak M., L. Kosec, A. Smolej: Mikrostruktura zlitin aluminija z veliko koncentracijo železa izdelanih po postopku hitrega strjevanja ..... KZT 28 (1994) 1-2, 213-217

Borchardt G., R. Turk, S. Javorič: Protection of Carbon/Carbon Composites against Oxidation ..... KZT 28 (1994) 4, 613-617

Bratina Janez, A. Rozman: Optimalna raba energentov v obločni peči ..... KZT 28 (1994) 1-2, 101-104

Brecelj F., A. Pregelj, K. Zupan: Optimizacija sinteze magnetodielektrika na osnovi karbonilnega železa ..... KZT 28 (1994) 1-2, 423-425

Breže Borivoj: Orientacijski izračun za sestavo nosilnega endo plina in plinske atmosfere za nikotriranje ..... KZT 28 (1994) 1-2, 189-193

Breže Borivoj: Račun fizikalno-kemijskih količin nitridov Fe_2-3N za temperaturi 298 in 843 K ..... KZT 28 (1994) 3, 502-505

Bricelj Erika, V. Marinković, F. Vodopivec: Nastajanje izločkov med deformacijo ..... KZT 28 (1994) 1-2, 121-123

Cajner Franjo: Prilog istraživanju svojstava popuštenog martenzita i popuštenog bainita ..... KZT 28 (1994) 3, 533-538

Crnjak Orel Z.: Electrochemical and Optical Properties of CeO_2 and Mixed CeO_2/SnO_2 Coatings ..... KZT 28 (1994) 1-2, 441-443

Cvelbar R., I. Emri: Analiza predhodnega pojava pri merjenju lezenja viskoelastičnih materialov ..... KZT 28 (1994) 1-2, 359-362

Demšar A., J. Lindav, K. Nemeš, S. Cencič, M. Lukač, B. Orel: Dielectric Laser and Ar Coatings for 2,94 μm ..... KZT 28 (1994) 1-2, 419-421

Dimitrievski Ilija, T. Malavašič: Vpliv dodatkov poliuretanskih ionomerov na vulkanizacijo matrik naravnega in akrilonitrilnega kavčuka ter vplivi matrike akrilonitrilnega vulkanizata na "in situ" poliadicije poliuretanskih ionomerov ..... KZT 28 (1994) 1-2, 311-315

Doberšek M., A. Osojnik, I. Kosovinc: Vpliv Cu' in cinka na preoblikovalne lastnosti belega zlata ..... KZT 28 (1994) 1-2, 179-182

Dretnik D., M. Iglar, A. Paulin: Predelava sekundarnih surovin z majhnim deležem plemenitih kovin ..... KZT 28 (1994) 1-2, 091-094

Dretnik D., R. Ozimic, M., Girth: Uporaba kisika v proizvodnji svinca ..... KZT 28 (1994) 1-2, 175-177

Eleršek A., J. Šoba, H. Mikuž: Ognjevzdržni oblikovanci iz betona z nizko vsebnostjo cementa ..... KZT 28 (1994) 1-2, 275-277

Emri Igor, N. W. Tschoegl: Determination of Mechanical Spectra from Experimental Responses ..... KZT 28 (1994) 3, 506-511

Fajdiga B., Z. Šušterič: Ojačevalni učinek saj na kavčukove zmesi ..... KZT 28 (1994) 1-2, 383-386

Germič L.: Priprava membran s fazno inverzijo na osnovi difuzijskih procesov ..... KZT 28 (1994) 1-2, 333-337

Gliha V., D. Toplak: Primerjava lastnosti toplotno vplivanega področja večvarkovnega zvara na jeklu Nionicral 70 pri dveh različnih vnostih toplote ..... KZT 28 (1994) 1-2, 135-140

Glogovac Branimir, T. Kolenko, B. Sicherl, F. Pavlin: Celotna toplotna prestopnost na vložek pri ogrevanju plošč v potisni peči .....KZT 28 (1994) 1-2, 263-265

Godec M., M. Jenko, F. Vodopivec, M. Ambrožič, \. Mandrino, L. Kosec, M. Lovrečič Saražin: Določanje teksture z metodo jedkalnih figur ..... KZT 28 (1994) 1-2, 105-109

Gontarev V., J. Lamut, M. Pirnat, M. Purg: Vpliv kakovosti katranske smole za fizikalne lastnosti anod ..... KZT 28 (1994) 1-2, 219-221

Grozdanić Vladimir: General Solution of Heating and/or Cooling of Metallurgical Furnace Wall by Means of Jacobi #3 Function ..... KZT 28 (1994) 3, 539-541

Gspan P.: Začetne temperature za reakcije v tankoplastnih sistemih Me/SnTe in Me/PbTe ..... KZT 28 (1994) 1-2, 415-418

Horvat S., L. Kosec, V. Gontarev, D. Kmetič: Prenos ogljika v reži med dvemi jekli ..... KZT 28 (1994) 1-2, 195-197

Jenko Monika, F. Vodopivec, M. Godec, D. Steiner, B. Praček, L. Kosec: AES karakterizacija površinske segregacije antimona v neorientirani elektro pločevini ..... KZT 28 (1994) 1-2, 153-157

Jenko Monika, F. Vodopivec, M. Godec, D. Steiner-Petrovič, H. Viefhaus, M. Lucas, M. Milun: Surface Activated Recrystallization of Antimony Alloyed Non-Oriented Electrical Steel Sheet ..... KZT 28 (1994) 4, 561-565

Kadivec I., N. Trček, Z. Šušterič: Ugotavljanje učinkovitosti peptizatorja pri masticiranju naravnega kavčuka z gelsko propustnostno kromatografijo ..... KZT 28 (1994) 1-2, 387-390

Kaker Henrik: Napake na valjih za hladno valjanje ..... KZT 28 (1994) 3, 543-547

Kastelic M., M. Žigon, T. Malavašič: Sinteza in karakterizacija poliestrskih zamreževal ..... KZT 28 (1994) 1-2, 379-382

Keber Zlatko, I. Emri: Napetostna korozija modificiranega polistirena ..... KZT 28 (1994) 1-2, 403-406

Kejžar Rajko: Platiranje konstrukcijskih jekel z navarjanjem .... KZT 28 (1994) 1-2, 095-100

Kejžar Rajko, B. Kejžar: Dodajni materiali na osnovi izbranih sintetičnih repromaterialov z dodatkom alkalijskih oksidov ..... KZT 28 (1994) 3, 516-519

Kejžar Rajko, L. Kosec: Quality of Surfaced Running Wheels .. KZT 28 (1994) 4, 589-593

Klinar Milan: Pregled, uporaba, primerjava in lastnosti v ognjuodpornih materialov, ki se uporabljajo za obzidavo livnih ponovc v Jeklarni Bela ..... KZT 28 (1994) 3, 553-556

Kobe-Beseničar S., B. Saje, G. Dražič, : Use of the HDDR Process in Preparation of Zirconia Doped Nd-Dy-Fe-B High Coercivity Powder ..... KZT 28 (1994) 4, 567-570

Kolenko Tomaž, M. Hodošček, T. Šuštar, B. Glogovac: Uvajanje programske opreme za procesno vodenje na potisno peč ..... KZT 28 (1994) 1-2, 257-262

Koller L., M. Jenko, S. Spruk, D. Railič: Študij lastnosti po-

zlačenega kontaktnega materiala Palladec 21 v odvisnosti od obrabe in atmosfere v hermetičnem okrovu ..... KZT 28 (1994) 1-2, 465-468

Koroušić Blaženko: Use of a Mathematical Model GPRO to Describe Complexe Gas - Metal Reactions ..... KZT 28 (1994) 4, 609-611

Kosec Bojan, T. Kolenko, F. Pavlin: Temperaturno polje v valjih pri kontinuirnem litju aluminijevih trakov ..... KZT 28 (1994) 3, 520-522

Kosec Ladislav: Kompoziti ..... KZT 28 (1994) 1-2, 019-024

Košir A., B. Šarler: Modeliranje strjevanja pri kontinuiranem ulivanju z dvojno recipročno robno integralsko metodo ..... KZT 28 (1994) 1-2, 237-243

Križman Alojz, I. Anžel, L. Gusel: Vpliv parametrov pri kontinuirnem litju na mehanske lastnosti zlitine Cu-Cr-Zr ..... KZT 28 1994) 1-2, 131-134

Kundak M., J. Črnko: Influence of the Scaling upon the Heating Process of Steel Slabs in a Pushe-type Furnace ..... KZT 28 (1994) 4, 619-622

Kuščer Danjela, M. Hrovat, J. Holc, D. Kolar, D. Sušnik: Sinteza katodnega materiala za visokotemperaturne gorivne celice ..... KZT 28 (1994) 1-2, 291-294

Lapanje Helena, I. Anžur, T. Malavašič: Sinteza poliakrilatnih disperzij z različnimi količinami zamreževala ..... KZT 28 (1994) 1-2, 395-398

Lavrenčič-Štangar U., B. Orel: Electrochromism of Mixed Phpsphotungstic Acid - Titanium Oxide Xerogel Thin Solid Films ..... KZT 28 (1994) 1-2, 445-449

Leben Stanko, A. Šebenik: Kopolimerizacija substituiranih acetilenov ..... KZT 28 (1994) 1-2, 345-348

Legat Franc: Razvoj jekel za ladijske verige ..... KZT 28 (1994) 3, 549-551

Leskovšek N., L. Tušar, M. Tušar, J. Zupan: Uporaba nevronskih mrež in statističnih metod pri razvoju premaznih sredstev ..... KZT 28 (1994) 1-2, 321-325

Leskovšek Vojteh, A. Paulin, T. Kolenko: Razvoj indukcijsko segrevane laboratorijske peči za toplotno obdelavo v zvrtinčeni plasti ..... KZT 28 (1994) 3, 525-531

Maček M., F. Švegl, B. Orel: Fe_2O_3 Sol-gel Derived Optical Coatings for Electrochromic Device ..... KZT 28 (1994) 1-2, 437-439

Malavašič Tatjana: Smeri razvoja na področju polimernih materialov ..... KZT 28 (1994) 1-2, 025-030

Marinček Miloš: Temeljne mehanske lastnosti konstrukcijskih materialov ..... KZT 28 (1994) 1-2, 031-038

Marinović Tatjana: Uporaba koagentov pri peroksidnem premreževanju etilen-propilen-dienskega kavčuka ..... KZT 28 (1994) 1-2, 317-319

Medved J., A. Rosina, J. Ilievski: Raziskave električne prevodnosti žlinder pri postopku EPŽ ..... KZT 28 (1994) 1-2, 111-113

Metlikovič P., I. Emri: Analiza procesa lezenja viskoelastičnih materialov pod vplivom strižne obremenitve ..... KZT 28 (1994) 1-2, 407-409

Milat Ognjen, Gustaaf Van Tendeloo, Jef Van Landuyt, Severin Amelincky: Characterization of Materials by High-Resolution Electron Microscopy ..... KZT 28 (1994) 1-2, 039-044

Mirčeva A., T. Malavašič: Sinteza in karakterizacija blokiranih poliuretanskih vodnih sistemov ..... KZT 28 (1994) 1-2, 399-402

Mozetič M., M. Kveder, A. Zalar: Rekombinacija atomov vodika na površini polikristalinskega bakra ..... KZT 28 (1994) 1-2, 461-463

Musil Vojko, G. Radonjič: Smeri razvoja novih materialov na podlagi polimernih mešanic in zlitin ..... KZT 28 (1994) 3, 493-495

Nemanič V.: Vakuumska ploskovna izolacija - Kovinska alternativa ekološko oporečnim izolacijskim penam ..... KZT 28 (1994) 1-2, 451-455

Obal M., S. Rozman, A. Osojnik: Pasivni postopek saniranja kislih izcednih voda ..... KZT 28 (1994) 1-2, 231-235

Opresnik M., A. Šebenik: Radikalska fotopolimerizacija stirena in akrilatov z disulfidnimi iniciatorji ..... KZT 28 (1994) 1-2, 349-353

Panjan Peter, B. Navinšek, A. Cvelbar: Kontrola čistosti površin kovin med ionskim jedkanjem ..... KZT 28 (1994) 1-2, 457-459

Pavšek V., I. Emri: Vpliv količine difundirane vlage na mehanske lastnosti polimerov ..... KZT 28 (1994) 1-2, 411-413

Plimon G., L. Kosec, F. Mlakar: Utrujenost valjev za valjanje kovin v vročem ..... KZT 28 (1994) 1-2, 209-212

Požun K., B. Paradiž: Tankoplastni polimerni kapacitivni senzor relativne vlažnosti ..... KZT 28 (1994) 1-2, 431-432

Pregelj Andrej, M. Mozetič, A. Paulin: Vakuumski helijev kriostat za doseganje superprevodnosti mikrovalovnega resonatorja ..... KZT 28 (1994) 1-2, 427-430

Rak Inoslav, M. Kocak, S. Yao, K. Seifert, H. Lampe: Lomnožilavostne lastnosti toplotno vplivanega področja mikrolegiranega jekla tipa StE 355Ti za zahtevne konstrukcije ..... KZT 28 (1994) 1-2, 141-146

Rodič Jože, K. Habijan, J. Dolenc, A. Rodič, D. Sikošek, I. Kos, K. Zalesnik: Specialni dodajni materiali in elektrode ..... KZT 28 (1994) 1-2, 199-202

Rodič Jože, K. Habijan, J. Dolenc, A. Jagodic, A. Rodič: Kobaltove zlitine v lesni industriji ..... KZT 28 (1994) 1-2, 203-208

Rozman B., T. Marinović, T. Malavašič: Obstojnost mešanice nitrilnega in polisulfidnega kavčuka v topilih ..... KZT 28 (1994) 1-2, 391-393

Rozman M., M. Drofenik: Hidrotermalna sinteza feritov ..... KZT 28 (1994) 1-2, 283-286

Runove Franc: Computer-Aided Modeling and Simulation of Fabrication Steps in Semiconductor Processes ..... KZT 28 (1994) 3, 512-515

Saje B., S. Kobe-Beseničar, Z. Samardžija, D. Kolar, A. E. Platts, I. R. Harris: Mikrostruktura in magnetne lastnosti zlitin v sistemu Sm-Fe-Ta ..... KZT 28 (1994) 1-2, 147-151

Schlomchack G. G., I. Mamuzič, F. Vodopivec: Deformation Anomalies of Higher Order during the Plastic Extention of Rheologically Complex Materials ... KZT 28 (1994) 4, 583-587

Schlomchack G. G., I. Mamuzič, F. Vodopivec: The Role of Contact Friction and Rheology in the Deformation at Plastometric Tests of Rheologically Complex Materials ..... KZT 28 (1994) 4, 579-582

Smolej A., M. Gnamuš, S. Vehovar: Razvoj superplastične zlitine AlZnMgCu ..... KZT 28 (1994) 1-2, 079-083

Spruk S., L. Koller, M. Jenko, A. Rodič, L. Kosec: Mikrostruktura laserskih zvarov kovin in zlitin za elektroniko ..... KZT 28 (1994) 1-2, 227-230

Stadler Zmago: Brezazbestni torni kompoziti ..... KZT 28 (1994) 1-2, 295-297

Steiner D., M. Jenko, F. Vodopivec, L. Kosec: Rast rekristaliziranih zrn v razogljičenem jeklu z 1,8 % Si in 0,025 % Sb ..... KZT 28 (1994) 1-2, 125-129

Stropnik Č.: Polimerne asimetrične porozne membrane ..... KZT 28 (1994) 1-2, 327-331

Šalamun Igor, A. Stritar, B. Šarler: Spremljanje parametrov kontinuiranega ulivanja na osebnem računalniku - II ..... KZT 28 (1994) 1-2, 245-250

Šarler Božidar, A. Košir: Modeliranje prenosa toplote in snovi pri kontinuiranem ulivanju - modela ACRONI Jesenice in IMPOL Slovenska Bistrica ..... KZT 28 (1994) 1-2, 163-167

Šegel Jože, F. Grešovnik: Metalurške raziskave za podporo kakovosti ..... KZT 28 (1994) 1-2, 053-055

Šegel Jože, A. Vučko, L. Ranc: Vodenje tehnoloških procesov v jeklarni s pompčjo mreže osebnih računalnikov ..... KZT 28 (1994) 1-2, 159-162

Šemen F., M. Huskić, A. Šebenik: Polimerizacija metil metakrilata s PVC-ksantantnim makroiniciatorjem ..... KZT 28 (1994) 1-2, 355-357

Šoba J., A. Eleršek, H. Mikuž, F. Golčman, R. Grabner: Rezultati poskusne monolitne obzidave vmesnih ponovc pri kontinuirnem ulivanju jekla ..... KZT 28 (1994) 1-2, 271-274

Štok B., B. Bukovec, B. Koroušič: Matematično modeliranje termičnih stanj pri strjevanju ..... KZT 28 (1994) 1-2, 169-174

Šuštaršič Borivoj, M. Torkar, M. Jenko, B. Breskvar, V. Leskovšek, A. Rodič, F. Vodopivec: Procesi atomizacije kovinskih gradiv in konsolidacija kovinskih prahov (4. del) ..... KZT 28 (1994) 1-2, 085-090

Šuštaršič B., B. Breskvar, V. Leskovšek, A. Rodič: Properties of Cu-based Alloys - powders for Brazing Prepared by Water Atomization ..... KZT 28 (1994) 4, 601-608

Šušterič Z.: Dinamične lastnosti mešanic elastomer/polietilen .. .. KZT 28 (1994) 1-2, 307-309

Šventner Kosmos A., Z. Samardžija, D. Sušnik, D. Kolar: Razvoj in značilnosti grobozrnate korundne keramike ..... KZT 28 (1994) 1-2, 299-301

Tasevski M., K. Požun, A. Demšar: Uporaba naparjenih kovin za polprepustna zrcala za avtomobilsko smerno svetilko ..... KZT 28 (1994) 1-2, 475-478

Topolovec Ksenija, V. Musil, T. Malavašič: Raziskave mešanic polietrni termoplastični poliuretan/kopolimer stiren-akrilonitril ..... KZT 28 (1994) 3, 496-498

Torkar Matjaž, B. Šuštaršič, J. Žvokelj: Vodna atomizacija in zgoščevanje Ni-superzlitine ..... KZT 28 (1994) 1-2, 073-078

Ulčnik M., B. Žerjal, I. Ban: Termogravimetrija - metoda za opredeljevanje lastnosti mešanic polimerov ..... KZT 28 (1994) 1-2, 367-370

Ule Boris, V. Leskovšek, B. Breskvar, K. Kuzman, D. Švetak, F. Kofol: Cockroft - Latham Fracture Criterion and Bulk Formability of Copper Base Alloys KZT 28 (1994) 4, 595-600

Uršič Vito, I. Surina, S. Semenič, M. Tonkovič-Prijanovič: Razvoj in preiskava domačih kompleksnih cepiv za sivo litino z lamelastim grafitom ..... KZT 28 (1994) 1-2, 251-255

Valant Matjaž, D. Suvorov: Mikrovalovni materiali z visoko dielektričnostjo ..... KZT 28 (1994) 1-2, 279-282

Vasevska Trajanka: Vpliv toplotne predelave in specifične deformacije na preoblikovalno trdnost zlitine AlMg3 pri predelavi v hladnem stanju ..... KZT 28 (1994) 1-2, 223-226

Vehovar Leopold, I. Zakrajšek, F. Mlakar: Raziskava korozijske odpornosti visokolegiranih jeklenih litin s silicijem v močno oksidacijskih midijih ..... KZT 28 (1994) 1-2, 115-119

Velej Marjan, F. Kosel: Reologija in premiki konstrukcijskih elementov iz zlitin z oblikovnim spominom ..... KZT 28 (1994) 1-2, 069-071

Verko N., Č. Stropnik: Kemijska modifikacija polimernih membran iz polisulfona ..... KZT 28 (1994) 1-2, 371-373

Vižintin J., E. Tomšič, F. Uranc, F. Grešovnik, J. Šegel: Primerjalno preizkušanje obrabne obstojnosti orodnih jekel ..... KZT 28 (1994) 1-2, 057-068

Vižintin Nada, M. Kovačevič: Vpliv posameznih komponent v surovinah na lastnosti mas in izdelkov v keramični industriji .... KZT 28 (1994) 3, 499-501

Vodopivec Franc: Jeklo po letu 2000 ..... KZT 28 (1994) 1-2, 045-052

Vodopivec Franc, B. Ule, L. Vehovar, J. Žvokelj, V. Verbič: Macro and Micromorphology of Service Cracking and Fracture of Turbine Blades ..... KZT 28 (1994) 4, 571-577

Vojvodič Gvardjančič Jelena, B. Ule, S. Ažman: Razvoj in uvajanje visokotrdnih drobnozrnatih mikrolegiranih jekel za uporabo v procesni industriji in gradbeništvu ..... KZT 28 (1994) 1-2, 183-187

Zupan K., F. Brecelj, E. Perman, J. Maček: Uporaba EGA metode za spremljanje sol-gel sinteze za pripravo #2-Fe_2O_3 ..... KZT 28 (1994) 1-2, 479-482

Zupančič N., D. Kolar, D. Sušnik, Z. Samardžija: Mehanizem tvorbe kalcijevega sulfoaluminata 3CaO.3Al2O3.CaSO4 in vpliv Fe2O3 na njegov nastanek ..... KZT 28 (1994) 1-2, 287-290

Žagar Ema, M. Žigon, T. Malavašič: Reakcije različnih diizocianatov z bis(hidroksimetil)propionsko kislino ..... KZT 28 (1994) 1-2, 363-366

Žerjal B.: Mehanske in morfološke lastnosti mešanic termoplastičnega poliuretana s stiren-akrilonitrili ..... KZT 28 (1994) 1-2, 303-305

Žnidaršič Andrej, M. Drofenik: Nova generacija Mn-Zn feritov za močnostne aplikacije ..... KZT 28 (1994) 1-2, 267-270

Župane-Mežnar Lea: Razvoj in optimizacija postopka izdelave zaslonov z luminoforom P-53 ..... KZT 28 (1994) 1-2, 471-473

HIGH AND ULTRA-HIGH VACUUM COMPONENTS

416 PAGES 38 CATEGORIES
10 SECTIONS 4 CURRENCIES
2 INDEXES ...

1 CATALOGUE

CABURN MDC

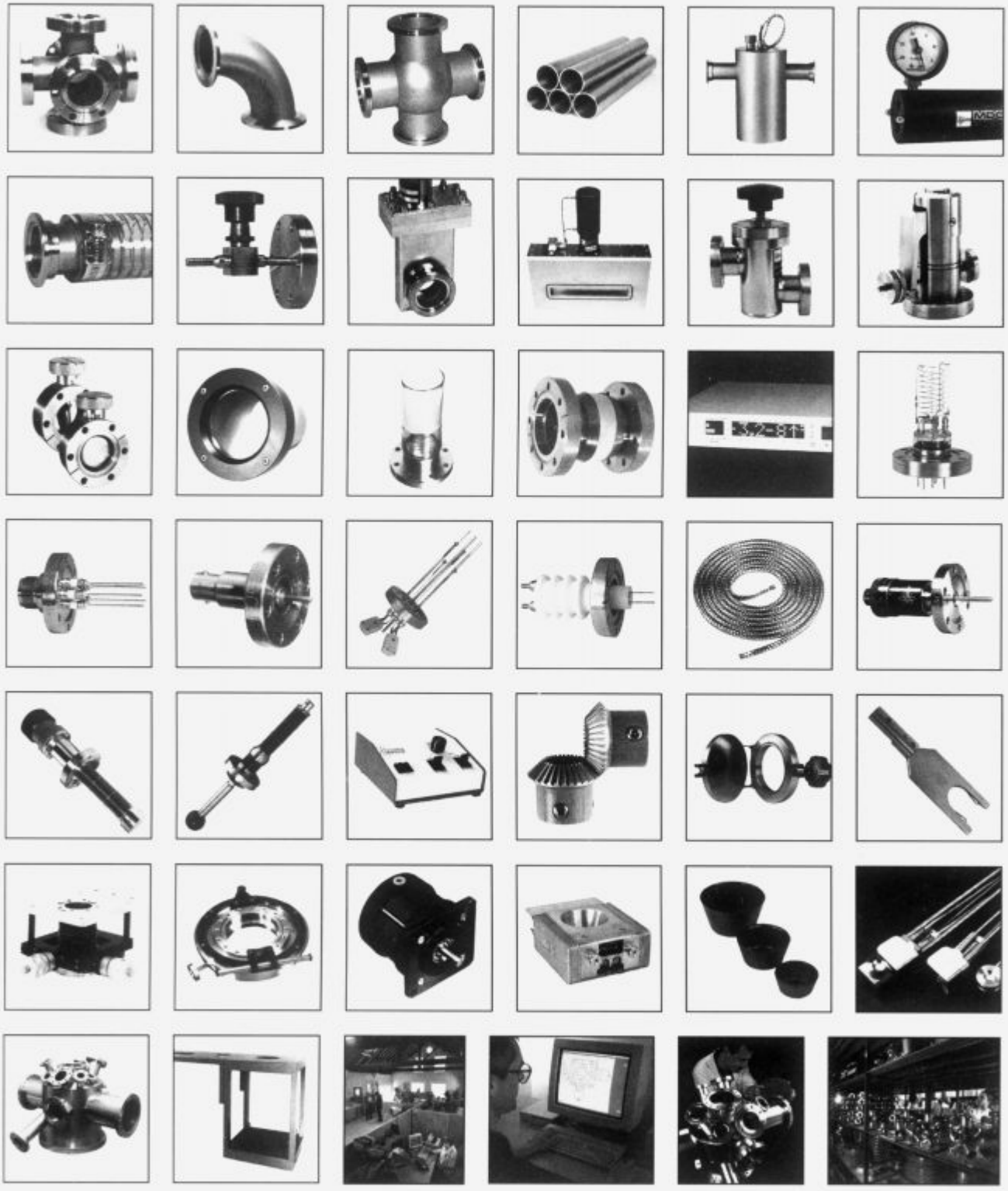

Head Office

Caburn-MDC Limited
The Old Dairy, The Street,
Glynde, East Sussex
BN8 6SJ United Kingdom

Tel: +44 (0)273 858585
Fax: +44 (0)273 858561

Berlin

Caburn-MDC
Ostendstrasse 1
D-12459 Berlin
Germany

Tel: +49 (0) 30 6953 9840
Fax: +49 (0) 30 635 3786

Lyon

Caburn-MDC S.A.R.L.
Novacité-Alpha
B.P. 2131
F-69603 Villeurbanne Cedex
France

Tel: (+33) 78 94 56 30
Fax: (+33) 72 44 34 85

Torino

Caburn-MDC
(Alberto Rava)
Str. Molinetti 41, Il Molino
10098 Rivoli, Torino
Italy

Tel: +39 (0) 11 95 85 134
Fax: +39 (0) 11 95 66 515

Are you satisfied with the air in your factory when heating up the ladles?

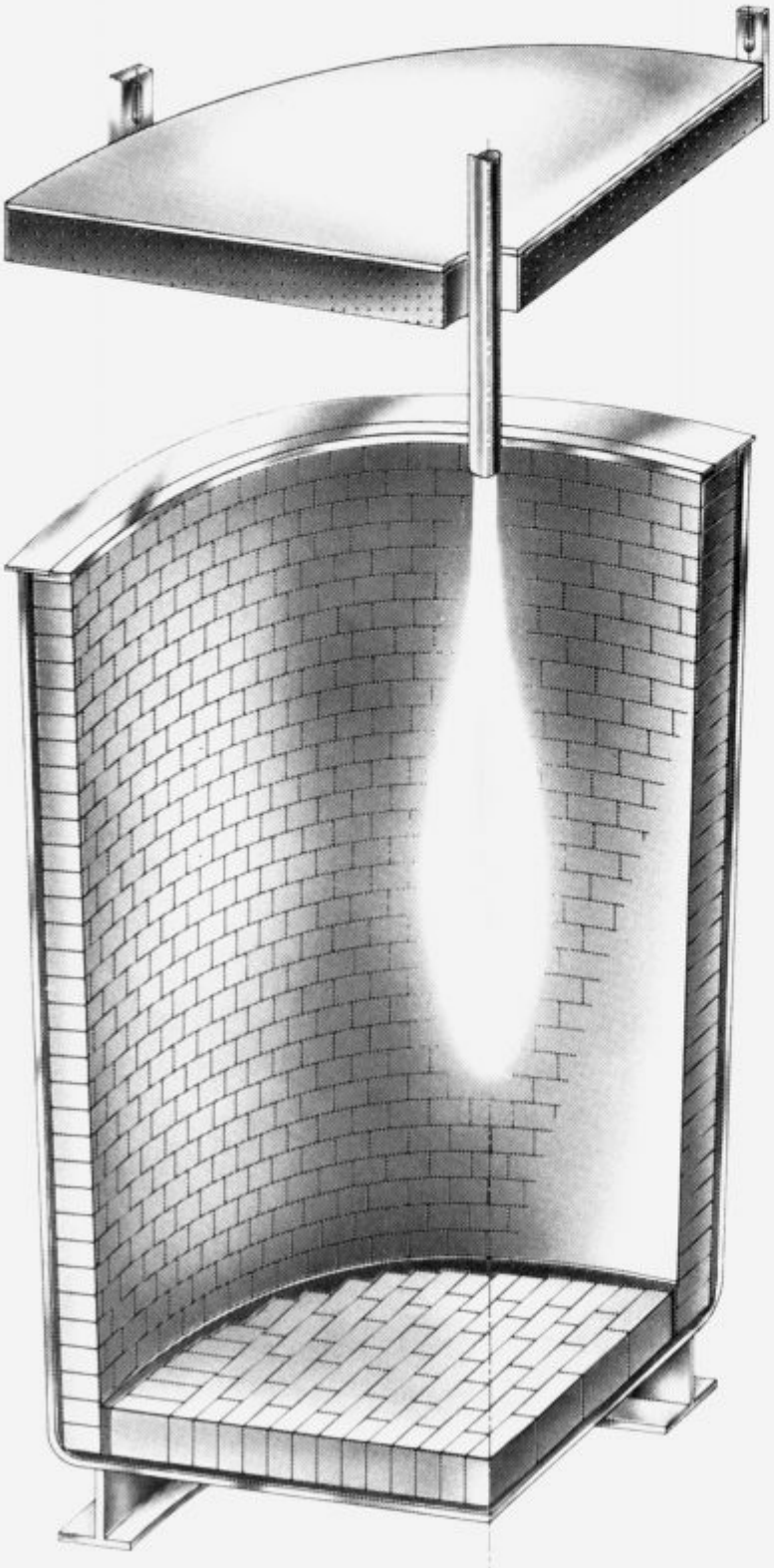

In spite of good ladle burners, fumes and bad odours are directly emitted into the factory when heating up carbon containing refractory linings

The newly delveloped bonding system (Major Improvement in Ladle Emission)

solves the problems you could encounter with fumes and odours.

Our quality assurance system ISO 9001 guarantees the highest continous quality and lining life for these new refractory products.

Your partner for pure air in the steel plant.

ISO 9001

VEITSCHER